MODELING OF FLUORIDE MOLTEN SALT REACTOR DEPLETION IN SCALE

A Dissertation
Presented to
The Academic Faculty

by

Christopher Bayne

In Partial Fulfillment
of the Requirements for the Degree
Masters of Science in Nuclear Engineering in the
Nuclear and Radiological Engineering, G. W. Woodruff School of Mechanical Engineering

Georgia Institute of Technology
December 2023

MODELING OF FLUORIDE MOLTEN SALT REACTOR DEPLETION IN SCALE

Approved by:

Date Approved:

Dr. Bojan Petrovic, Advisor

[August 18, 2023]

Nuclear & Radiological Engineering,

School of Mechanical Engineering

Georgia Institute of Technology

Dr. Dan Kotlyar

Nuclear & Radiological Engineering,

School of Mechanical Engineering

Georgia Institute of Technology

Dr. Stephen Biegalski

Nuclear & Radiological Engineering,

School of Mechanical Engineering

Georgia Institute of Technology

ACKNOWLEDGEMENTS

This work was supported, in part, by the Nuclear Energy eXperimental Testing Research Alliance (NEXTRA) with funding provided by Natura Resources, LLC, as well as through research cyberinfrastructure resources and services provided by the Partnership for an Advanced Computing Environment (PACE) at the Georgia Institute of Technology, Atlanta, Georgia. Additionally, this research made use of Idaho National Laboratory computing resources which are supported by the Office of Nuclear Energy of the U.S. Department of Energy and the Nuclear Science User Facilities under Contract No. DE-AC07-05ID14517. [1]

TABLE OF CONTENTS

LIST OF TABLES

LIST OF FIGURES

LIST OF SYMBOLS AND ABBREVIATIONS

CE	Continuous-energy (in reference to cross section libraries)
MG	Multigroup (in reference to cross section libraries)
MSR	Molten salt reactor
MTIHM	Metric tons of initial heavy metal
NEXTRA	Nuclear Energy eXperimental Testing Research Alliance
ORNL	Oak Ridge National Laboratory
PNNL	Pacific Northwest National Laboratory
SNL	Sandia National Laboratory
US DOE	United States Dept. of Energy
US NRC	United States Nuclear Regulatory Commission

SUMMARY

Molten Salt Reactors (MSRs) are Gen IV nuclear reactor designs that use fissile material dissolved in high-temperature molten salt. MSRs feature safety and economic benefits through their low operating pressure, combined fuel and coolant into one component, and high thermal efficiency. Due to the historically limited demand for modeling MSRs, there has been no established tool explicitly designed for such a task. The SCALE reactor modeling software suite, developed and maintained by Oak Ridge National Laboratory (ORNL), is selected as a tool to examine MSR modeling capabilities. SCALE has been widely used, verified, and benchmarked for modeling of light water reactors (LWRs) and it would prove beneficial to demonstrate and evaluate its use for MSRs.

This thesis focuses on graphite-moderated, FLiBe-fueled MSRs. It aims to determine the impacts and trade-offs for a given SCALE MSR depletion model between the user-defined simulation parameters, accuracy of the depletion simulation results and the computational resources. Accuracy of the depletion simulations was determined through comparison of criticality estimates (k_{eff}) and isotopic compositions of key nuclides across the lifetime of the reactor simulation. The simulation parameters considered include: depletion sub-interval schemes (coarse vs fine depletion step schemes); trace-element tracking (addnux parameters 2 through 4), self-shielding methods (CENTRM vs BONAMI); cross-section libraries (ENDF/B-VII.1 252-multigroup vs continuous-energy); and specific power (10 MW/MTIHM vs 20 MW/MTIHM). All analyses were conducted up to burnups of 62 GWd/MTIHM. Additionally, the parallel performance on two supercomputing clusters

(Idaho National Laboratory's Sawtooth cluster and Georgia Institute of Technology's PACE-Firebird cluster) was analyzed. Major findings include:

- From coarser to finer depletion schemes. Maximum actinide percent differences experienced little effect (~ 0.32%), but percent difference of nuclides of significant radioactivity experienced significantly higher (~5.10%). Computational runtime was affected linearly with each additional depletion step introduced into the scheme. k_{eff} was statistically unaffected (<10 pcm difference).
- From BONAMI to CENTRM self-shielding, runtime experienced relatively small change (6.81% increase), ~226 ppm average difference in $k_{eff,}$ and ~2.51% maximum difference of actinides and nuclides of significant radioactivity.
- From addnux=2 to addnux=4 nuclide tracking, runtime experienced only a 6.33% increase for MG. k_{eff} was significantly affected (167 pcm difference, growing to ~500 pcm at EOL). For CE addnux variation, the criticality and isotopic concentration differences were near indistinguishable from that of MG, but the computational runtime experienced a ~4.7x increase from addnux=2 to addnux=4. The difference between addnux=2 and addnux=3 was significantly smaller than that of addnux=3 to addnux=4, suggesting that addnux=4 contains nuclides with significantly more effect on reactivity for fluoride-fueled, graphite-moderated MSRs (potentially H-3 and He-3 stemming from larger Li-7 concentrations).
- From MG to CE runtime experienced significant increase (~10x longer). Actinide maximum difference was ~7%, while the nuclides of significant radioactivity exhibited ~4% maximum difference.

- Depletion at 20MW/MTIHM over 10 MW/MTIHM yielded differences that were expected due to the inherent changes in the reactor core physics, thus suggesting that analyses presented in this thesis can be scaled to other fluoride-fueled, graphite-moderated MSRs of different specific powers

1 INTRODUCTION

1.1 Background

Molten Salt Reactors (MSRs) are a Gen IV nuclear reactor design that utilizes nuclear fuel dissolved in high-temperature molten salts. MSRs feature safety benefits through their low (near-atmospheric) operating pressure and the combining of fuel and coolant into one component (thus loss of coolant leads to subcriticality). MSRs also feature economic benefits through their high (700+ ºC) operating temperatures which yield higher thermal efficiencies in the power cycle.

The potential benefits of MSRs demand that they be explored and analyzed effectively. The Molten Salt Reactor Experiment (MSRE) of Oak Ridge National Labs (ORNL) in the 1960's yielded the most significant amount of experimental data on high-temperature, thermal-spectrum MSRs. Due to the historically limited demand for modelling MSRs and limited experimental data, there has been no established and validated tool designed for such a task. The novelty of the MSRs flowing liquid fuel (as opposed to typical solid fuel rods), the largely unstudied chemical composition of the fuel, and the uncommon neutron energy spectrum combine to yield uncertainties within MSR simulations that have largely been unverifiable by current experimental data.

The SCALE [1] reactor modeling software suite, developed and maintained by Oak Ridge National Laboratory (ORNL), has been selected as a tool to verify MSR modeling capabilities due to its development and verification under contract with the U.S. Nuclear Regulatory Commission (NRC), U.S. Dept. of Energy (DOE), and National Nuclear

Security Administration (NNSA). SCALE has experienced widely verified and benchmarked use in the modeling of light water reactors (LWRs) and it would prove beneficial for this software suite to be configurable for advanced nuclear reactors, particularly for MSRs within the scope of this thesis.

1.2 Objective and Scope

The objective of this report is to determine the effects of various SCALE depletion modeling parameters within the scope of graphite-moderated, fluoride-salt MSRs. The reasons for the choice of graphite-moderated, fluoride-salt MSRs is to narrow the scope of analysis to the MSR design with arguably the most significant support by the scientific and commercial industry. The particular MSR design selected for analysis is based on publicly available information on the NEXT Research Alliance (NEXTRA) Molten Salt Research Reactor (MSRR). [2] NEXTRA is a four-university consortium, including the Abilene Christian University (ACU) and its Nuclear Energy eXperimental Testing (NEXT) Lab, Georgia Institute of Technology, Texas A&M University, and The University of Texas at Austin. Supported by funding of Natura Resources LLC, NEXTRA aims to design, license and commission MSRR on ACU campus. Several features present in the MSRR have been simplified or modified for this research and thus the model does not accurately reflect the current MSRR design in all details.

Within this objective, studies are performed on the effects of various inputs to the reactor simulation such as: specific power; depletion interval lengths (burnsteps); trace-element tracking, self-shielding methods; choice of cross-section library. Overall, the results yielded by reactor physics modeling options pertinent to MSRs are evaluated based on the

necessary accuracy of keff, radionuclide concentrations, and radiation spectra results for given depletion applications.

The work of this report is intended to lay the groundwork for future depletion modeling of liquid-fueled MSRs in SCALE under configurations optimized for particular necessities in result accuracy and computational resource allowance. This depletion modeling will be serviceable for reactivity, shielding, and fuel cycle analysis of MSR designs and will thus provide support in making design decisions effectively.

1.3 Introduction to SCALE

The SCALE Code System is a modeling and simulation suite for nuclear safety analysis and design that is developed, maintained, tested, and managed by the Reactor and Nuclear Systems Division (RNSD) of Oak Ridge National Laboratory (ORNL). [1]

For this study, SCALE's TRITON module is used to perform 3D Monte Carlo transport calculations (KENO/CSAS) and isotopic depletion (ORIGEN) in order to simulate the criticality and isotopic environment of a graphite-moderated, FLiBe-fueled MSR.

The TRITON module requires a constructed input containing many input blocks. Those important to this study (accounting for most input blocks) include:

- In-house SCALE modeling parameters
    - Cross-section library
    - Self-shielding solution method
    - Trace-element tracking (addnux parameter)
- Model geometry

- Model material compositions
- Depletion parameters
    - Specific power
    - Depletion time-length
- Monte Carlo Parameters (per transport calculation)
    - # of MC generations (gen parameter)
    - # of MC histories/particles per generation (npg parameter)
    - # of skipped generations (nsk parameter)

1.4 Literature Review

Significant work has been done to model fluoride MSRs in several nuclear modeling software suites, with the majority of this work focusing on criticality evaluations of the atypical material characteristics (i.e. flowing liquid fuel) and neutron spectrum (more epithermal than typical nuclear reactors). These characteristics of MSRs present challenges in nuclear transport calculations due to the historical endeavors of the industry in optimizing water cooled reactor modeling (i.e. methods revolving around solid-fueled, water-cooled, heavily-thermalized reactors).

1.4.1 Functional Needs of MSR Modelling

When considering MSR modelling, it is useful to keep in mind the primary barrier-to-entry that will determine whether a modelling software/method/etc. will be used for real-world MSR design: regulatory and licensing requirements.

The licensing of a nuclear reactor design through the US Nuclear Regulatory Commission (NRC) is a complex and arduous process. A 2019 study published by Betzler et al. [3] attempted to utilize the Safety Analysis Report (SAR) process of the NRC licensing process to determine the functional needs of a given MSR modelling system that must be satisfied in order for NRC license approval[a]. In particular interest is SAR/DCD Chapter 4, which includes the nuclear design licensing component. Within this licensing component, the functional needs were weighted based on frequency of necessity during the process of obtaining two key advanced reactor licensing outcomes [3]:

1. Mechanistic source term estimation for prediction of radioactive release and atmospheric transport of the released radioactivity (highest priority), and
2. Analysis of design basis accidents, including undercooling or over-cooling events, reactivity accidents, and other events such as potential disruption of the primary coolant boundary (high priority)

The results of this analysis are provided in Figure 1. Of note is that MSR fuel depletion is the most significant functional needs of MSR modelling in the licensing process.

[a] This determination of functional needs attempted to cover both liquid- and solid-fuelled MSRs.

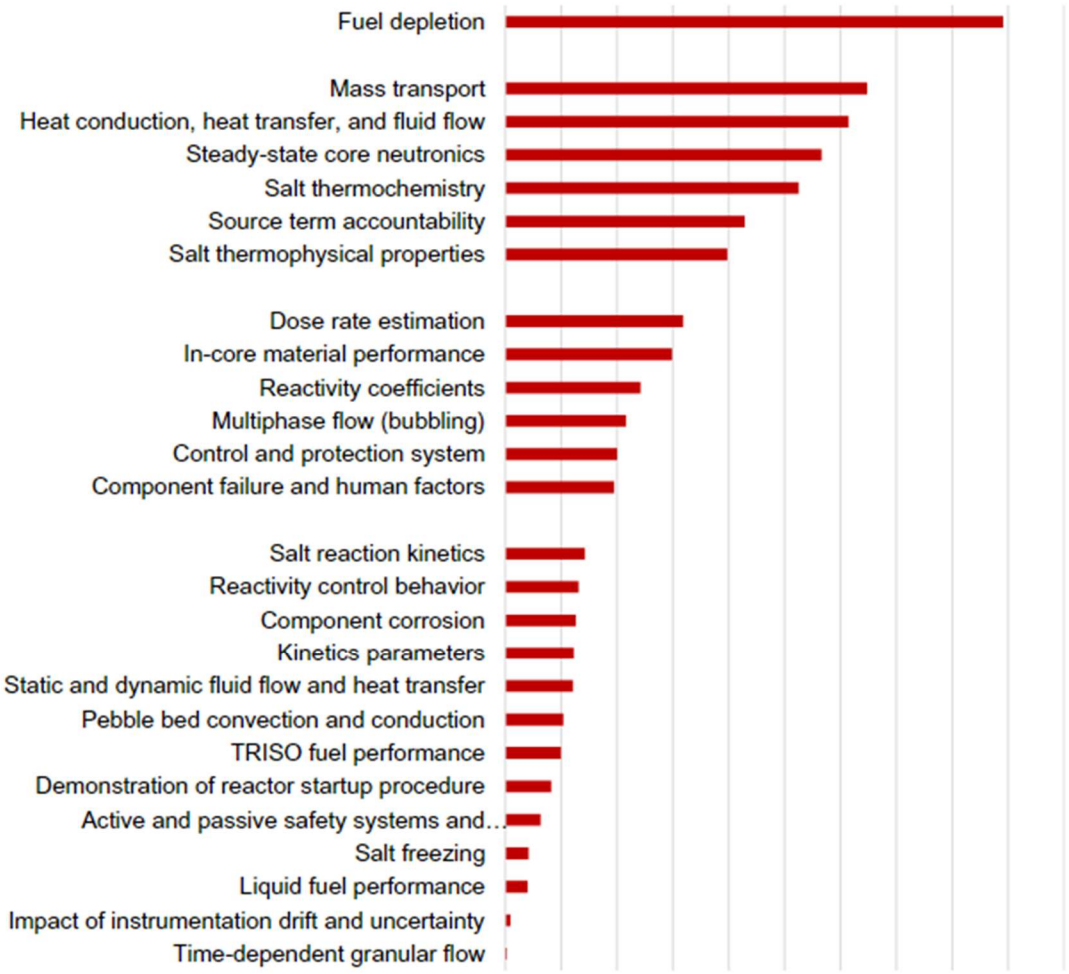

Figure 1. Prioritized functional needs with their relative importance scores for licensing [3]

1.4.2 Novel Interactions of fluoride-MSRs

Standard cross-section libraries (ENDF/B) have had to evolve to account for previously neglected interactions that have now gained importance in MSR modeling.

A 2022 study [4] published by Bostelmann et al. attempted to perform an MSRE benchmark published in the 2019 version of the International Handbook of Evaluated

Reactor Physics Benchmark Experiments (IRPhEP) [5] through SCALE 6.2.4. The study noted that when comparing ENDF/B continuous-energy cross-section libraries:

- ENDF/B-VII.0 overestimates the $^{6}Li(n,t)\alpha$ reaction in the thermal energy range of <0.01 eV by a factor of ~2 when compared to ENDF/B-VII.1
- ENDF/B-VII.0 and ENDF/B-VII.1 experience significant differences in thermal energy capture cross-sections of Carbon
- Prior to ENDF/B-VIII.0, graphite was considered a perfect crystal lattice with 0% porosity. ENDF/B-VIII.0 added the function of defining 0%, 10%, and 30% porosity graphite
- ENDF/B-VIII.0 and ENDF/B-VII.1 exhibit differences in neutron multiplicity and capture cross sections of ^{235}U

The results of the study showed that utilizing SCALE 6.2.4's Monte Carlo neutron transport kernel, KENO-6, and the continuous-energy cross-section library ENDF/B-VIII.0 over ENDF/B-VII.1 yielded a roughly 265 pcm increase in k_{eff}. It was concluded that this effect was largely caused by the updates to ^{235}U.

The study also yielded results suggesting that the changes to ^{6}Li and C cross-sections did not yield statistically dissimilar k_{eff} due to the slightly harder neutron spectrum of the MSRE (i.e. less affected by thermal energy cross-section changes).

Lastly, the study noted that identical MSRE benchmarks through both SCALE and SERPENT yielded ~2000 pcm greater k_{eff} than the benchmark indicates. The suggested resolution to this discrepancy is that while the blueprints, design documents, and design dimensions were well documented, they were done so before actual construction and at

room temperature. Any changes made during construction may not have been documented, and thermal expansion was assumed using a uniform temperature of 911 K by the benchmark authors. Additionally, there are conflicting MSRE fuel composition documents and the eigenvalue bias may be up to 450 pcm based on the selected composition.

1.4.3 MSR Fuel Salt Flow

The novelty of MSRs to operate with liquid fuel that flows through the primary loop poses a concern regarding the migration of delayed neutron precursors. This transfer of materials through fluid flow is known as advection, and the neutronic solutions to the material advection and material diffusion terms within the reaction equation are generally disregarded when considering MSR depletion modelling [6]. This is due to the computationally expensive process of modelling fluid behavior, for material migration. Instead, the typical approach for long-term depletion analysis (i.e. steady state) is to assume the MSR primary loop to be a homogeneously mixed system and to scale the flux (or reactor power) to accommodate the fraction of fuel salt that is being irradiated at any given time [6]. Advection-diffusion problem solutions are a current area of research, being particularly important for modelling transients and source term distribution.

1.4.4 k_{eff} Sensitivity to MSR Model Parameters

A sensitivity study [7] published by Bae et al. attempted to perform correlation studies on a 750 MWth, graphite-moderated, LiF-UF_4 fueled, molten salt demonstration reactor (MSDR) model. This MSR model utilized fuel feed, gas removal, and noble-metal removal. The goal of this study was to identify the parameter uncertainties in the model

and the effects that these uncertainties would have on the selected responses (i.e. k_{eff}, Uranium, Plutonium, Curium, and Tritium concentrations).

It was determined that the parameters (within this study) which most significantly affect BOC and EOC k_{eff} were graphite density, specific power, and temperature. The correlation matrix that arose from this study is provided in Figure 2; wherein the positive or negative effects of various parameters (y-axis) on various responses (x-axis) can be seen.

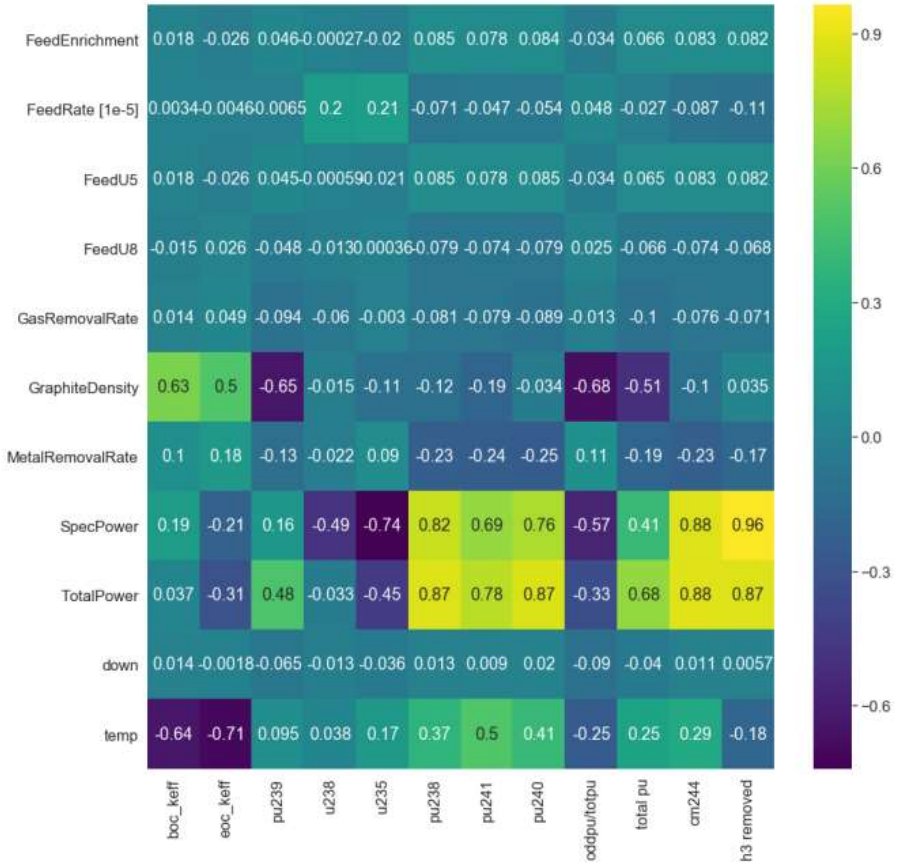

Figure 2. Correlation heatmap for MSDR model results to model uncertainties (value of ±1 equates to absolute correlation) [7]

However, the study only looked at responses in keff, and Uranium, Plutonium, Curium, and Tritium isotope concentrations and only perturbed fuel salt characteristics, feed/removal rates, power, and temperature. Additionally, the study perturbed multiple parameters at once (reconciled through perturbation theory applications performed by the researchers) resulting in less accurate correlation values between perturbations and responses. Thus, this study should be expanded to cover additional responses (i.e. radiation spectra and a more comprehensive isotopic list) and perturbations (i.e. histories, depletion timesteps, self-shielding methods, and multigroup cross section library variations) while also performing individual perturbations to converge on more accurate correlations. Lastly, these sensitivity studies do not utilize a response within the topic of "computational expense".

There have been a number of publications [b]studying the sensitivity of thermal MSR model perturbations in SCALE, but studies on the sensitivities of the following parameter perturbations have received limited attention:

- Monte Carlo neutron transport history parameters
- Length of depletion timesteps
- Self-shielding methods
- Multigroup cross section library

[b] [7] [6] [28] [27] [29] [4]

Additionally, most current studies primarily focus on a single response, keff, while neglecting other potential responses of interest such as isotopics and radiation spectra.

2 METHODOLOGY

2.1 Approach

Typical MSR steady-state depletion analysis generally utilizes primary loop-averaged power to forgo the significant computational resources that would be needed to model fuel advection and diffusion outside of the core (e.g., for analysis of transients and accidents). Current depletion analysis also generally utilizes continuous energy neutron cross-section libraries (i.e. the most accurate, but most resource intensive method). The goal of this thesis is to identify costs, benefits, and proposed applications of SCALE depletion modelling parameters. With this in mind, the following research plan has been implemented as a path towards this goal:

1. Develop a model of a representative MSR design (graphite-moderated & FLiBe-fueled). The MSR design of interest is chosen to be the Molten Salt Research Reactor, MSRR, introduced in Ch. 1. [2]
2. Quantify the effects of different MSR specific power.
3. Quantify the sensitivity of the MSR depletion analysis to native SCALE simulation parameters between the continuous-energy (CE) library model and multigroup (MG) library models.
    a. Cross-section libraries (CE vs MG)
    b. Depletion interval length
    c. Self-shielding methods
    d. Trace-element tracking (i.e. addnux)

The defined research plan can be separated into groups of perturbation parameters and responses as shown in Table 1.

Table 1. Research Plan Perturbations and Responses

Depletion Parameters	Responses
MSR specific power	
Cross-section library	k_{eff}
Depletion interval length	Isotopic concentrations
Self-shielding method	Computational resources
Impurities and trace-element tracking	

2.2 MSR Model

2.2.1 Model Geometry

The MSR model used for depletion analysis in SCALE is based on the Molten Salt Research Reactor (MSRR), a 1-MWth research reactor under development by the Nuclear Energy Experimental Testing Research Alliance (NEXTRA) consortium with funding by Natura LLC. The MSRR model used in this thesis is based on the publicly available information (PSAR submitted to U.S. NRC [2]) and does not necessarily represent the actual or most recent design configuration.

Figure 3, Figure 4, and Figure 5 show the reactor core geometry and additional thermal and radiation shielding layers. The reactor is primarily composed of a cylindrical graphite-moderated core and FLiBe-UF_4 flowing fuel salt. Within the model, the reactor core is contained by an SS316 reactor vessel. Above the reactor vessel is a pipe leading to primary loop components (primary loop heat exchanger, piping, and pump). Below the reactor vessel is a pipe leading to the drain tank, which sits, alongside the reactor vessel, surrounded by a hot air gap followed by a Kaowool-based thermal insulation layer. Beyond the insulation layer is an ambient-temperature air gap followed by a polyethylene-based shielding layer, another ambient-temperature air gap, a SS316 enclosure, a final air gap, and lastly an M1-concrete sacrificial shield. An XZ-cut of the model is shown in Figure 6. The graphite core is composed of a hexagonal lattice of graphite stringers with fuel flow channels. This core is structurally supported by a SS316 lower gridplate. The control rod (CR) channels are of a larger radius to account for both fluid flow and a control rod thimble in the channel. Figure 6 and Figure 7 show an independently developed SCALE model of the MSRR design. General dimensions of the design are provided in Table 2.

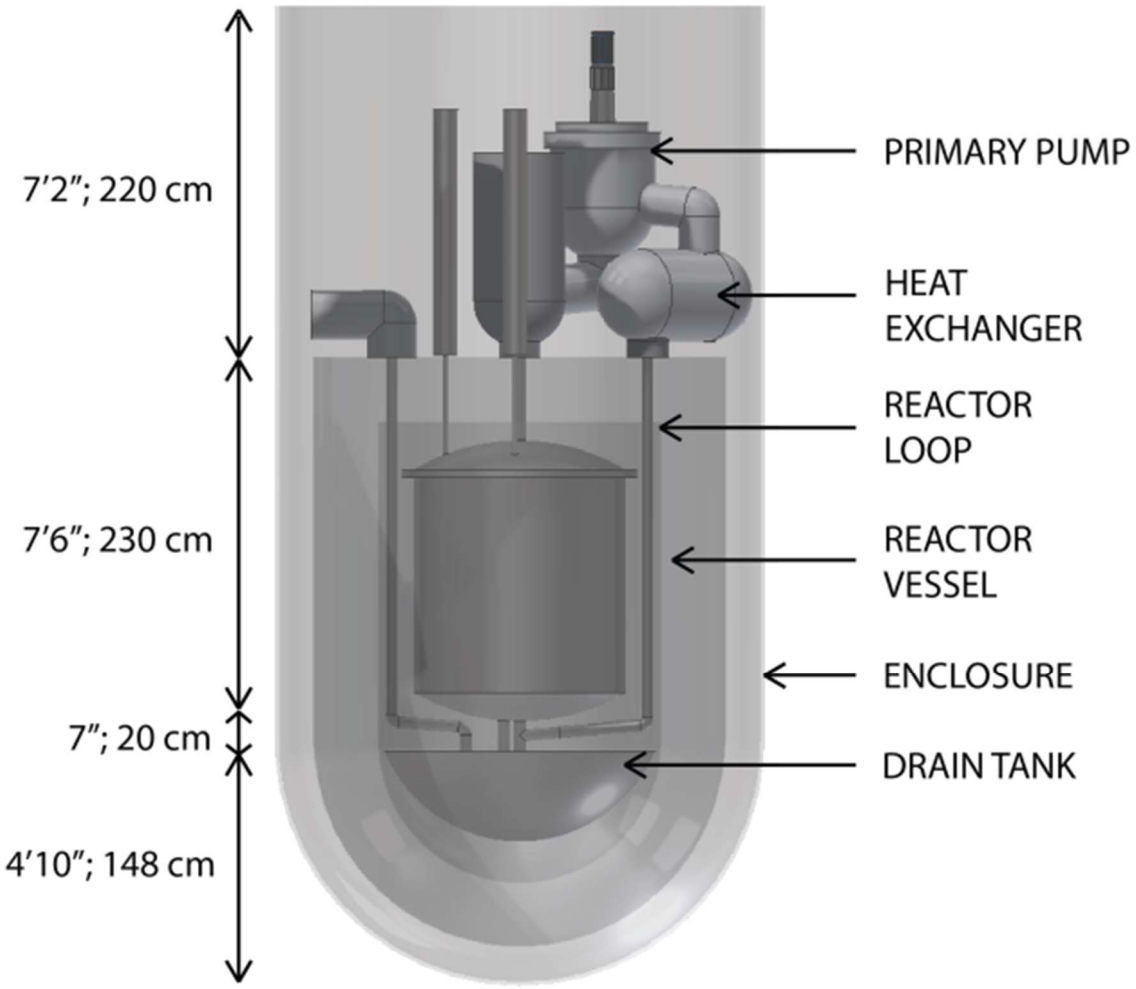

Figure 3. Reactor system major internals and approximate dimensions [2]

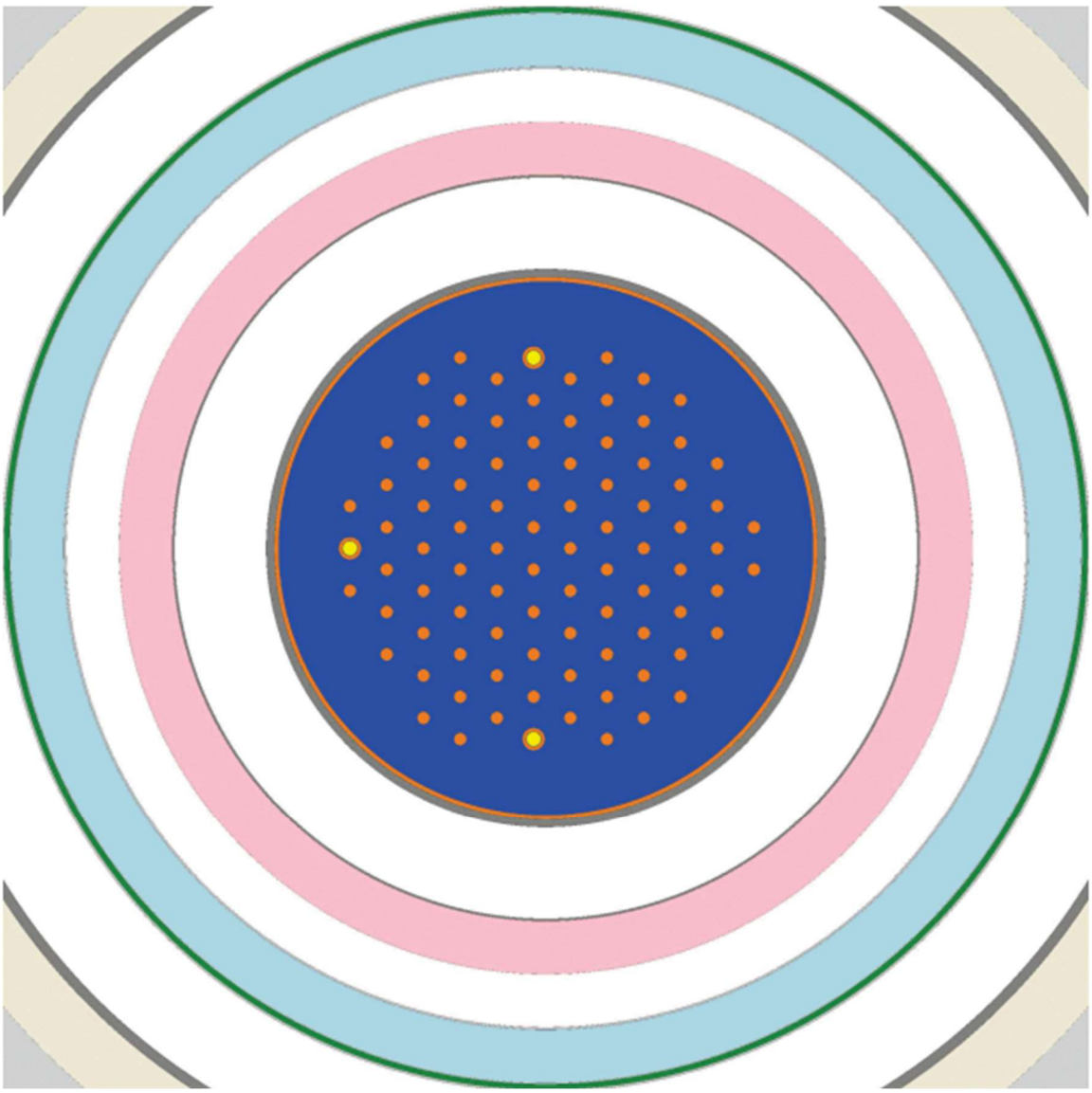

Figure 4. XY-cut of the MSRR [2]

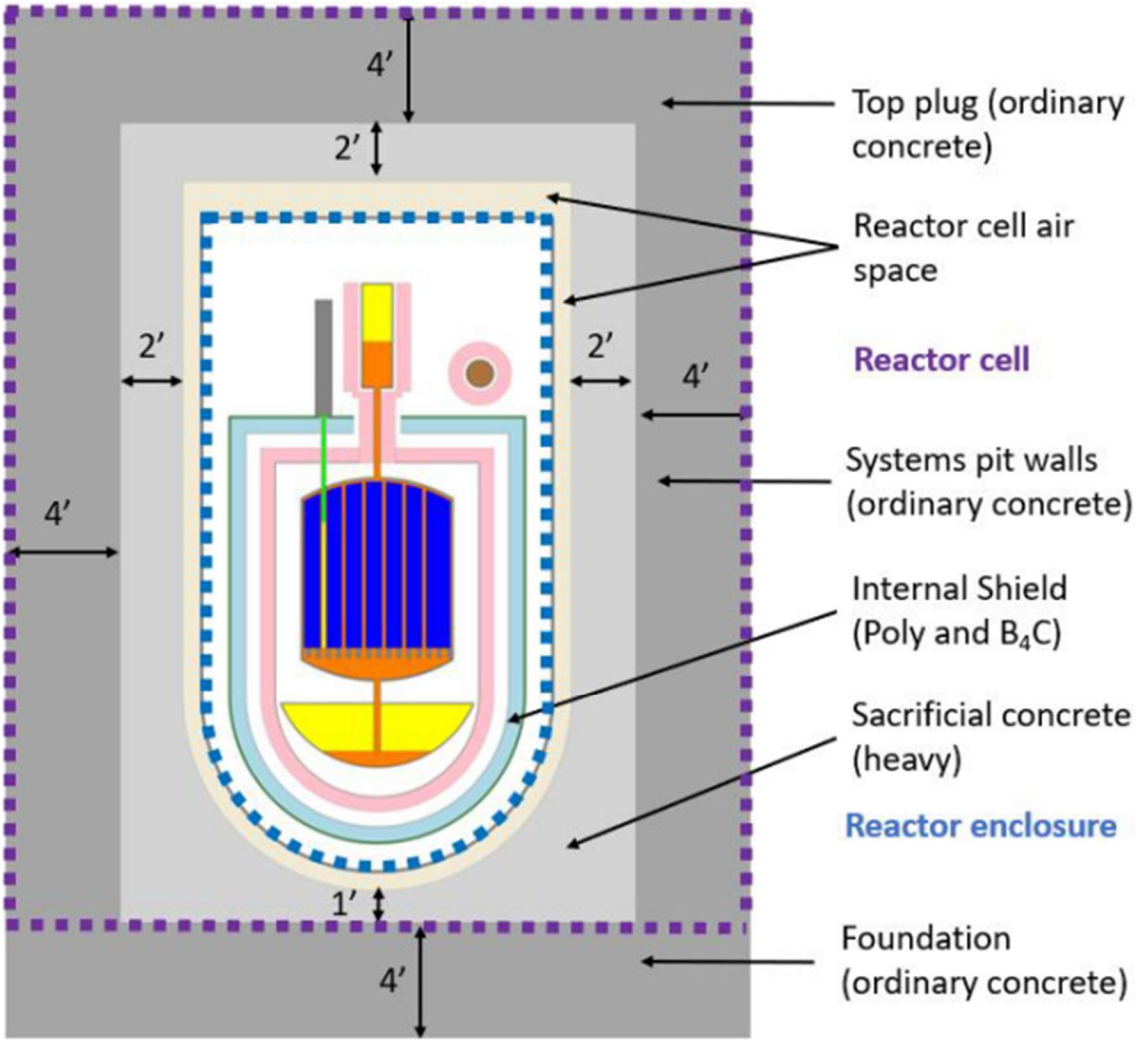

Figure 5. Configuration and thickness of biological shield layers [2]

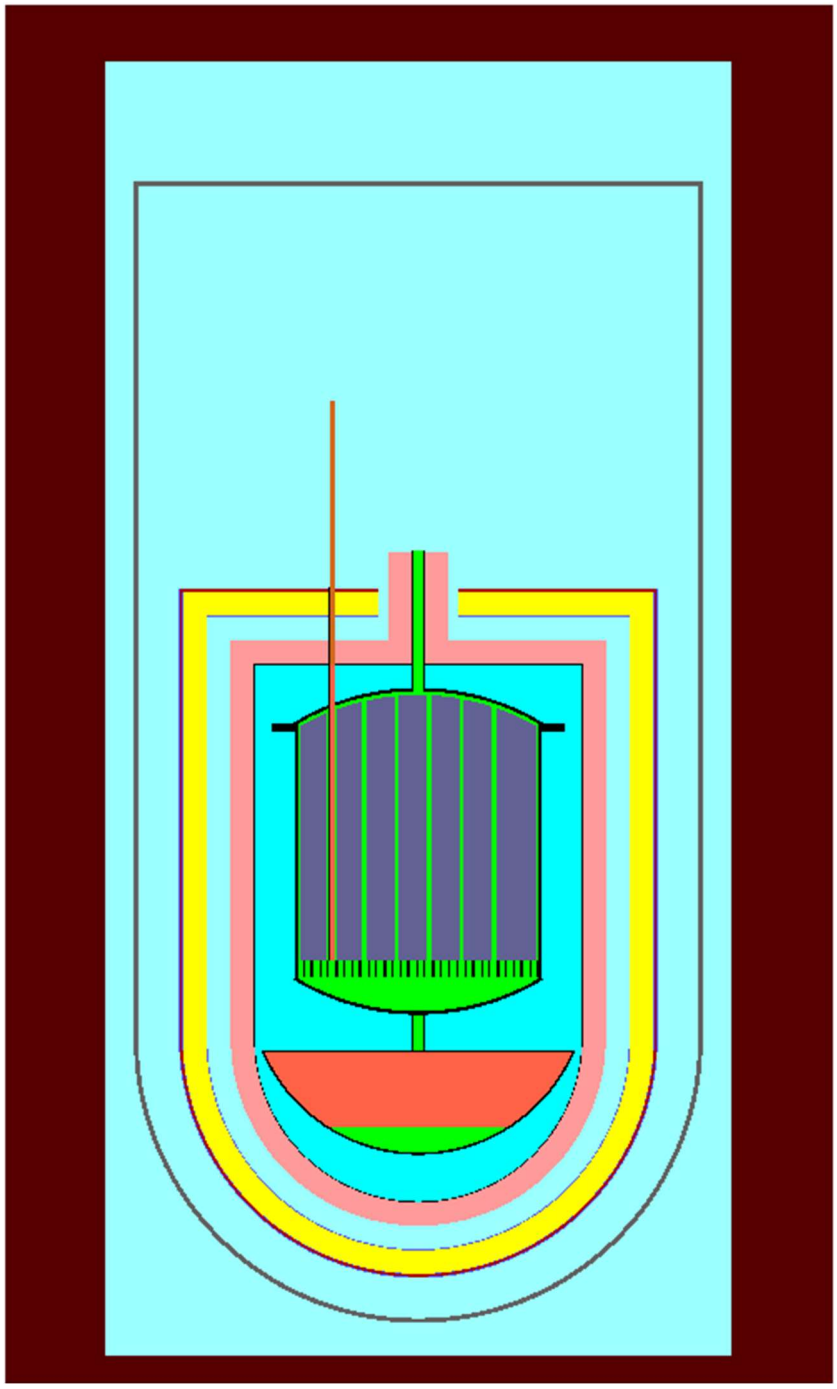

Figure 6. MSR SCALE model XZ-cut (slate gray: graphite core | lime green: FLiBe fuel salt | black: SS316 reactor vessel and core gridplate | peach: Helium fill gas | sky blue: air | pink: thermal insulation | yellow: polyethylene shield | red: B_4C shield | dark gray: SS316 enclosure | brown: M1-concrete)

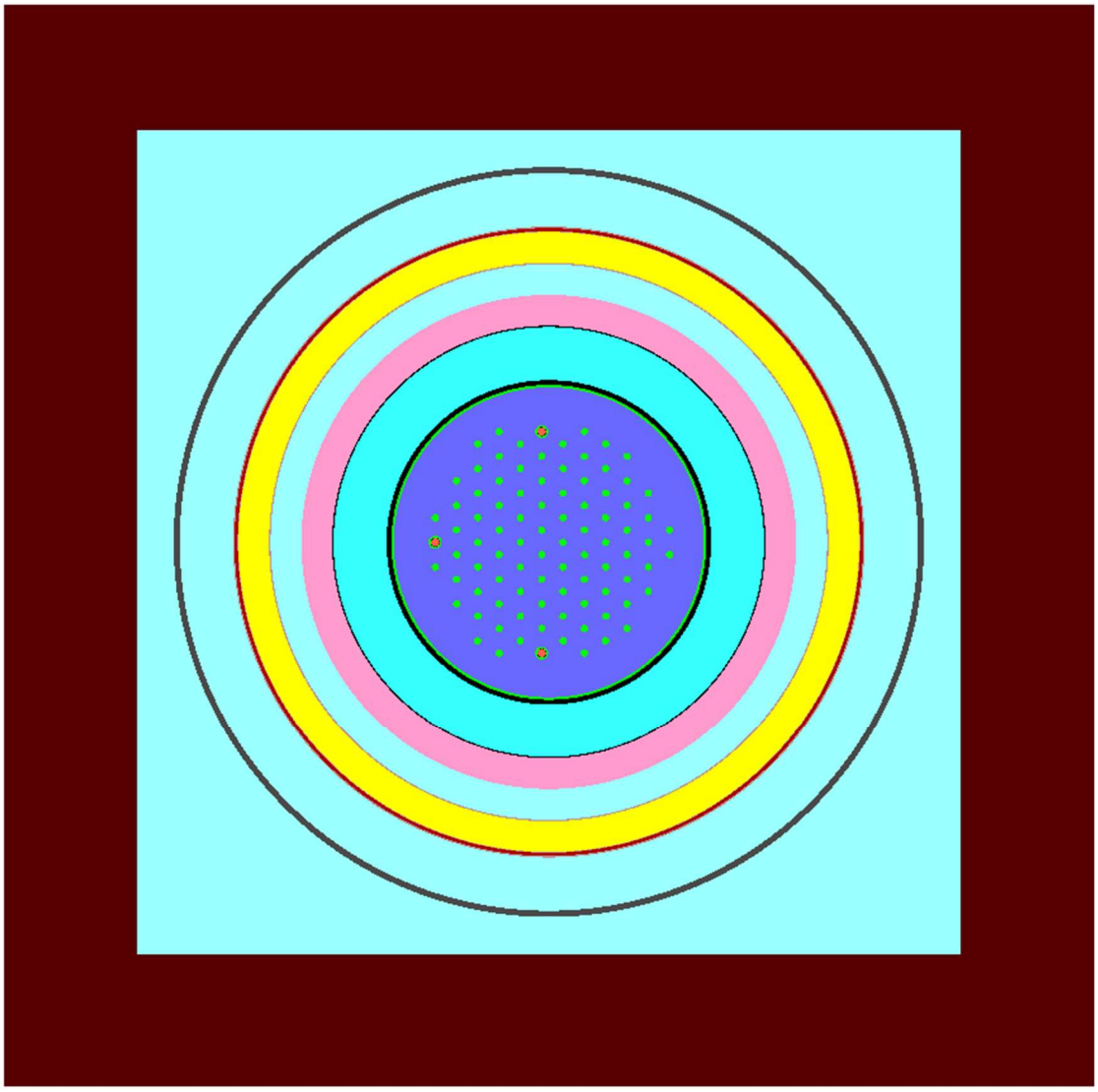

Figure 7. MSR SCALE model XY-cut (colors correspond as in Figure 7)

Table 2. MSR Model Geometry [2][c]

Parameter	Value
Graphite Core Height [cm]	145.42
Graphite Core Radius [cm]	64
Reactor Vessel Outer Radius [cm]	67
Insulation Inner Radius [cm]	88.9
Insulation Thickness [cm]	13.3
Shielding Inner Radius [cm]	114.9
Shielding Thickness [cm]	15.5
Enclosure Inner Radius [cm]	152.4
Enclosure Thickness [cm]	2.54
M1-shield Inner Radius [cm]	170.18
M1-shield Thickness (sides) [cm]	54.82
M1-shield Thickness (top) [cm]	30.48
Total M1-shield Outer Diameter [cm]	450
Total M1-shield Height [cm]	751.84

2.2.2 Material Compositions

All materials of the model were identified by explicit indication in the MSRR PSAR and with compositions defined either in said PSAR or the 2021 edition of Pacific Northwest National Laboratory's Compendium of Material Composition Data for Radiation Transport Modeling [8]. These materials and the components they make up are identified in Table 3.

[c] All dimensions collected from the publicly available MSRR PSAR

Table 3. Predefined Materials and their Components

Material	Component
Graphite (nuclear-grade; moderator)	Core
SS316H	Reactor vessel, drain tank, lower grid plate, piping, CR thimble, insulation structural liner, enclosure
Air (dry; sea-level)	Air gaps between reactor vessel, thermal insulation, shielding, enclosure, and sacrificial shielding
Insulation (Kaowool)	Thermal insulation
Al6061-O	Shielding structural liner
High-density polyethylene (HDPE)	Shielding
Boron Carbide (B_4C)	Shielding
M1-concrete	Sacrificial shield

The fuel salt is composed of 67LiF-28BeF_2-5UF_4, the numbers indicating molar percent. All three molecules are defined in the Comp. of Materials, while the Li-7 and U-235 enrichments are adjusted to 99.99 wt% and 19.75 wt% respectively.

2.2.3 Source Convergence

In order to achieve a converged fission source distribution for performing accurate transport calculations, a certain number of neutron generations must be skipped. As more particles/generations are performed, the source distribution spatially converges from the initial guess to the fundamental mode. (In this study the initial distribution is uniform over the entire MSR reactor vessel including the unfuelled graphite and stainless steel vessel). The number of skipped cycles/generations is particular to individual models, and the convergence is measured through both k_{eff} and Shannon Entropy convergence. In order to determine an appropriate number of skipped histories/generations for the primary work in this thesis, source convergence simulations were conducted.

2.3 SCALE Depletion Modeling

The depletion analysis utilizes the TRITON module of SCALE 6.2.4 (specifically the t6-depl sequence) to perform 3D eigenvalue Monte Carlo analysis for criticality (KENO-VI module) and to perform isotopic depletion and decay calculations (ORIGEN module) in tandem. This modeling utilizes a predictor-corrector depletion process, wherein the cross-section processing and transport calculations are performed for the anticipated isotope concentrations at the *midpoint* of the depletion subinterval (also defined by user input), then the depletion calculations are performed over the full subinterval using those midpoint-predicted cross-sections and flux distributions. This process is iterated until all depletion subintervals have been processed. A visual representation of this process can be seen in Figure 8. [1]

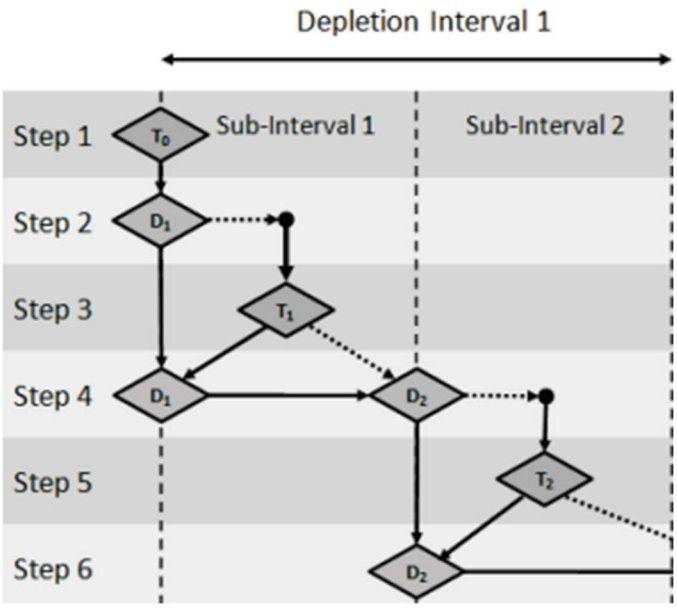

Figure 8. Predictor/corrector depletion algorithm used by TRITON (Step 1: initial transport calculation | Step 2: depletion calculation to midpoint of the first depletion subinterval | Step 3: transport calculation using previous midpoint-depletion calculation | Step 4: depletion calculation to end of first depletion subinterval using cross-sections and flux distributions of previous midpoint-transport calculation | Step 5-6: reiteration of steps until all subintervals have been processed) [1].

The t6-depl sequence of SCALE requires an input file specifying several parameters: a selection of the sequence a neutron cross-section library; a selection of the number of trace isotopes to track (defined by the SCALE addnux function); defined materials with isotopic concentrations; problem geometry utilizing the defined materials; depletion interval(s) at a defined specific power; number of Monte Carlo active and skipped generations; number of Monte Carlo histories per generation; and many optional additional specifications (parameters) for the model and simulation.

2.3.1 Reactor Physics Models

When considering the model simulation, a few parameters can be considered "reactor physics parameters". These parameters are the SCALE self-shielding method selection, the cross-section library selection, the detailed isotopics (i.e. through the SCALE addnux parameter); and the specific power. These parameters are dependent on user input of the model and define reactor physics methods by which SCALE simulates the environment.

2.3.2 Numerical Parameters

When considering the model simulation, a few parameters can be considered "numerical parameters", wherein they are attributed to the numerical aspect of the simulation. These parameters differ from "reactor physics parameters" in that they do not change any of the methods by which the environment is simulated, only that they change the extensiveness of the Monte Carlo histories simulation, the computational resources used in the simulation, and/or the depletion interval and subinterval lengths. These parameters include: the depletion interval scheme and the parallel performance of different SCALE implementations (i.e. supercomputing cluster used).

For the analysis of parallelization, identical simulations are conducted on two different computing clusters; namely, Georgia Institute of Technology's FIREBIRD cluster and Idaho National Laboratory's SAWTOOTH cluster.

2.4 Metrics of Quantifying Differences

The parameters identified in SCALE Depletion Modeling define the perturbations used in the SCALE MSRR depletion analysis. The effects that these perturbations have on the

depletion results are numerous but can be narrowed to only a few considerable metrics. For reactor design, k_{eff} of the system, radiation spectra, and isotopic composition of the fuel are of the utmost importance. These metrics of interest have ramifications on the geometry, materials, neutron poison off-gassing, radiation shielding, and fuel cycle of the reactor design.

For all references of "difference from X to Y" (ex. difference in U-235 concentration from MG to CE) will utilize Equations 1 and 2.

$$\Delta(X \rightarrow Y) = Y - X \quad \textbf{1}$$

Where:

$\Delta(X \rightarrow Y)$ = difference from X to Y

$$\%\Delta(X \rightarrow Y) = \frac{Y - X}{X} \quad \textbf{2}$$

Where:

$\%\Delta(X \rightarrow Y)$ = percent difference from X to Y

2.4.1 k-eff

The effective multiplication factor, k_{eff}, is a measure of the change in the fission neutron population from one neutron generation to the following generation. The reactivity of the system is defined by the deviation of k_{eff} from unity and expresses the exponential trend of the neutron population over time.

Understanding the reactivity and effective multiplication factor are essential to begin and maintain a safe, critical configuration of the system. Identifying the effects on k_{eff} from the previously mentioned perturbations is important to determine the necessary reactivity insertions (i.e. fuel addition/subtraction, control rod position, reactor geometry/volume, off-gassing concentration/rate, etc.) and thus affect nearly every design area of the reactor core.

2.4.2 Isotopic Concentrations

The isotopic concentrations of the fuel salt (and secondarily in the structural materials through depletion and transmutation) is intuitively understood as the amount of each isotope in each material. This changes over time as materials are exposed to the system's neutron field and as radioactive elements decay. These isotopic concentrations ultimately lead to the reactivity and radiation spectra of the system, but their purpose in this analysis is with material characteristics (i.e. chemical properties, structural properties, nuclear weapons proliferation value, waste management, etc.) in mind. Identifying the effects of the previously identified perturbations on isotopic concentrations is important to manage and plan around the material properties throughout the fuel cycle. Table 4 through Table 9 identify groupings of nuclides of interest to satisfy robust analyses of isotopic concentrations changes with adequate coverage of nuclides of varying types of interest. Nuclides in Table 4 indicate the nuclides that were explicitly requested to be output by SCALE 6.2.4, but they account for many more nuclides than used for analysis within this thesis. For instance, H-3 is not used for any analysis within this thesis. These nuclides were selected based on their mention in all literature references made within this thesis,

regardless of their importance to the analyses made in this thesis. The table is provided to encourage similar robustness of future analyses of nuclide concentrations through SCALE.

Table 4. Nuclides of Interest

Element	Z	N	SCALE Symbol
H	1	3	h-3
Li	3	6	li-6
Li	3	7	li-7
Be	4	9	be-9
B	5	10	b-10
C	6	12	c-12
C	6	13	c-13
O	8	16	o-16
F	9	19	f-19
Si	14	28	si-28
Cr	24	51	cr-51
Cr	24	53	cr-53
Fe	26	56	fe-56
Ni	28	60	ni-60
Ni	28	62	ni-62
Cu	29	64	cu-64
Ga	31	67	ga-67
Ga	31	68	ga-68
Se	34	79	se-79
Kr	36	85	kr-85
Kr	36	81m	kr-81m
Sr	38	89	sr-89
Sr	38	90	sr-90
Y	39	90	y-90
Y	39	91	y-91
Zr	40	89	zr-89
Zr	40	90	zr-90
Zr	40	91	zr-91
Zr	40	93	zr-93

Table 4 continued

Zr	40	94	zr-94
Zr	40	95	zr-95
Zr	40	97	zr-97
Nb	41	95	nb-95
Mo	42	95	mo-95
Mo	42	97	mo-97
Mo	42	99	mo-99
Tc	43	99m	tc-99m
Ru	44	103	ru-103
Ru	44	106	ru-106
Pd	46	107	pd-107
Ag	47	110m	ag-110m
Cd	48	113	cd-113
In	49	111	in-111
Sn	50	126	sn-126
Sn	50	121m	sn-121m
Te	52	132	te-132
I	53	125	i-125
I	53	129	i-129
I	53	131	i-131
I	53	133	i-133
Xe	54	133	xe-133
Xe	54	135	xe-135
Xe	54	131	xe-131
Cs	55	134	cs-134
Cs	55	135	cs-135
Cs	55	136	cs-136
Cs	55	137	cs-137
Ba	56	140	ba-140
La	57	140	la-140
Ce	58	143	ce-143
Sm	62	149	sm-149
Sm	62	151	sm-151
Sm	62	153	sm-153

Table 4 continued

Gd	64	155	gd-155
Gd	64	157	gd-157
Re	75	188	re-188
Ra	88	223	ra-223
Ra	88	226	ra-226
Ra	88	228	ra-228
Ac	89	225	ac-225
Ac	89	227	ac-227
Th	90	229	th-229
Th	90	230	th-230
Th	90	232	th-232
U	92	232	u-232
U	92	233	u-233
U	92	234	u-234
U	92	235	u-235
U	92	236	u-236
U	92	238	u-238
Np	93	236	np-236
Np	93	237	np-237
Pu	94	238	pu-238
Pu	94	239	pu-239
Pu	94	240	pu-240
Pu	94	241	pu-241
Pu	94	242	pu-242
Pu	94	243	pu-243
Pu	94	244	pu-244
Am	95	241	am-241
Am	95	243	am-243
Am	95	242	am-242
Cm	96	242	cm-242
Cm	96	243	cm-243
Cm	96	244	cm-244
Cm	96	244	cm-244
Cm	96	245	cm-245

Table 4 continued

Cm	96	246	cm-246
Cm	96	247	cm-247
Cm	96	248	cm-248
Cf	98	252	cf-252

Table 5. Actinides

Element	Z	N	SCALE Symbol
Ac	89	225	ac-225
Ac	89	227	ac-227
Th	90	229	th-229
Th	90	230	th-230
Th	90	232	th-232
U	92	232	u-232
U	92	233	u-233
U	92	234	u-234
U	92	235	u-235
U	92	236	u-236
U	92	238	u-238
Np	93	236	np-236
Np	93	237	np-237
Pu	94	238	pu-238
Pu	94	239	pu-239
Pu	94	240	pu-240
Pu	94	241	pu-241
Pu	94	242	pu-242
Pu	94	243	pu-243
Pu	94	244	pu-244
Am	95	241	am-241
Am	95	243	am-243
Am	95	242m	am-242m
Cm	96	242	cm-242
Cm	96	243	cm-243

Table 5 continued

Cm	96	244	cm-244
Cm	96	244	cm-244
Cm	96	245	cm-245
Cm	96	246	cm-246
Cm	96	247	cm-247
Cm	96	248	cm-248
Cf	98	252	cf-252

Table 6. Nuclides of Significant Radioactivity

Element	Z	N	SCALE Symbol
Se	34	79	se-79
Kr	36	85	kr-85
Sr	38	90	sr-90
Tc	43	99	tc-99
Te	52	132	te-132
Xe	54	133	xe-133
Xe	54	135	xe-135
Cs	55	137	cs-137
Sm	62	151	sm-151
Cm	96	242	cm-242
Cm	96	243	cm-243
Cm	96	244	cm-244
Cm	96	244	cm-244
Cm	96	245	cm-245
Cm	96	246	cm-246
Cm	96	247	cm-247
Cm	96	248	cm-248
Cf	98	252	cf-252

Table 7. LiF-BeF_2-UF_4 Nuclides

Element	Z	N	SCALE Symbol
Li	3	6	li-6
Li	3	7	li-7
Be	4	9	be-9
F	9	19	f-19
U	92	234	u-234
U	92	235	u-235
U	92	238	u-238

Table 8. Primary Uranium

Element	Z	N	SCALE Symbol
U	92	235	u-235
U	92	238	u-238

Table 9. Top 30 Nuclides by EOL Mass

Element	Z	N	SCALE Symbol
Li	3	7	li-7
Be	4	9	be-9
Kr	36	85	kr-85
Sr	38	90	sr-90
Zr	40	90	zr-90
Zr	40	91	zr-91
Zr	40	93	zr-93
Zr	40	94	zr-94
Zr	40	95	zr-95
Zr	40	97	zr-97
Tc	43	99	tc-99
Pd	46	107	pd-107
I	53	129	i-129
Xe	54	133	xe-133

Table 9 continued

Cs	55	134	cs-134
Cs	55	136	cs-136
Sm	62	149	sm-149
U	92	233	u-233
U	92	234	u-234
U	92	236	u-236
Np	93	236	np-236
Np	93	237	np-237
U	92	238	u-238
Pu	94	238	pu-238
Pu	94	239	pu-239
Pu	94	240	pu-240
Pu	94	241	pu-241
Pu	94	242	pu-242
Sn	50	121m	sn-121m

3 RESULTS AND DISCUSSION

The different SCALE simulations and their demonstrated differences are presented within this chapter. The simulations ran are listed in Table 10, along with the specified parameters. Simulations are selectively chosen for comparison across specific parameter differences (specified in 2.3 SCALE Depletion Modeling).

Table 10. Simulations and Respective Parameters

Model	Run	Addnux	Est. MTIHM	Depletion Scheme	Self-shielding	Library	Cluster	gen	npg	nsk	MPI Processes	Average Parallel Efficiency [%]	Wallclock time [hours]	Average k_eff Uncertainty [pcm]
0001	v01	4	0.292513	NA	C	MG	INL-ST	310	400000	10	96	64.070	0.367	8.8
0001	v02	4	0.292513	NA	C	MG	INL-ST	400	400000	100	96	64.890	0.462	9.0
0002	v02	4	0.292513	20-2	C	MG	INL-ST	350	400000	50	240	26.495	13.589	9.8
0002	v03	4	0.292513	20-3	C	MG	INL-ST	350	400000	50	240	26.084	20.719	9.8
0002	v04	4	0.292513	20-4	C	MG	INL-ST	350	400000	50	240	26.137	27.338	10.0
0002	v05	4	0.292513	20-8	C	MG	INL-ST	350	400000	50	240	26.427	54.051	10.2
0003	v02	4	0.292513	10-2	C	MG	INL-ST	350	400000	50	240	26.350	13.680	9.6
0003	v03	4	0.292513	10-3	C	MG	INL-ST	350	400000	50	240	26.104	20.945	9.7
0003	v04	4	0.292513	10-4	C	MG	INL-ST	350	400000	50	240	26.143	27.444	9.4
0003	v05	4	0.292513	10-8	C	MG	INL-ST	350	400000	50	240	26.143	53.989	9.7
0004	v02	3	0.292513	10-4	C	MG	INL-ST	350	400000	50	240	26.852	25.761	9.5
0004	v03	2	0.292513	10-4	C	MG	INL-ST	350	400000	50	240	27.123	24.876	10.2
0005	v01	4	0.292513	10-4	B	MG	INL-ST	350	400000	50	240	26.417	25.428	9.6
0006	v01	4	0.292513	10-2	C	CE	INL-ST	250	300000	50	1440	36.722	18.630	13.0
0006	v02	4	0.292513	10-4	C	CE	INL-ST	350	400000	50	1440	48.196	53.324	10.2
0007	v01	3	0.292513	10-2	C	CE	INL-ST	250	300000	50	720	45.175	15.893	13.5
0007	v02	3	0.292513	10-2	C	CE	INL-ST	250	300000	50	720	33.441	8.748	14.1
0009	v01	4	0.292513	365	C	MG	INL-ST	340	200000	40	48	75.850	1.447	13.5
0009	v02	4	0.292513	365	C	MG	GT-FB	340	200000	40	48	51.455	1.404	15.5
0009	v03	4	0.292513	365	C	MG	INL-ST	340	200000	40	24	86.455	2.533	13.5
0009	v04	4	0.292513	365	C	MG	GT-FB	340	200000	40	24	82.780	1.747	13.5
0009	v05	4	0.292513	365	C	MG	INL-ST	340	200000	40	12	93.285	4.829	14.0
0009	v06	4	0.292513	365	C	MG	GT-FB	340	200000	40	12	91.015	3.028	14.0

3.1 Source Convergence

For this model, a simulation was performed using SCALE's 3D Monte Carlo transport solver, KENO/CSAS 6, and convergence of k_{eff} and Shannon Entropy were plotted to indicate convergence of the fission source.

The parameters for this simulation are provided in Table 11, the Shannon entropy convergence in Figure 9, and the k_{eff} convergence in Figure 10.[d] As shown in Figure 9 and Figure 10, the source has arguably converged through both measures by anywhere between 10 and 30 generations, so a conservative estimate for # of generations until true convergence for this model was selected to be 50 generations and this number was used in subsequent simulations. Additionally, the 10 generations skipped in simulation 0001-v01 were enough to approach satisfactory Shannon Entropy convergence with respect to the built-in convergence tests in SCALE 6.2.4 [1]. The Shannon Entropy convergence was diagnosed across a 5x5x5 region mesh over the reactor vessel (width/depth/height [cm] ≈ 26.8/26.8/65.9). The results of these tests can be found in A.1 (0001-v01 Convergence Test Results).

Table 11. Source Convergence Simulation Parameters

Model	Run	Model Descriptor	Module	Addnux	Est. MTIHM	Self-shielding	Library	gen	npg	nsk	Total Number of
0001	v01	CR-in;v01	csas6	4	0.29251	CENTRM	252-MG 7.1	310	400000	10	1.2E+08

[d] Replica simulations were run with a different random number seed in order to verify accuracy of convergence. The results were indistinguishable and thus were not included.

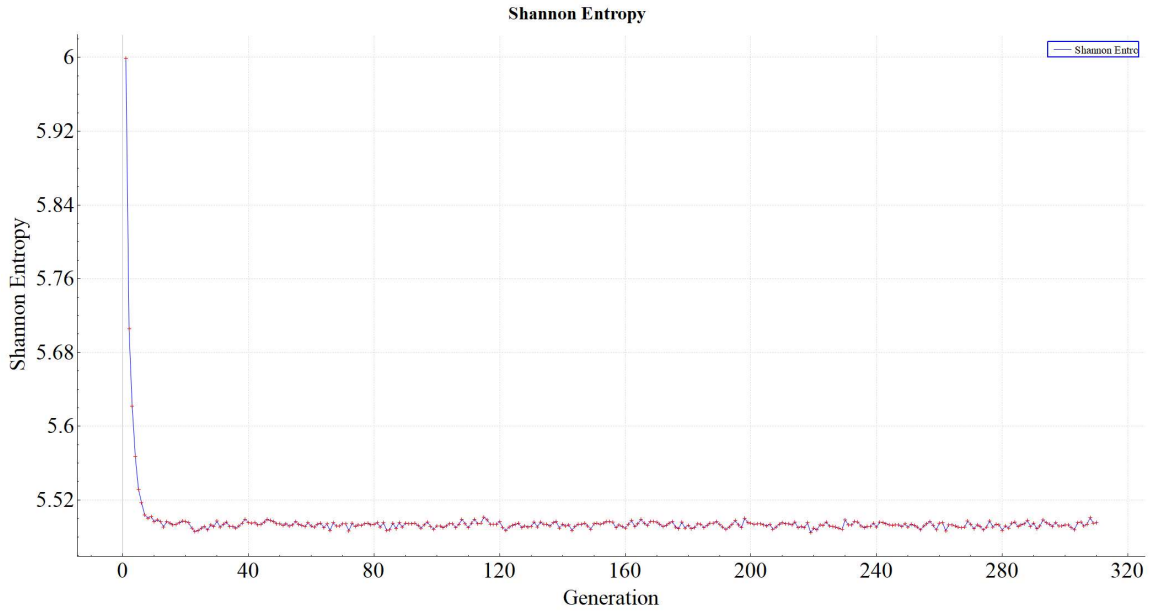

Figure 9. Shannon entropy convergence for 0001-v01 CSAS simulation.

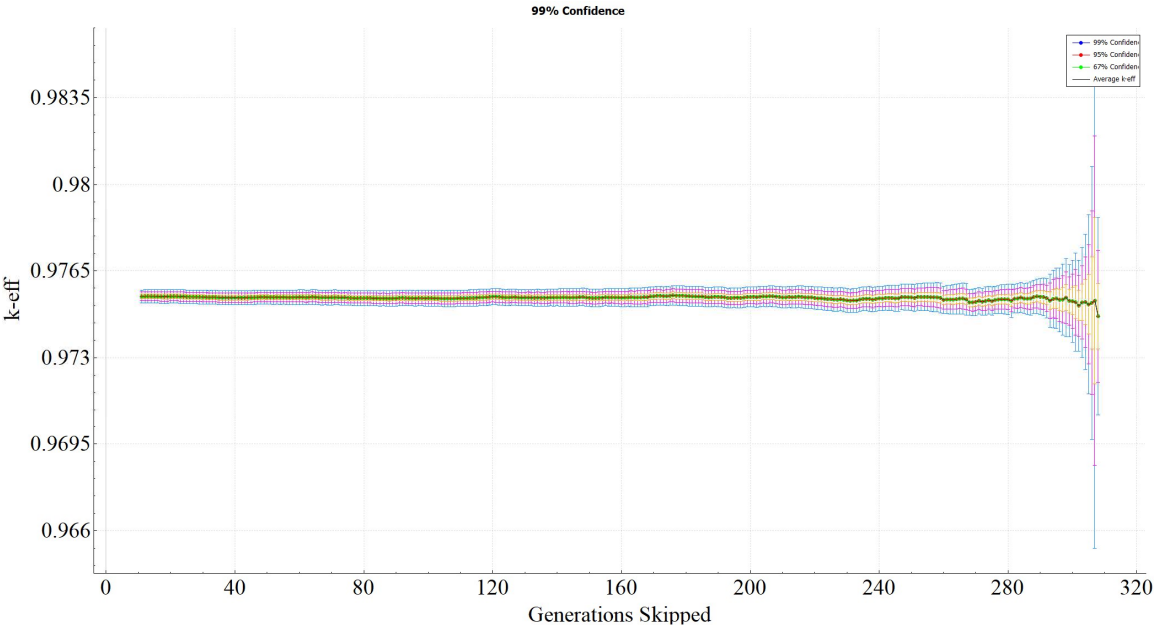

Figure 10. k_{eff} convergence for 0001-v01 CSAS simulation.

3.2 Numerical Parameters

The numerical parameters of analysis prove to be the simplest to implement and thus lead the analysis.

3.2.1 Depletion Sub-intervals

For analysis of meaningful k_{eff} and radionuclide concentration differences, the total depletion interval is set to equal an EOL burnup of 62 GWd/MTIHM regardless of the specific power of the model, and an arbitrary course depletion sub-interval scheme is provided in Table 12 under the name "Scheme 10-1". This course depletion sub-interval scheme will be that which is input into the SCALE-TRITON "**read depletion**" input block, and the **"nlib=**" (also found in the same block) will be used to equally subdivide each of these coarse steps into finer depletion schemes for comparisons.

The transformation/alteration/modification of depletion subintervals is intuitively studied by conducting several SCALE simulations of replica models and parameters *except* for the user-defined depletion subintervals. The depletion sub-intervals of each simulation can be grouped into "burnup schemes"; each of these plans are represented in Table 12 through Table 13, and in A.2 (Add. Depletion Sub-interval Schemes). The methods are titled in the following format: "**Scheme {specific_power}-{nlib_subdivisions}**", where "nlib_subdivisions" represents the subdivisions imposed on the coarse depletion scheme (Table 12) by the "nlib" SCALE-TRITON depletion parameter. For instance, "Scheme 10-1" is the coarse depletion scheme under a specific power of 10-MW/MTU.

As shown, the finest depletion scheme (A.2 | Table 26) allows depletion step-lengths of no more than 75 days (i.e. 0.75 GWd/MTIHM). These step-lengths are expected to be adequate for convergence towards meaningful solutions and appropriate for comparison [9]. The simulations used in this study of depletion sub-intervals have been extracted from Table 10 and are presented in Table 14.

Table 12. Depletion Scheme 10-1.

Sub-interval [d]	Sub-interval [GWd/MTIHM]
0.00	0.00
20.00	0.20
80.00	0.80
200.00	2.00
400.00	4.00
800.00	8.00
1400.00	14.00
2000.00	20.00
2600.00	26.00
3200.00	32.00
3800.00	38.00
4400.00	44.00
5000.00	50.00
5600.00	56.00
6200.00	62.00

Table 13. Depletion Scheme 10-2.

Sub-interval [d]	Sub-interval [GWd/MTIHM]
(initialization) 0.00	0.00
10.00	0.10
20.00	0.20
50.00	0.50
80.00	0.80
140.00	1.40

200.00	2.00
300.00	3.00
400.00	4.00
600.00	6.00
800.00	8.00
1100.00	11.00
1400.00	14.00
1700.00	17.00
2000.00	20.00
2300.00	23.00
2600.00	26.00
2900.00	29.00
3200.00	32.00
3500.00	35.00
3800.00	38.00
4100.00	41.00
4400.00	44.00
4700.00	47.00
5000.00	50.00
5300.00	53.00
5600.00	56.00
5900.00	59.00
6200.00	62.00

Table 14. Self-shielding simulations used.

Model	Run	Addnux	Est. MTIHM	Depletion Scheme	Self-shielding	Library	Cluster	gen	npg	nsk	MPI Processes	Average Parallel Efficiency [%]	Wallclock time [hours]	Average k_eff Uncertainty [pcm]
0003	v02	4	0.292513	10-2	CENTRM	MG	INL-ST	350	400000	50	240	26.350	13.680	9.6
0003	v03	4	0.292513	10-3	CENTRM	MG	INL-ST	350	400000	50	240	26.104	20.945	9.7
0003	v04	4	0.292513	10-4	CENTRM	MG	INL-ST	350	400000	50	240	26.143	27.444	9.4

0003	v05	4	0.292513	10-8	CENTRM	MG	INL-ST	350	400000	50	240	26.143	53.989	9.7

3.2.1.1 Multiplication factor k_{eff}

In Figure 11, all depletion schemes are shown to yield statistically equivalent k_{eff} vs Burnup curves (difference between any two simulations k_{eff} is <10pcm, the uncertainty of k_{eff} results), thus suggesting that k_{eff} estimates are not significantly affected by changes in depletions sub-intervals within reasonable depletion schemes.

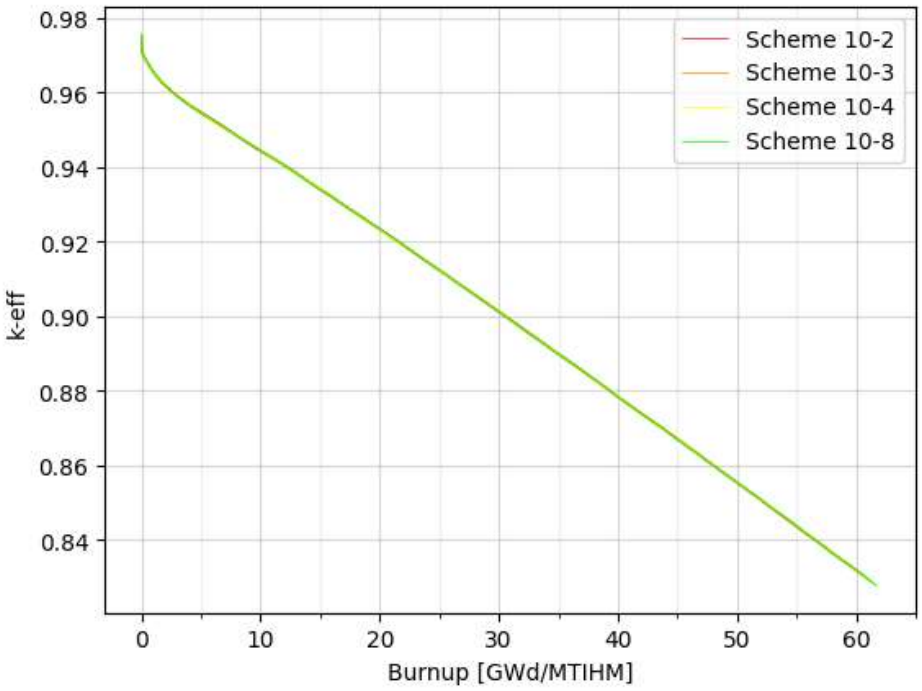

Figure 11. k_{eff} vs. burnup across schemes (individual curves are not visually distinguishable; ±σ error bars are shown but are too small to be visible)

3.2.1.2 Isotopic Concentrations

This section examines evolution (with burnup) of difference in isotopic concentration of previously identified groups of nuclides, as impacted by the depletion schemes. In Figure 12, the average maximum percent difference between actinides of different depletion

schemes are shown to decrease as the depletion schemes converge (e.g. percent differences for 10-2 to 10-8 are larger than 10-2 to 10-3). This was an expected result and is useful to help show that the depletion scheme comparisons are correct. This trend is shown in Figure 13, with all actinide concentrations of each depletion scheme being compared to those yielded in Scheme 10-8.

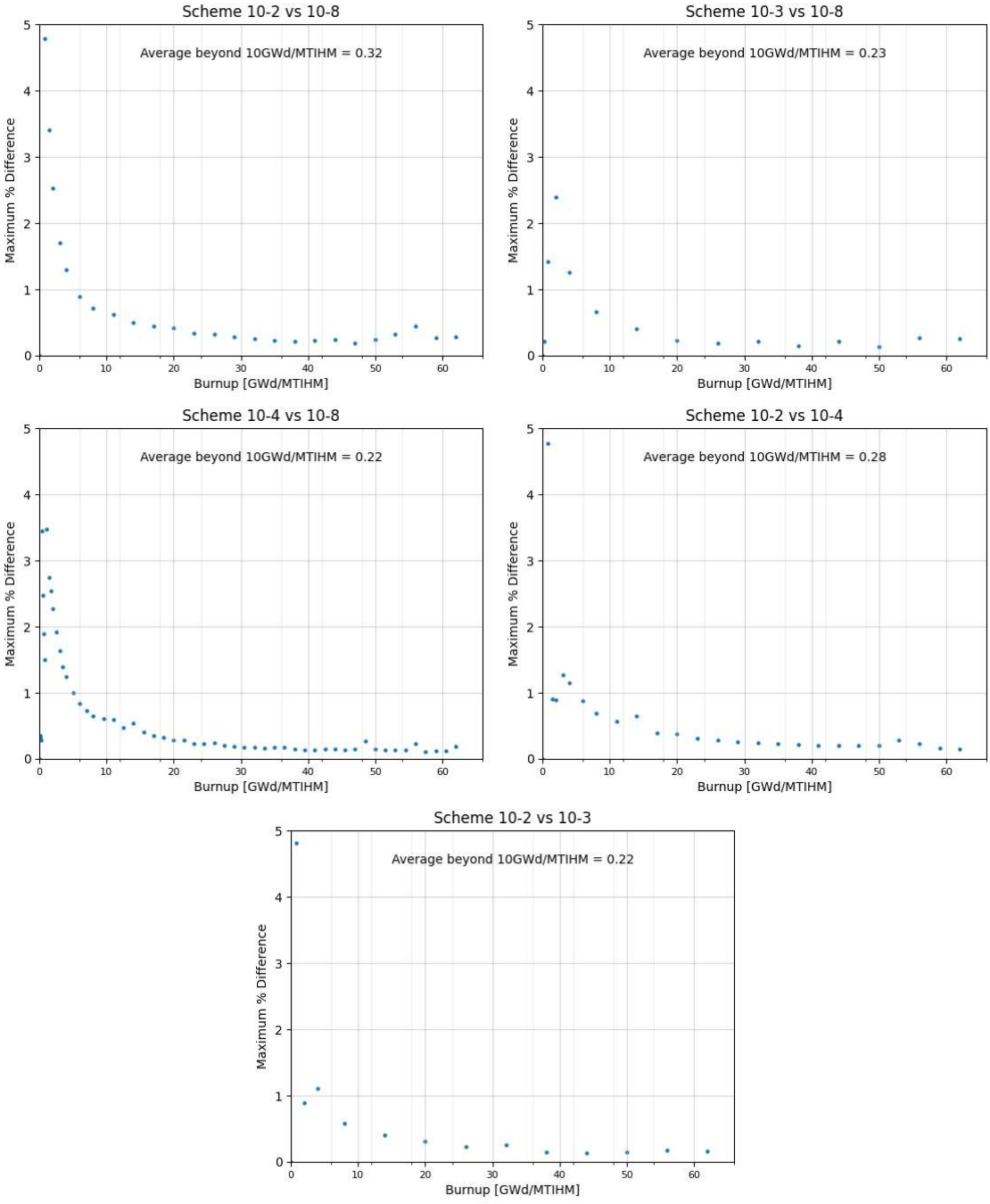

Figure 12. Maximum actinide percent differences.

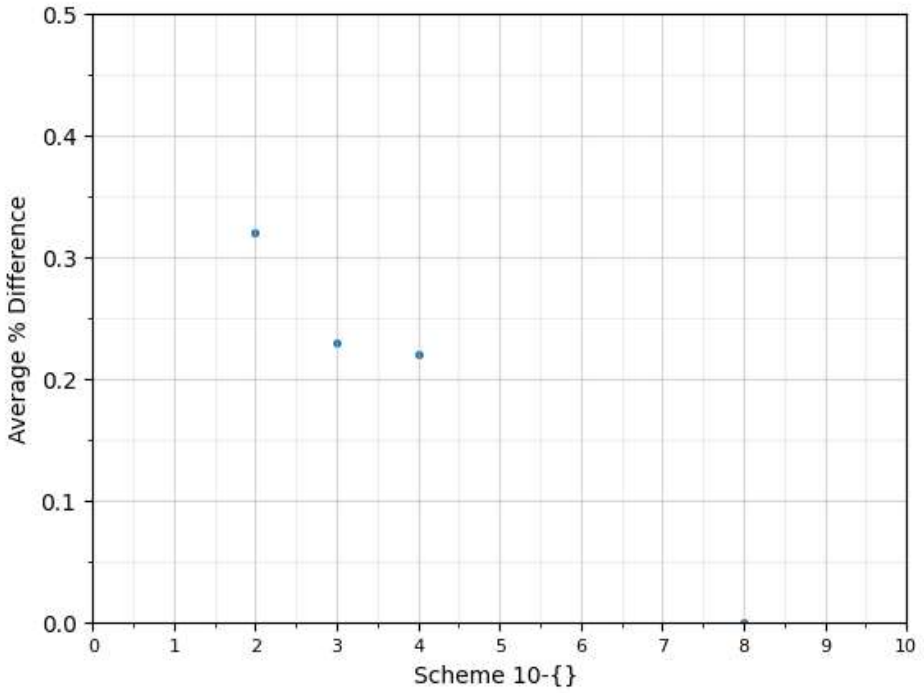

Figure 13. Average actinide percent difference of each depletion scheme relative to Scheme 10-8.

As expressed in Figure 14, the maximum percent difference in actinides is usually dominated by low-concentration nuclides, such as Pu-243, Ac-225, Th-229, Cm-243, and Am-242. Figure 15 shows that these particular nuclides yield near-zero concentrations, and thus any deviation purely through stochastic uncertainty can lead to significant percent differences across two independent simulations. This may suggest that these nuclides are not necessarily indicators of *true* difference between depletion scheme simulations. This provides the benefit that the *maximum percent difference of all actinides* may not be the most meaningful difference for comparison across depletion schemes. For this reason, Table 6, Table 7, and Table 8 were used to analyze the most significantly radioactive nuclides, the nuclides found in the FLiBe fuel, and Uranium isotopes of interest, respectively.

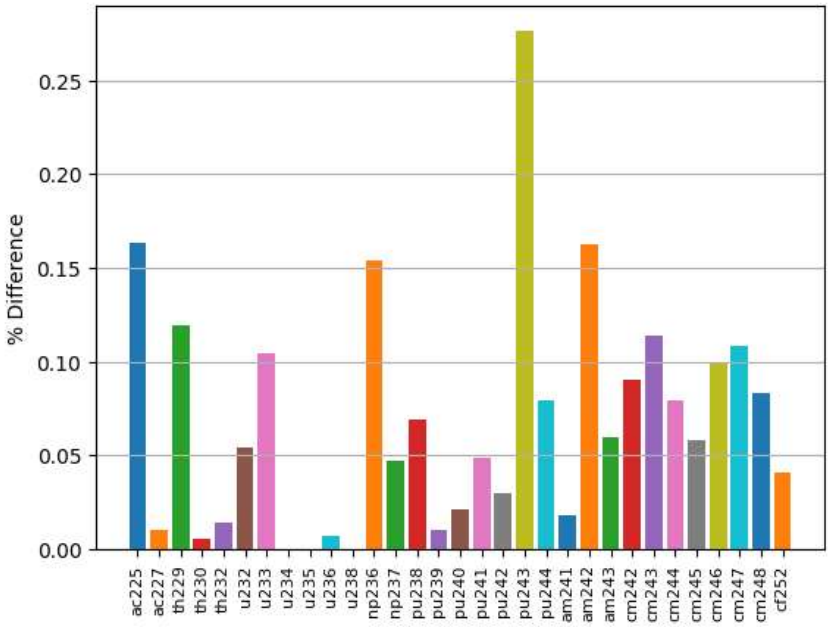

Figure 14. EOL actinide percent difference from depletion Scheme 10-2 to 10-8 (62 GWd/MTIHM).

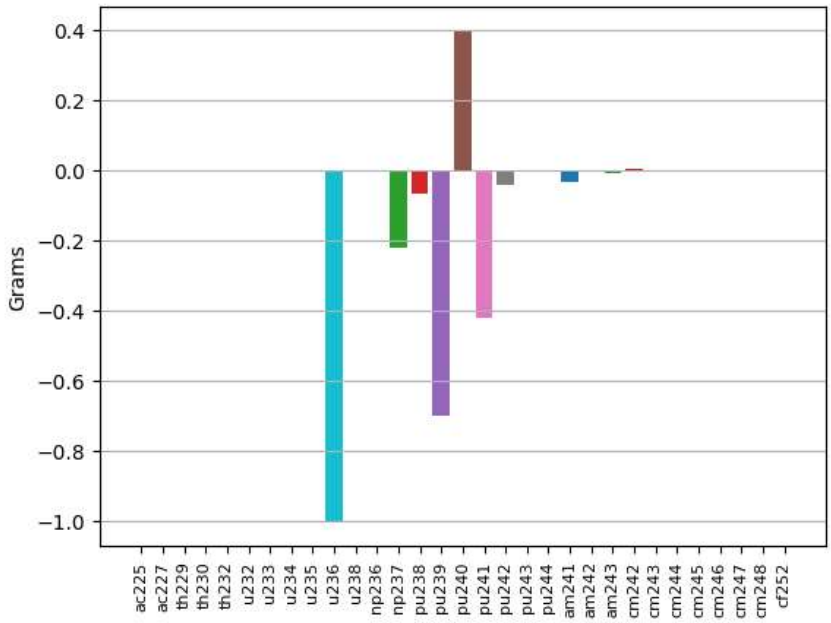

Figure 15. EOL actinide mass difference from Scheme 10-2 to 10-8 (62 GWd/MTIHM).

Figure 16 shows that Xe-133 yields the highest percent difference (~5%) at EOL from Scheme 10-2 to Scheme 10-8, but this corresponds to a relatively small mass difference (~0.14 grams). The maximum percent difference is always dominated by Xe-133 across all burnups in this case. A more significant radiation uncertainty may be seen in Tc-99, where a ~1.5% difference yields a mass difference of ~22.5 grams. All other analyzed nuclides of significant radiation were found to yield less than 0.15% difference from Depletion Scheme 10-2 to 10-8.

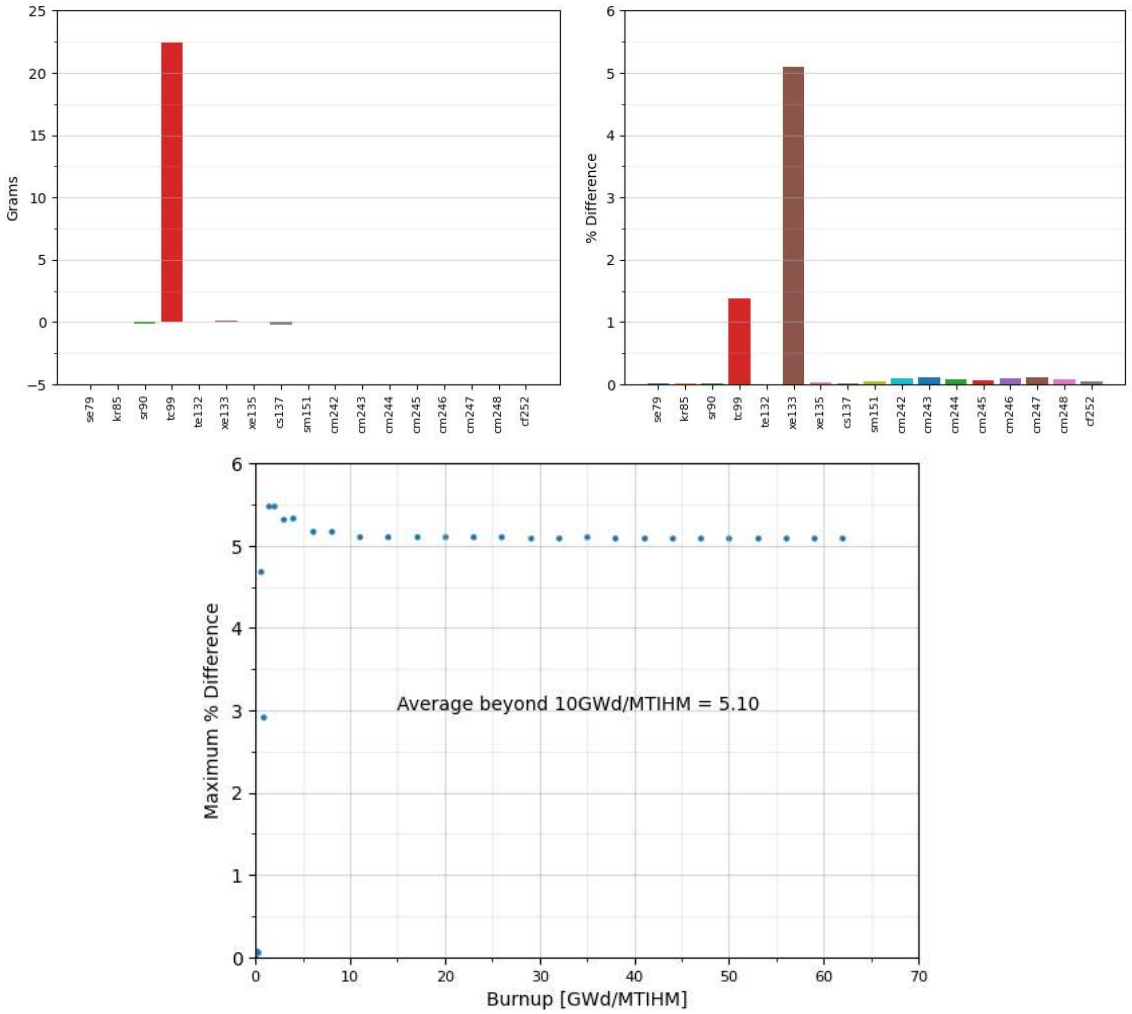

Figure 16. EOL concentration differences and maximum percent difference for significantly radioactive nuclides from Scheme 10-2 to 10-8.

Figure 17 and Figure 18 show even more favorable results than those of the actinides and significant radioactive nuclides. None of the FLiBe fuel salt nuclides experience significant differences from Depletion Scheme 10-2 to 10-8, with the maximum percent difference across all burnups being less than 0.01%, and the maximum percent difference being primarily dominated by Li-6 at all burnups.

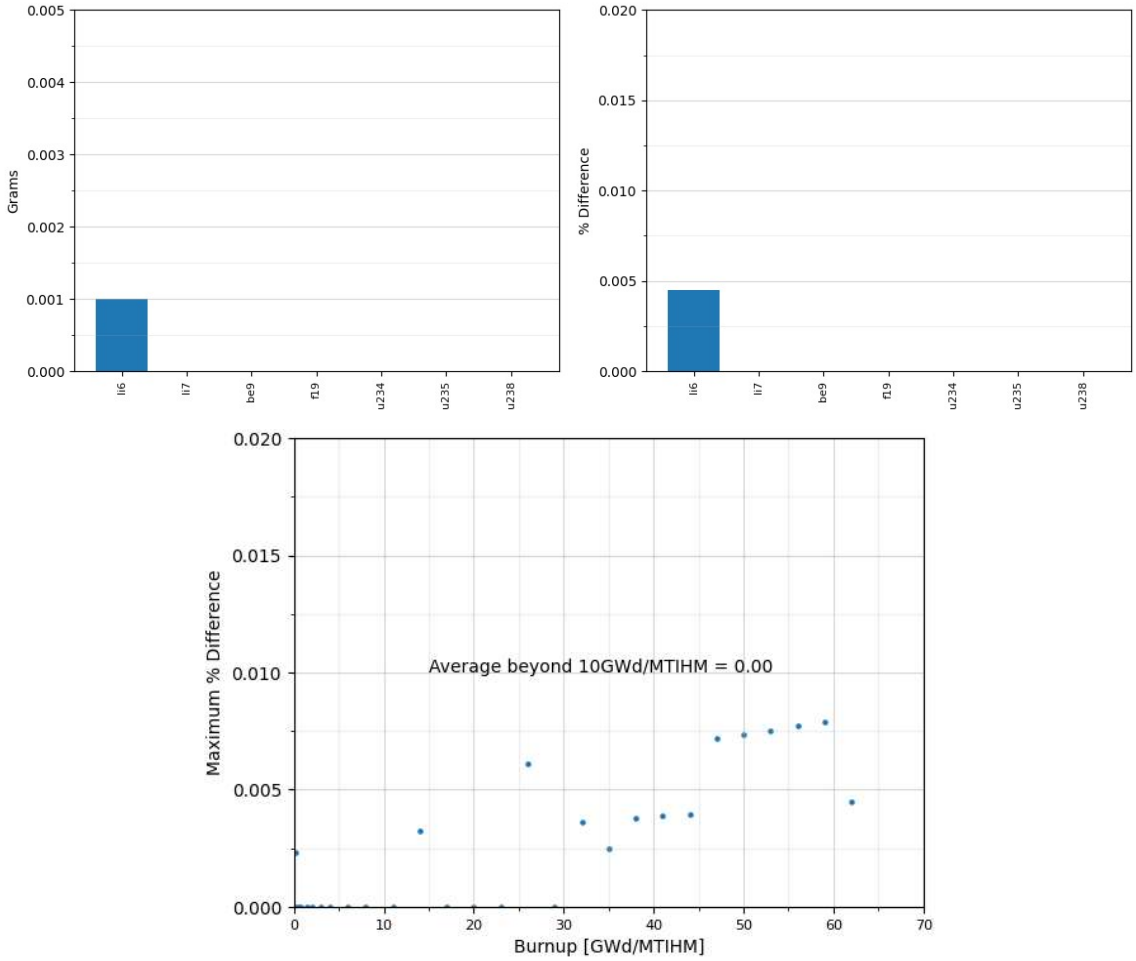

Figure 17. EOL concentration differences and maximum percent difference for fueled FLiBe nuclides from Scheme 10-2 to 10-8.

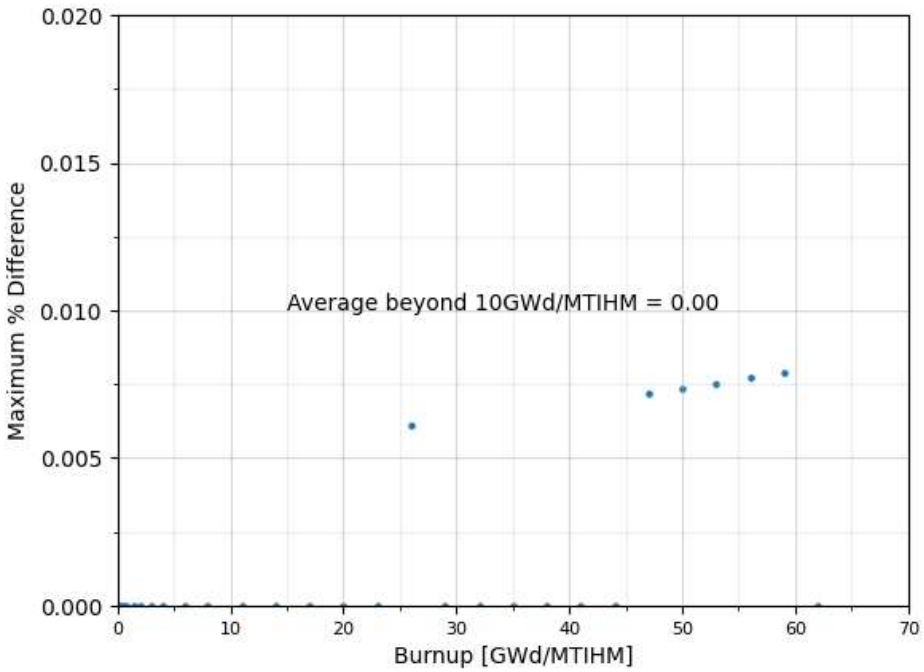

Figure 18. Maximum percent difference for U-235 and U-238 from Scheme 10-2 to 10-8.

3.2.1.3 Computational Resources

Figure 19 shows the computational resources necessary per number of depletion steps in a given simulation. For this particular model, this computational resource setup (INL's Sawtooth Cluster [10]), and this number of MPI processes used (240), the number of CPU-hours necessary to complete a simulation of a given number of depletion steps can be represented by a linear fit with a R^2 value of 0.999832. As shown, the estimated serial runtime for this particular model from 14 depletion sequences to 112 depletion sequences experiences a ~303% increase from ~846 hours to ~3411 hours (or ~ 30 serial hours for every additional depletion sequence). For the comparison of Scheme 10-2 to 10-8, 10-2 (~0.5 d) runs in 4x less time than 10-8 (~2.25 d) and at EOL yields a maximum 0.3%

percent difference across all important actinides, a 5.1% percent difference in Xe-133 (maximum at EOL), a 1.4% difference in Tc-99, a 0.9% difference in I-131, and <0.5% difference in all other analyzed nuclides. Decision whether to use a more accurate and more costly simulation, or less accurate but significantly faster depletion will depend on each specific application; quantification provided here may help guide that decision.

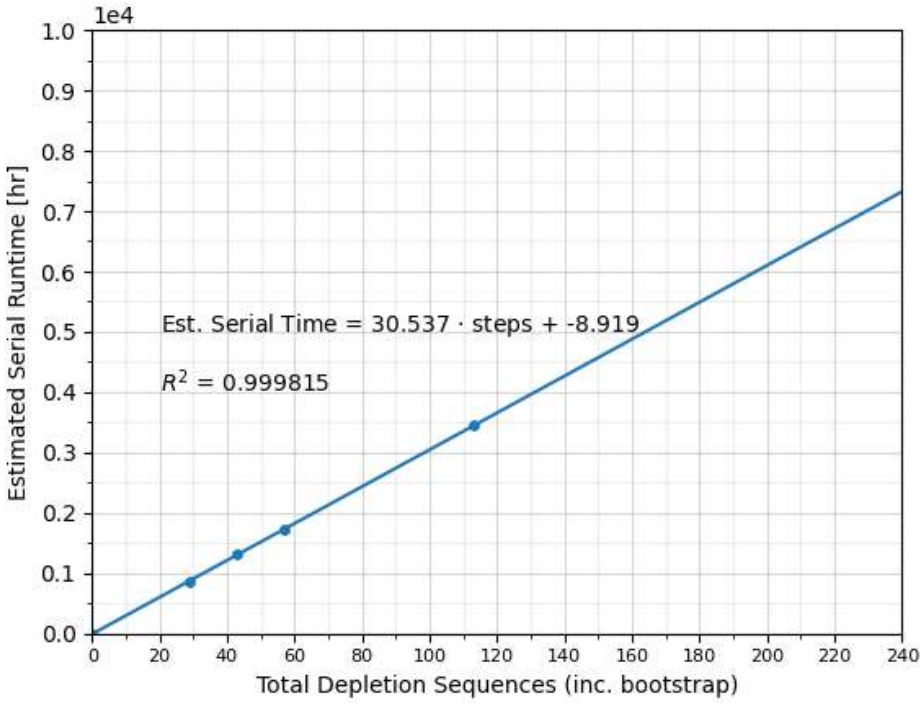

Figure 19. Estimated serial runtime vs number of depletion steps parameter for 240 MPI processes on INL's Sawtooth cluster

3.2.2 Parallel Performance

The transformation/alteration/modification of SCALE simulation parallelization is studied by conducting several SCALE simulations of identical models and parameters on separate parallelized SCALE builds (Idaho National Laboratory's Sawtooth Cluster and Georgia Institute of Technology's PACE Firebird Cluster) using a varying number of computer

nodes and computer cores. The clusters can be characterized by the information provided in Table 15. The parallelization of each simulation can be grouped into "builds": INL's Sawtooth SCALE build (INL-ST) and Georgia Institute of Technologies Firebird SCALE build (GT-FB).

Table 15 shows that INL-ST yields 48 cores per node while GT-FB yields 24 cores per node and that INL-ST should yield greater maximum CPU speeds. Figure 20, Figure 21, and Figure 22 show the variance in computational efficiency between INL-ST and GT-FB for identical simulations on SCALE 6.2.4. Unexpectedly, INL-ST across a full 48-core node was shown to yield calculation speeds nearly equivalent to GT-FB across two 24-core nodes (i.e. both on 48 cores). This was counter to predictions due to the expectation that cross-node communications would hinder the GT-FB simulation. This lends itself to the trend of INL-ST yielding slower calculation times than GT-FB on equivalent resources (both nodes and cores included). The cause of this may be shown through the process times, wherein INL-ST is shown to spend less time communicating with other cores but more time running parallel and serial computations than GT-FB. This may indicate that the SCALE build on INL-ST utilizes a parallelization process and/or read/write process that is not as efficient as the SCALE build on GT-FB.

Table 15. Cluster Specifications

	INL-ST	**GT-FB**
Architecture	x86_64	x86_64
CPU op-mode(s)	32-bit, 64-bit	32-bit, 64-bit
Byte Order	Little Endian	Little Endian

Table 15 continued

Thread(s) per core	2	1
Core(s) per socket	24	12
Socket(s)	2	2
NUMA node(s)	2	2
Vendor ID	GenuineIntel	GenuineIntel
CPU family	6	6
Model	85	85
Model name	Intel(R) Xeon(R) Platinum 8268 CPU @ 2.90GHz	Intel(R) Xeon(R) Gold 6226 CPU @ 2.70GHz
Stepping	7	7
CPU MHz	3500	3500
CPU max MHz	3900	3700
CPU min MHz	1200	1200

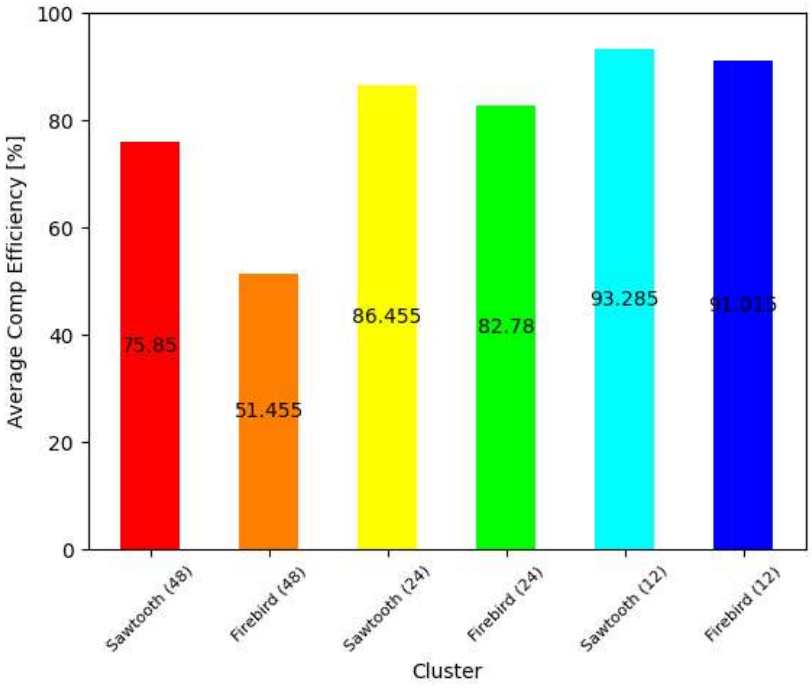

Figure 20. Average parallel efficiency for varying cores on INL-ST and GT-FB

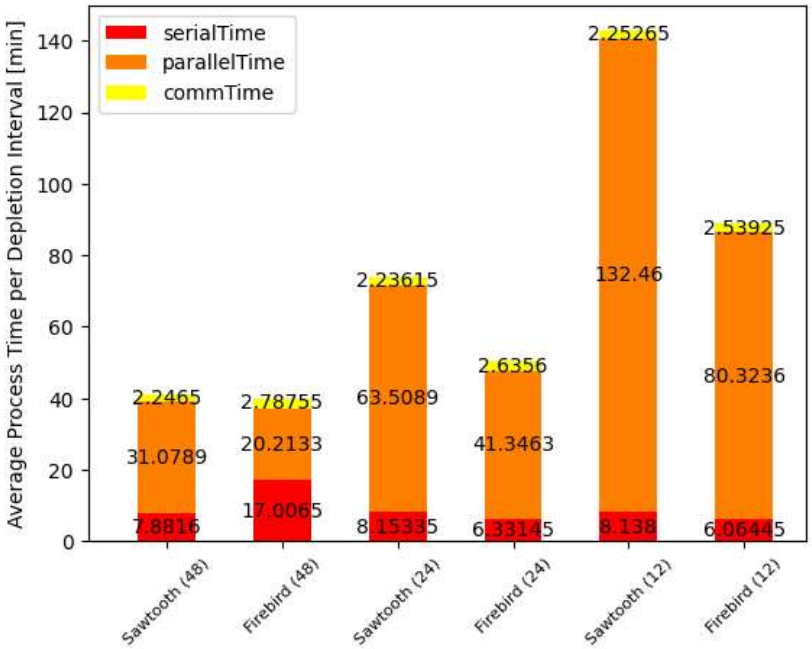

Figure 21. Average process time per depletion calculation

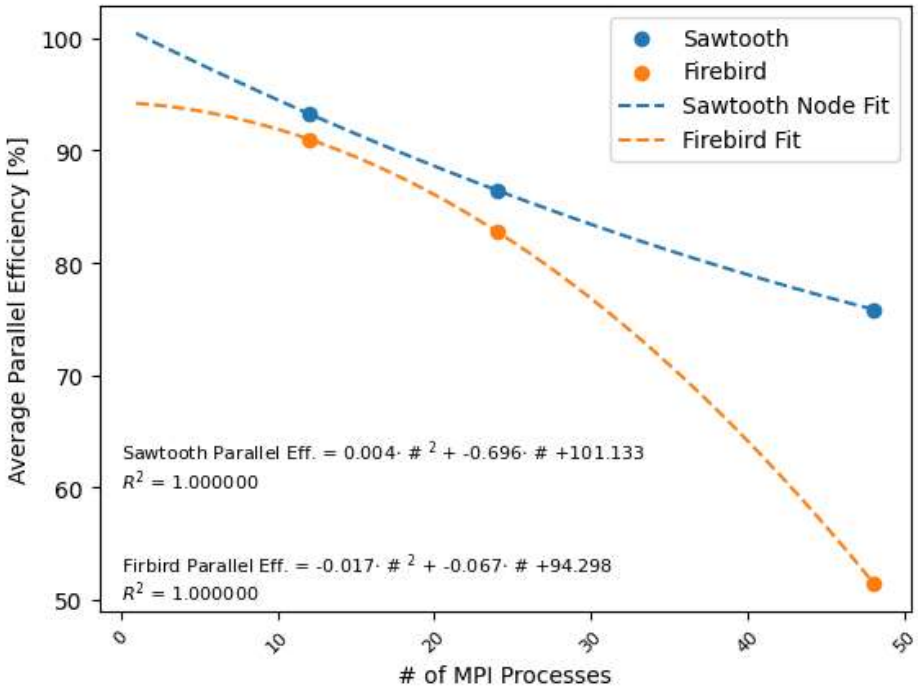

Figure 22. Average parallel efficiency vs # of MPI processes for INL-ST and GT-FB

3.3 Reactor Physics Models

3.3.1 Self-shielding method

For neutronic purposes, resonance self-shielding is the phenomenon that takes place when the energy dependent neutron flux experiences a depression in the resonance energy region of a given material due to an increased nominal absorption cross section of neutrons within the material. This is compounded with a spatial shielding effect wherein heterogenous cores (e.g. LWR fuel pins) experience a spatial shielding near the fuel surface due to the separation of moderator and fuel demanding that the neutrons leave the fuel to enter the moderator and then return to a fuel source to induce fission. The effect of these neutrons interacting with the fuel surface leads to a "shielding" of the inner layers of the fuel. This

effect is especially dramatic in the material's resonance energy region. SCALE implements two modules of accounting for the self-shielding phenomenon: BONAMI and CENTRM.

The BONAMI module performs the resonance self-shielding calculations based on the Bondarenko Method, wherein problem-independent cross-sections and Bondarenko shielding factors are acquired from a multigroup master library and used to generate self-shielded, problem-dependent MG cross-sections. This module holds the advantage of being simpler and faster than the CENTRM module. [1]

The CENTRM module performs the resonance self-shielding calculations through a pointwise deterministic transport calculation to generate continuous-energy neutron spectra for infinite lattice, which is then used as a problem-dependent weight function for MG averaging and resulting self-shielded, problem-dependent MG cross-sections. This module holds the advantage of generating problem-specific fluxes on a fine energy mesh (which may be used for generating self-shielding multigroup cross-section library). [1]

Additionally, the use of Dancoff factors is an element within the SCALE self-shielding method. The Dancoff factor, also known as the Dancoff coefficient, is a coefficient for the accountancy of the probability of neutrons escaping from the heterogenous nuclear fuel/moderator system before interacting with the surrounding moderator or coolant, and SCALE 6.2.4 allows the user to define it from their own calculations. [11] [12]

The analysis of the effects of each self-shielding method are evaluated through replica simulations using depletion scheme 10-4 with only the self-shielding parameter changed. The simulations used in this study of depletion sub-intervals have been extracted from Table 10 and are presented in Table 16.

Table 16. Self-Shielding Simulations Used.

Model	Run	Addnux	Est. MTIHM	Depletion Scheme	Self-shielding	Library	Cluster	gen	npg	nsk	MPI Processes	Average Parallel Efficiency [%]	Wallclock time [hours]	Average k_eff Uncertainty [pcm]
0003	**v04**	4	0.292513	10-4	CENTRM	MG	INL-ST	350	400000	50	240	26.143	27.444	9.4
0005	**v01**	4	0.292513	10-4	BONAMI	MG	INL-ST	350	400000	50	240	26.417	25.428	9.6

3.3.1.1 Multiplication factor k_{eff}

Figure 23 shows k_{eff} of the replica simulations for BONAMI and CENTRM self-shielding methods. Figure 24 shows k_{eff} from BONAMI to CENTRM experiences an average decrease of 226-pcm (i.e. BONAMI overestimates k_{eff} relative to CENTRM). This trend is particular to this model. Analyses of BONAMI vs CENTRM in other reactor models may show different results. A point can be made that this k_{eff} difference is not due to plutonium isotope resonance overlap because the k_{eff} difference is shown to begin at BOL of the depletion simulation (i.e. before plutonium has been bred).

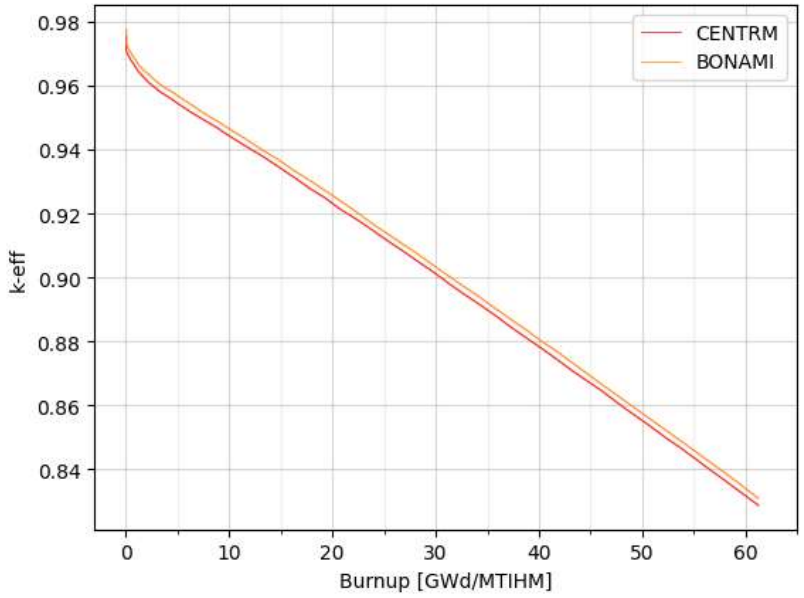

Figure 23. k_{eff} vs burnup of Scheme 10-4 for BONAMI and CENTRM (±σ error bars are shown but are too small to be visible)

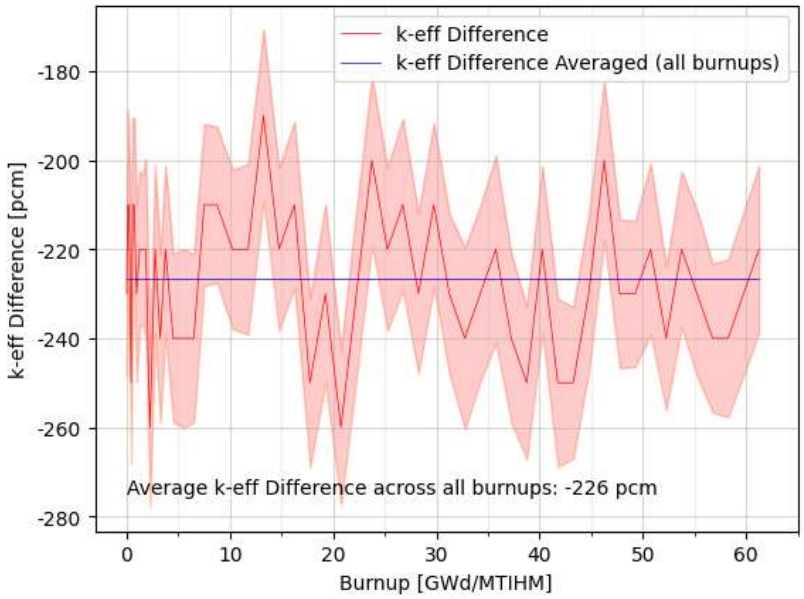

Figure 24. k_{eff} difference from BONAMI to CENTRM for all burnups (±σ error bars are shown)

3.3.1.2 Isotopic Concentrations

In Figure 25, the average maximum actinide percent difference from CENTRM to CENTRM is shown to be relatively consistent across all burnups (a range of 1.8% to 2.8% difference) and is primarily dominated by higher isotopes of curium (Cm-246 to Cm-248) beyond 10 [GWd-MTIHM^{-1}] (example given at EOL in Figure 27).

Figure 26 shows that these particular nuclides yield near-zero concentrations, and thus any deviation may be through stochastic uncertainty. This may again suggest that these nuclides are not necessarily indicators of *true* difference between depletion scheme simulations. This provides the benefit that the *maximum percent difference of all actinides* may not be the most meaningful difference for comparison across depletion schemes. For thorough analysis, Figure 27 and Figure 28 are provided to show EOL actinide percent difference and actinide mass difference, respectively.

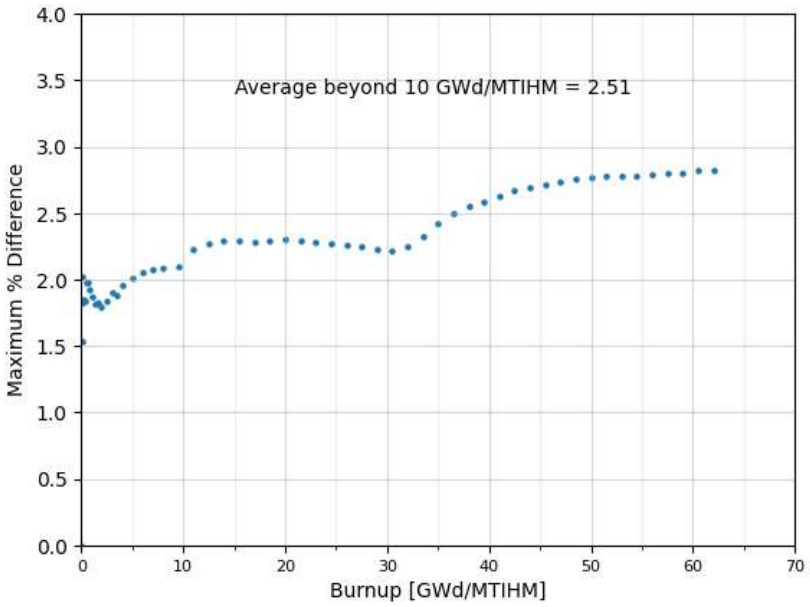

Figure 25. Maximum actinide percent differences from BONAMI to CENTRM.

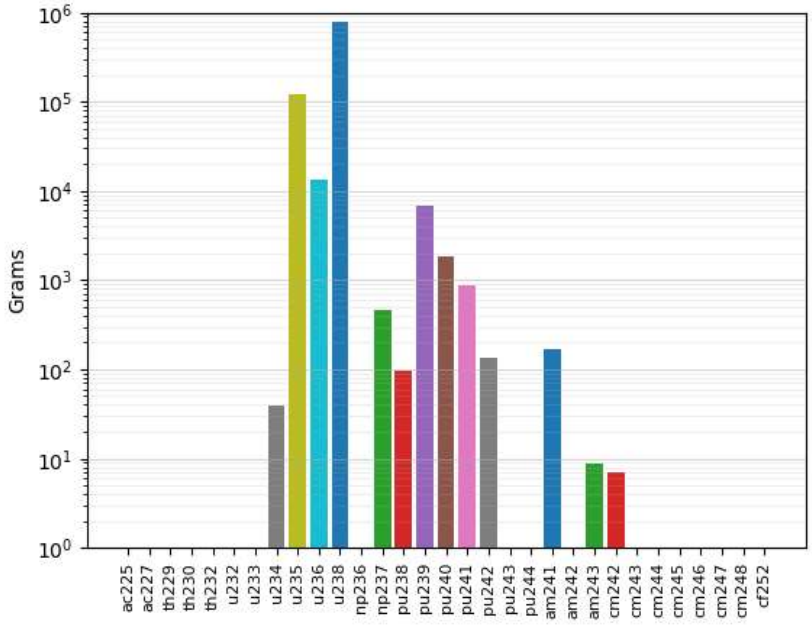

Figure 26. Average EOL actinide concentrations for BONAMI and CENTRM

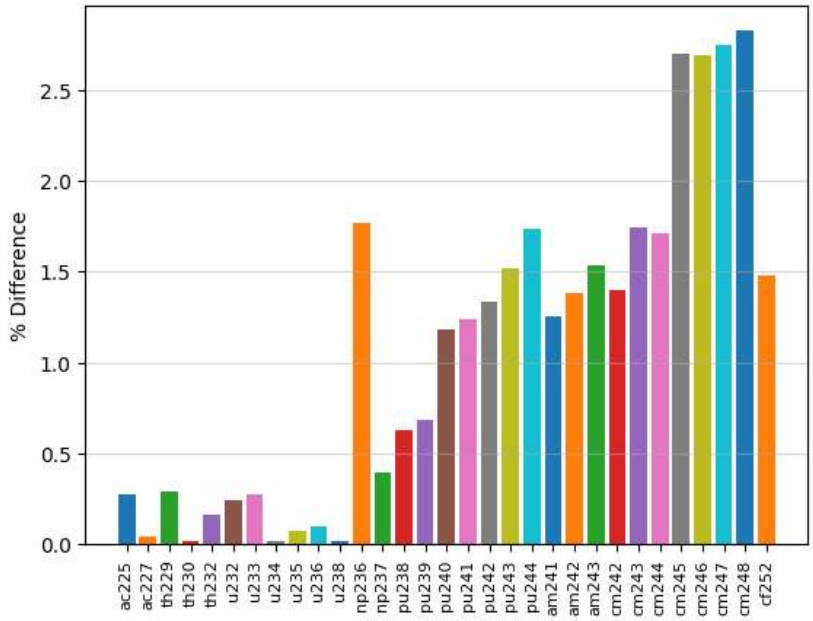

Figure 27. EOL actinide percent differences from BONAMI to CENTRM

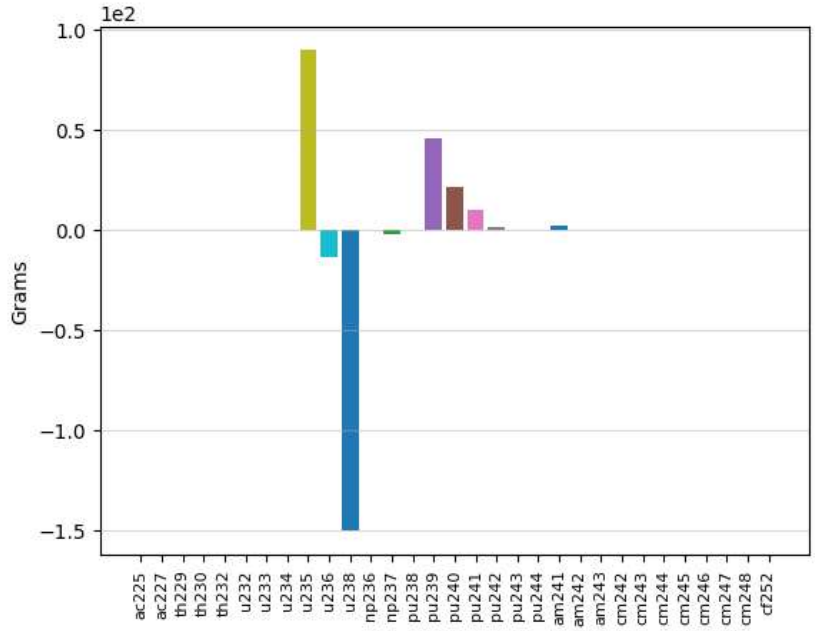

Figure 28. EOL actinide mass differences from BONAMI to CENTRM

Due to the questionability of the significance of the actinide maximum percent difference analysis, Figure 29, Figure 30, and Figure 31 were used to analyze the most significantly radioactive nuclides, the FLiBe fuel nuclides, and Uranium isotopes of interest, respectively.

Figure 29 shows that, again, curium nuclides yields the highest percent difference (~2.7%) at EOL from BONAMI to CENTRM, but this corresponds to a near zero mass difference. Notably, the maximum percent difference is always dominated by Curium nuclides across all burnups in this case. All nuclide differences yielded are below 1-gram; and if accounting for all but Sr-90, nuclide differences are all below 0.3-grams. Across all burnups beyond 10 GWd-MTIHM^{-1}, the maximum % difference (which can be read as maximum Curium difference) is 2.5%.

Figure 30 (for FLiBe) and Figure 31 (for uranium isotopes) show closer agreement than those of the actinides and significant radioactive nuclides. None of the fueled nuclides experience significant difference from BONAMI to CENTRM, with the maximum percent difference across all burnups being less than 0.1%, and the maximum percent difference being primarily dominated by U-235 at higher burnups.

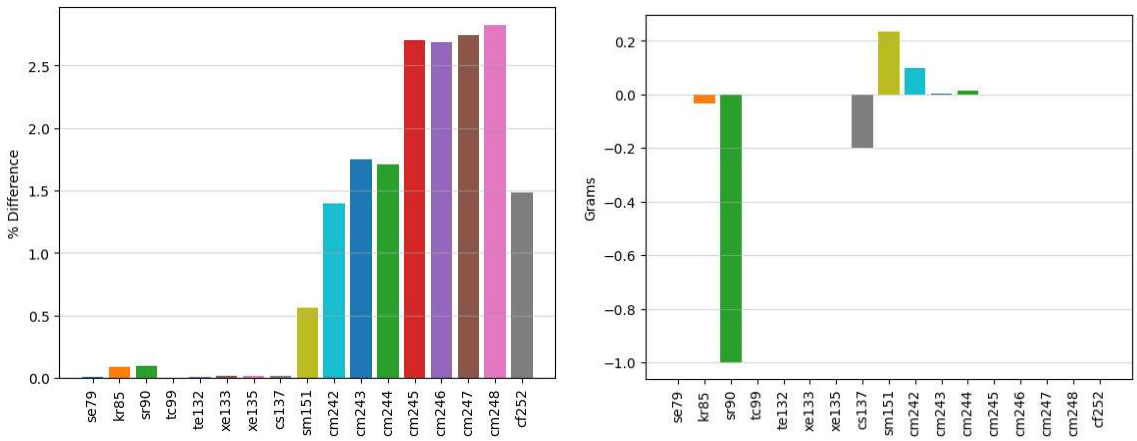

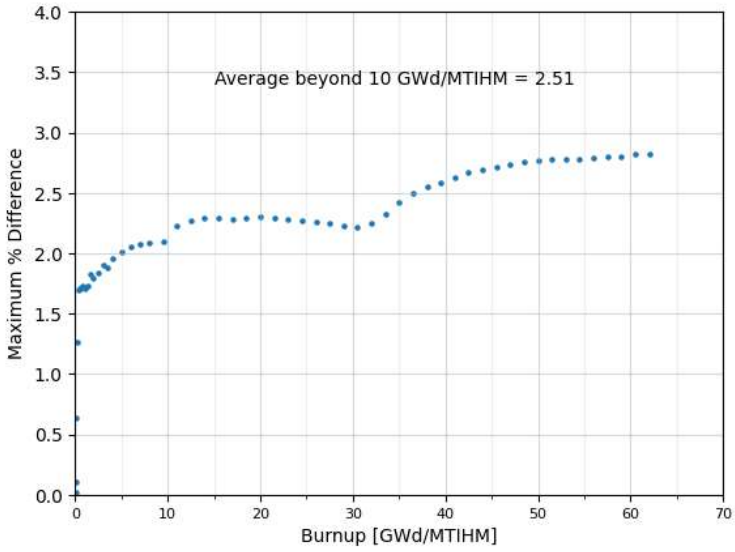

Figure 29. EOL concentration differences and maximum percent difference for significantly radioactive nuclides from BONAMI to CENTRM

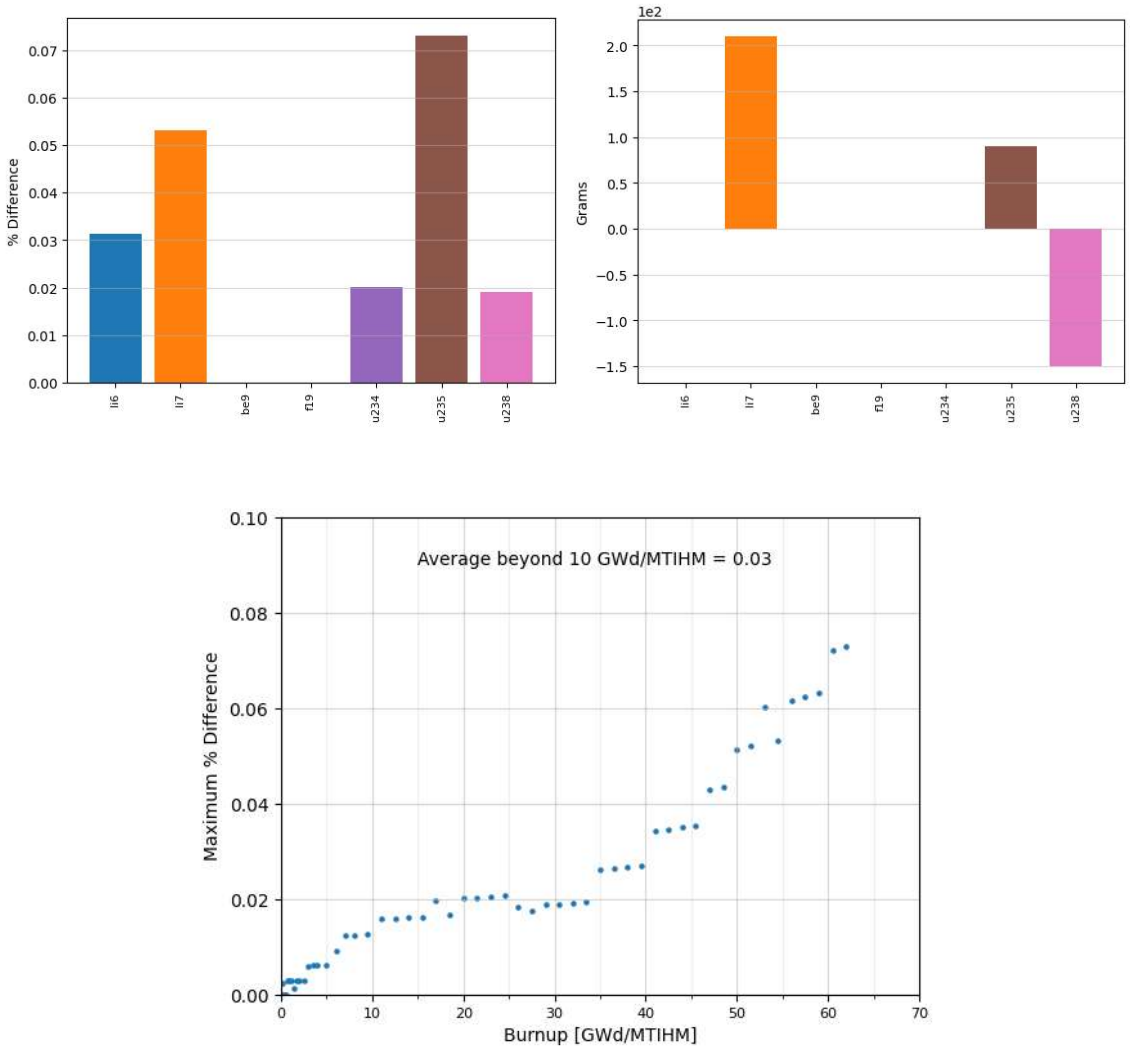

Figure 30. EOL concentration differences and maximum percent difference for fueled FLiBe from BONAMI to CENTRM

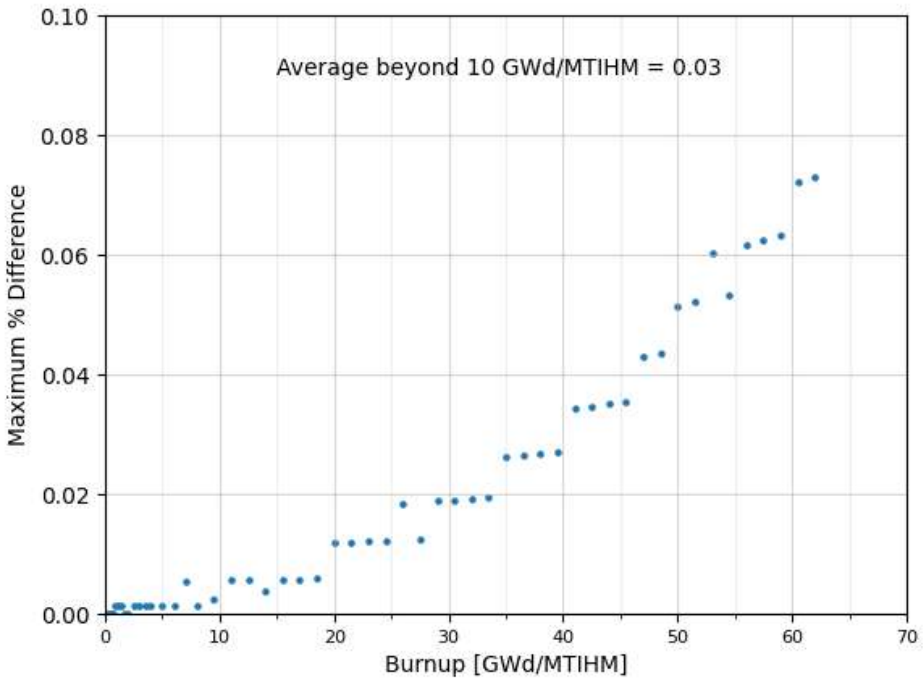

Figure 31. Maximum percent difference for uranium isotopes from BONAMI to CENTRM

3.3.1.3 Computational Resources

Figure 32 shows that, while there is an increase in serial runtime between BONAMI and CENTRM, the increase is relatively small (~7% increase), yielding a serial runtime increase of over 100-hours but only a wallclock runtime increase of 2 hours (from 25.4 to 27.3 hours). This result was somewhat unexpected because depletion studies employing simple models have shown a more substantial differences in runtimes.

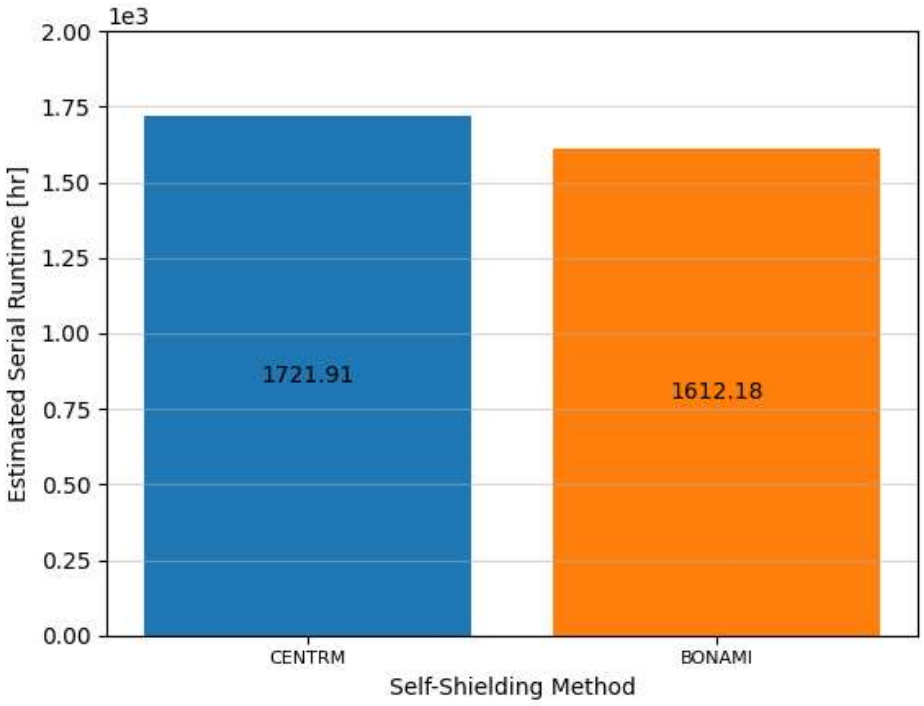

Figure 32. Estimated serial time vs self-shielding method for 240 MPI processes on INL's Sawtooth cluster

3.3.2 Cross-section Library

A crucial constituent of the depletion simulation is the choice of cross-section library. In particular, a prevalent method to reduce computational load in neutronics simulations is to collapse a given continuous-energy cross-section library (CE) into a multigroup cross-section library (MG). The reduction of discrete datapoints from tens-of-thousands per nuclide (as in CE) to only hundreds per nuclide (as in 252-group MG) yields significantly faster computations in the form of reduced loading times for the library and computational time for each transport calculation.

This analysis quantifies the differences between replica simulations using depletion scheme 10-2 with only the cross-section library changed between continuous-energy ENDF/B-VII.1 and 252-group ENDF/B-VII.1. The simulations used in this study of cross-section libraries have been extracted from Table 10 and are presented in Table 17. Note that CE simulations utilized 1440 MPI processes while the MG runs utilized only 240.

Table 17. Cross-Section Library Simulations Used.

Model	Run	Addnux	Est. MTIHM	Depletion Scheme	Self-shielding	Library	Cluster	gen	npg	nsk	MPI Processes	Average Parallel Efficiency [%]	Wallclock time [hours]	Average k_eff Uncertainty [pcm]
0003	**v02**	4	0.292513	10-2	CENTRM	MG	INL-ST	350	400000	50	240	26.350	13.680	9.6
0003	**v04**	4	0.292513	10-4	CENTRM	MG	INL-ST	350	400000	50	240	26.143	27.444	9.4
0006	**v01**	4	0.292513	10-2	CENTRM	CE	INL-ST	250	300000	50	1440	36.722	18.630	13.0
0006	**v02**	4	0.292513	10-4	CENTRM	CE	INL-ST	350	400000	50	1440	48.196	53.324	10.2

3.3.2.1 Multiplication factor k_{eff}

Figure 33 shows k_{eff} of the replica simulations for MG and CE cross-section libraries. Figure 34 shows that the k_{eff} from MG to CE experiences an average increase of ~148-pcm (i.e. MG underestimates k_{eff} relative to CE), with the k_{eff} difference converging towards zero as burnup increases.

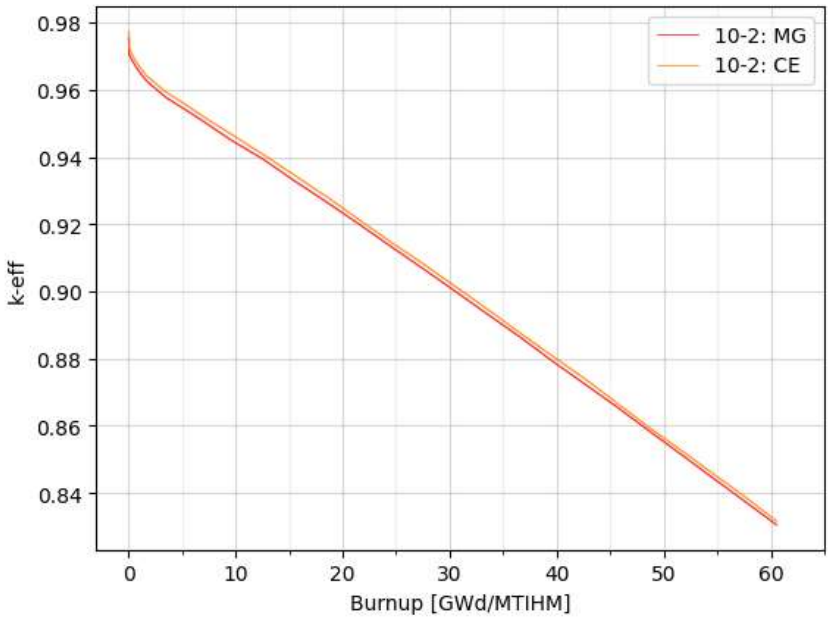

Figure 33. k_{eff} vs burnup of Scheme 10-2 for CE and MG (±σ error bars are shown but are too small to be visible)

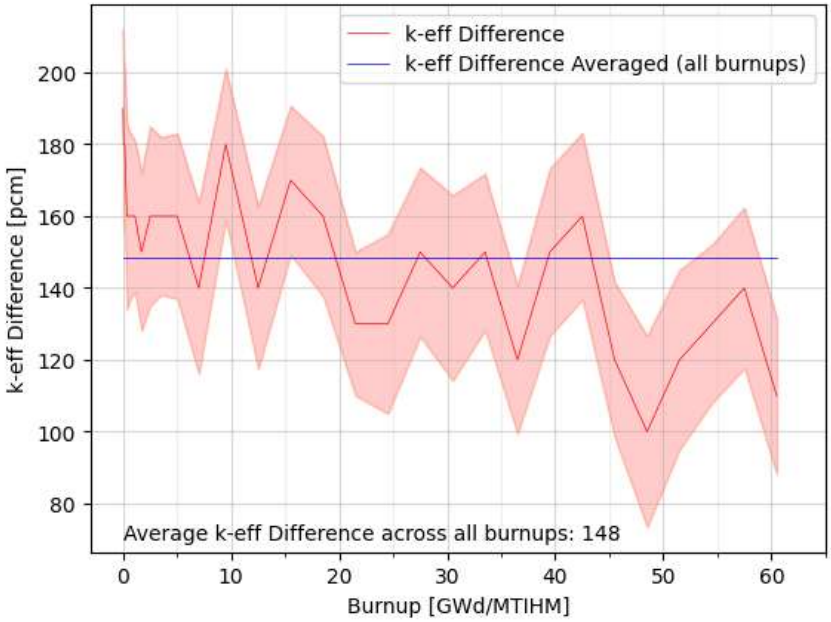

Figure 34. k_{eff} difference across all burnups from MG to CE

3.3.2.2 Isotopic Concentrations

In Figure 35, the average maximum actinide percent difference from MG to CE is shown to be relatively high at low burnups (>20% difference at <10 GWd/MTIHM) and is exclusively dominated by U-233. Interestingly, by 62 GWd/MTIHM, U-233 percent difference has converged to <1%. Beyond 35-GWd/MTIHM, the maximum actinide percent difference has converged to <5% and is exclusively dominated by Cm-243.

Figure 37 shows again that these particular nuclides yield near-zero concentrations and thus any deviation may be at least partly due to stochastic uncertainty. This may again suggest that these nuclides are not necessarily indicators of *true* difference between depletion scheme simulations. This provides the benefit that the *maximum percent difference of all actinides* may not be the most meaningful difference for comparison across depletion schemes. For thorough analysis, EOL actinide percent differences from MG to CE are provided in Figure 36.

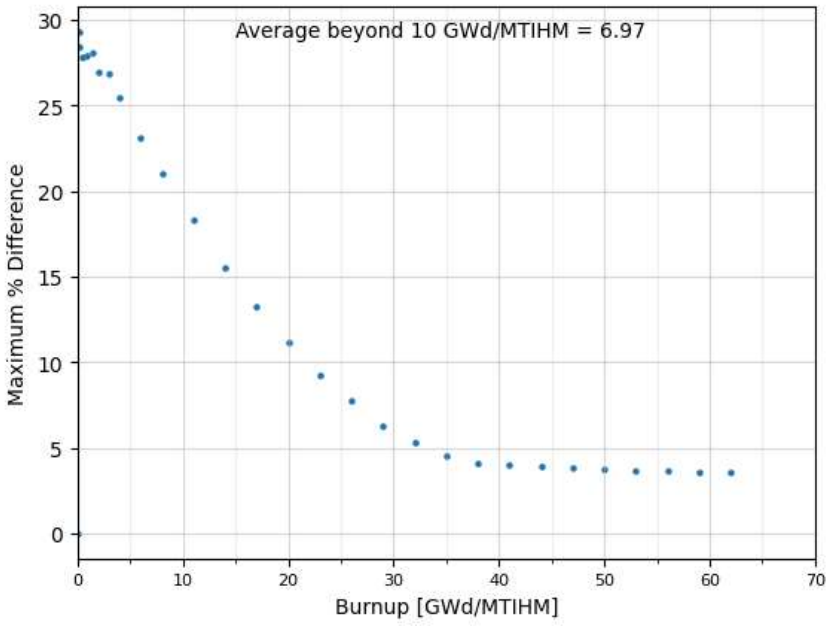

Figure 35. Maximum actinide percent differences across burnups from MG to CE

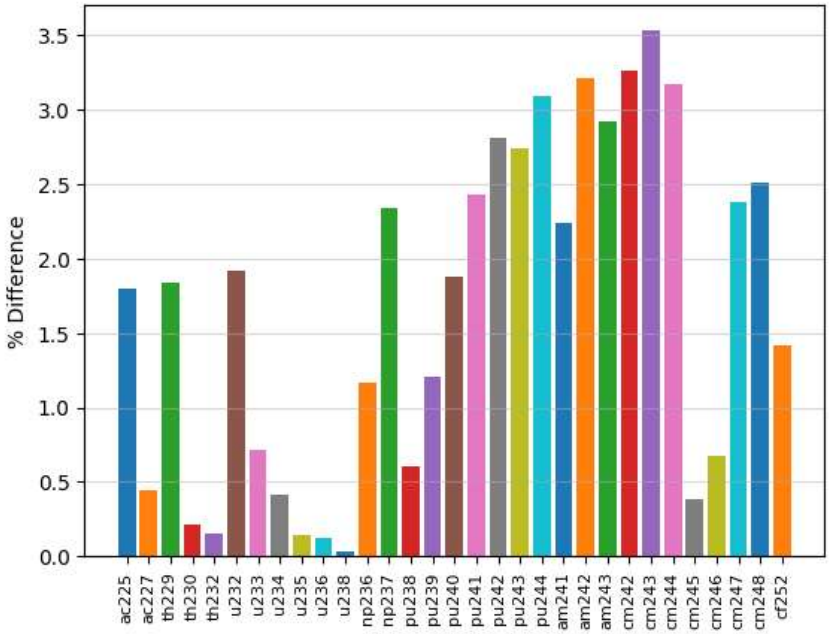

Figure 36. EOL actinide percent differences from MG to CE

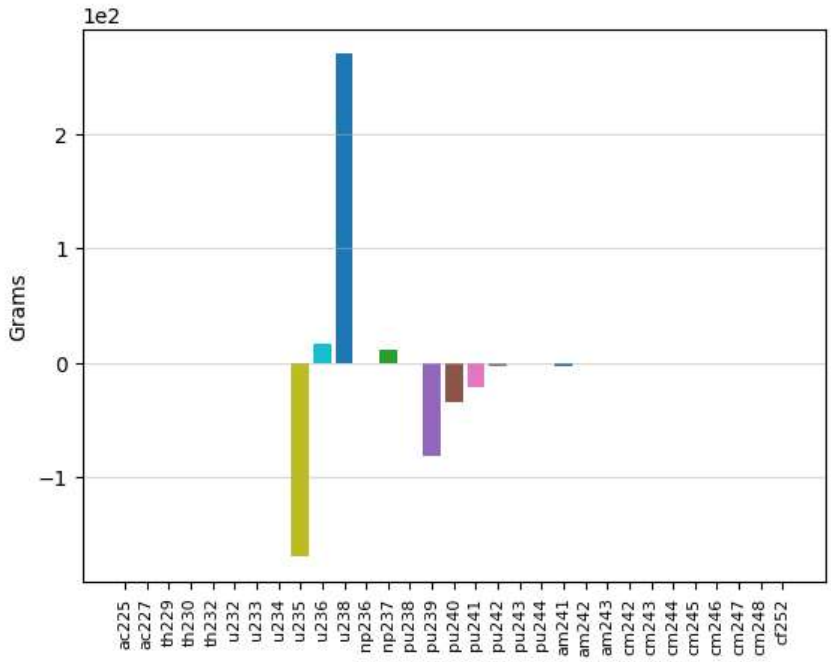

Figure 37. EOL actinide mass differences from MG to CE

Because of the questionable significance of the analysis of actinide max percent differences, Figure 38, Figure 39, and Figure 40 were used to analyze the most significantly radioactive nuclides, the FLiBe fuel nuclides, and Uranium isotopes of interest, respectively.

Figure 38 shows that, again, Curium nuclides yields the highest percent difference (~3.5%) at EOL from MG to CE, but this corresponds to a near zero mass difference. Notably, the maximum percent difference is always dominated by Curium nuclides across all burnups in this case. Besides Sr-90 and Tc-99, all analyzed significant radioactive isotopes differences yielded are below 0.5-grams. Across all burnups beyond 10 GWd/MTIHM, the maximum % difference (which can be read as maximum Curium difference) is 4.09%.

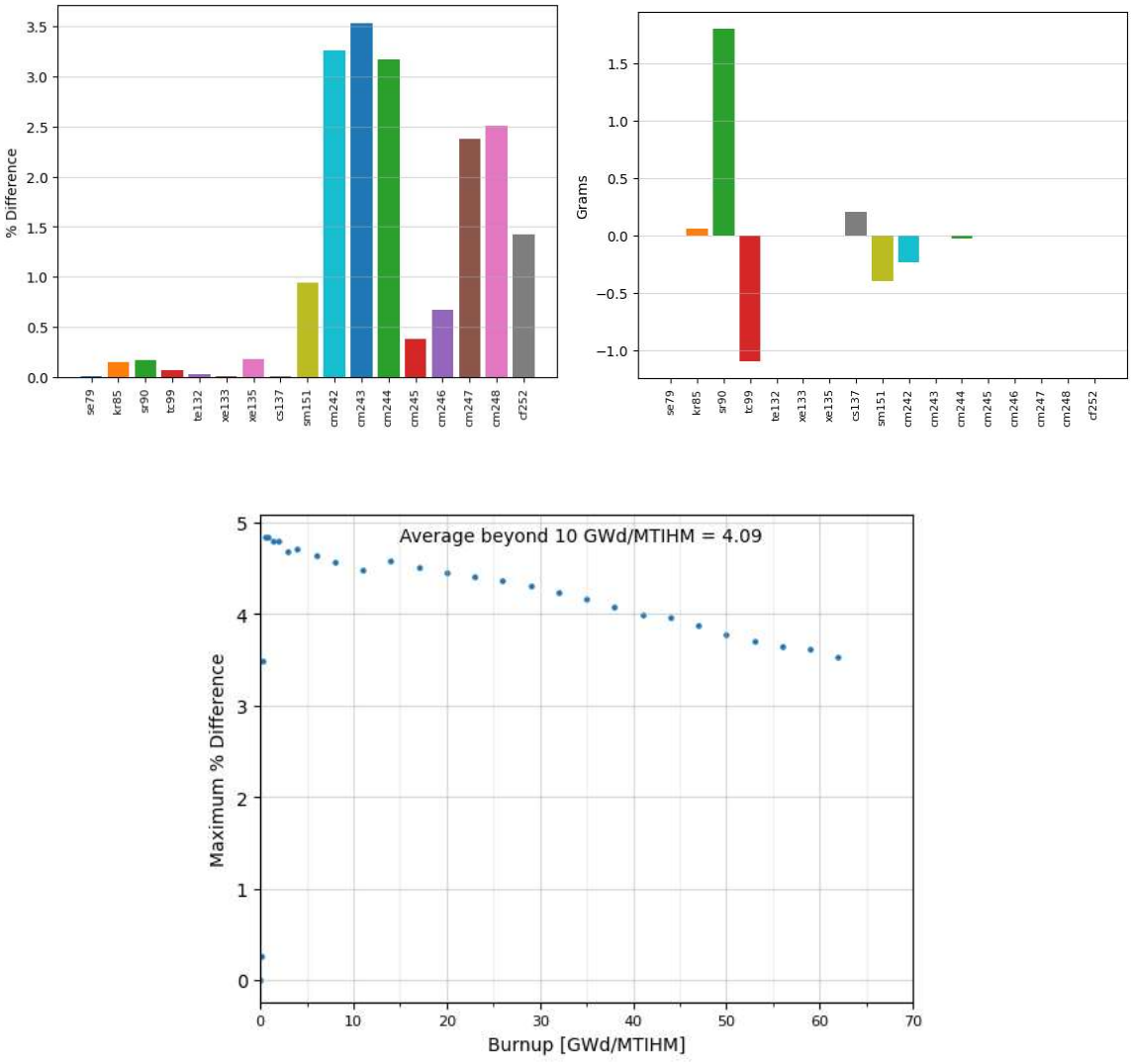

Figure 38. EOL concentration differences and maximum percent difference for significantly radioactive nuclides from MG to CE

Figure 39 and Figure 40 show again more favorable results than those of the actinides and significant radioactive nuclides. None of the fueled nuclides experience significant difference from MG to CE, with the maximum percent difference across all burnups being less than 0.5%, and the maximum percent difference being primarily dominated by U-234 at all burnups. Notably, U-235 experiences a significantly higher EOL percent difference

from MG to CE than U-238, but both remain below 2% difference. MG resulting in higher U-238 concentrations and lower U-235 concentrations may indicate an effective increase in the absorption cross-section of U-238 through the multigroup process from CE to 252-MG.

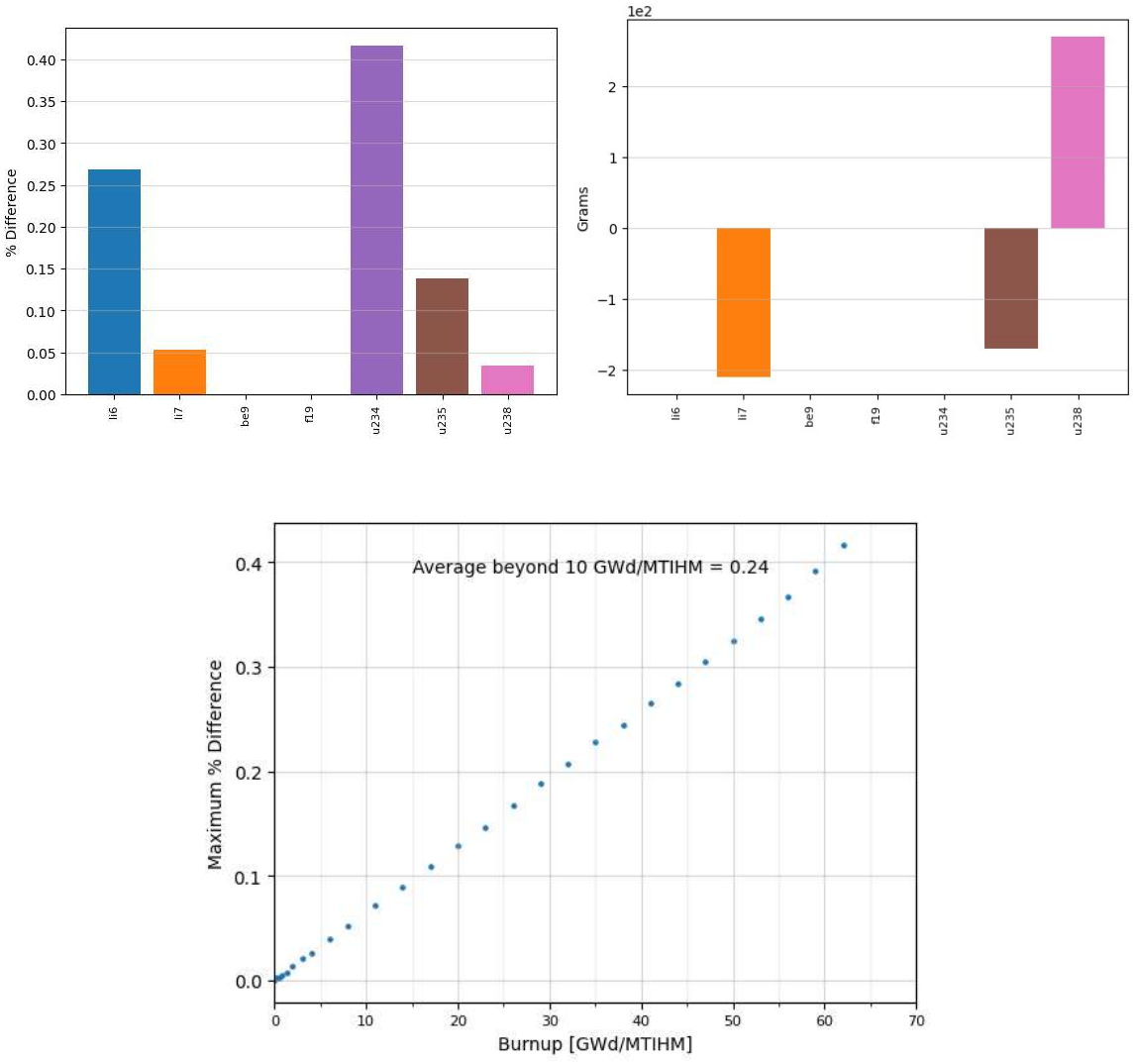

Figure 39. EOL concentration differences and maximum percent difference for fueled FLiBe from MG to CE

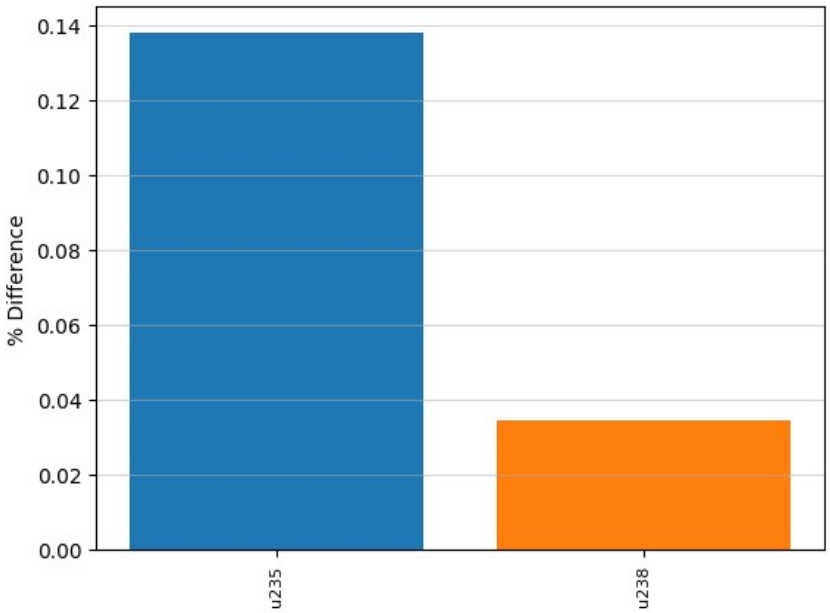

Figure 40. EOL percent difference for uranium isotopes from MG to CE

3.3.2.3 Computational Resources

Figure 41 shows a significant increase in serial runtime from MG to CE (11x greater or a ~1039% increase).

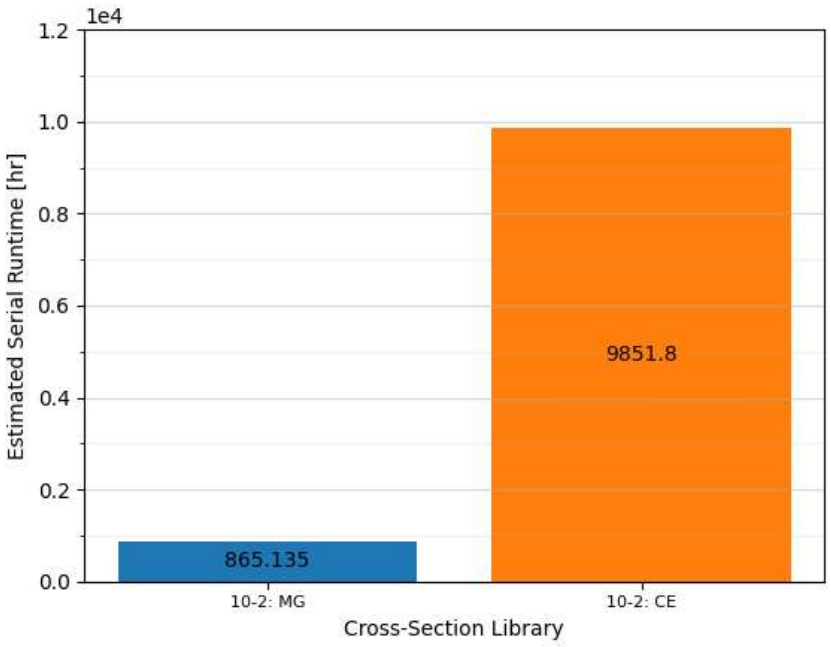

Figure 41. Estimated serial time vs cross-section library for 240 MPI processes on INL's Sawtooth cluster

3.3.3 Trace Elements (i.e. addnux)

SCALE cross-section processing and transport calculations are dependent on the tracked nuclides and as such, the "addnux" parameter is used to introduce trace quantities (~1 x 10^{-20} at/b-cm) of certain nuclides to the depletion inventories. The SCALE manual indicates explicitly that addnux=0 and addnux=1 are to be used **only** for testing purposes. The problem in these lower addnux parameters can be expressed through consideration of addnux=0: when additional nuclide tracking through addnux is forgone (i.e. addnux=0), then the depletion sequence may not account for many important nuclides and the error yielded from this lack of accounting will compound as burnup increases.

For this analysis, differences are quantified by comparing replica MG simulations of the depletion scheme 10-4 with varying addnux parameters from 2 (default; 95 add. nuclides) to 4 (highest; 388 add. nuclides). The simulations used in this study of trace element tracking through the addnux parameter have been extracted from Table 10 and are presented in Table 18.

Table 18. Trace Element Tracking (addnux) Simulations Used.

Model	Run	Addnux	Est. MTIHM	Depletion Scheme	Self-shielding	Library	Cluster	gen	npg	nsk	MPI Processes	Average Parallel Efficiency [%]	Wallclock time [hours]	Average k_eff Uncertainty [pcm]
0003	**v04**	4	0.292513	10-4	CENTRM	MG	INL-ST	350	400000	50	240	26.143	27.444	9.4
0004	**v02**	3	0.292513	10-4	CENTRM	MG	INL-ST	350	400000	50	240	26.852	25.761	9.5
0004	**v03**	2	0.292513	10-4	CENTRM	MG	INL-ST	350	400000	50	240	27.123	24.876	10.2
0006	v01	4	0.292513	10-2	CENTRM	CE	INL-ST	250	300000	50	1440	36.722	18.630	13.0
0006	v02	4	0.292513	10-4	CENTRM	CE	INL-ST	350	400000	50	1440	48.196	53.324	10.2
0007	v01	3	0.292513	10-2	CENTRM	CE	INL-ST	250	300000	50	720	45.175	15.893	13.5
0007	v02	3	0.292513	10-2	CENTRM	CE	INL-ST	250	300000	50	720	33.441	8.748	14.1

3.3.3.1 Multiplication Factor k_{eff}

Figure 42 shows k_{eff} of the replica simulations for varying addnux parameters. Figure 43 and Figure 44 show that from addnux=2 to addnux=4 the k_{eff} experiences a decrease of 167-pcm; and from addnux =2 to addnux=3 it experiences a ~7-pcm decrease.[e] Furthermore, the absolute difference in k_{eff} grows only slightly with increasing burnup for

[e] A figure for addnux=3 to addnux=4 was not added because it is indistinguishable from the addnux=2 to addnux=4 figure

addnux=2 vs addnux=3; while that absolute difference for addnux=2 to addnux=4 grows significantly as burnup increases. This suggests that there is an additional nuclide between addnux=3 and addnux=4 that yields significant effects on reactivity estimates with increasing burnups. Additionally, this additional nuclide being found in addnux=4 but not addnux=3 indicates that it is a nuclide that is found in significantly less quantities in LWRs. This can potentially be explained by the inclusion of H-3 and He-3 in addnux=4, which is produced significantly more by the $Li^7(n,\alpha, n)H^3$ reaction in FLiBe-fueled MSRs. H-3 decays to He-3, a significant thermal neutron absorber, by beta decay with a half-life of 12.3-years (the total lifetime of this simulation accounts for ~17 years). Because of the new accountancy of the H-3 → He-3 reaction and He-3 concentrations, it is possible that the k_{eff} difference growth over time was primarily dominated by accountancy of H-3 and He-3.

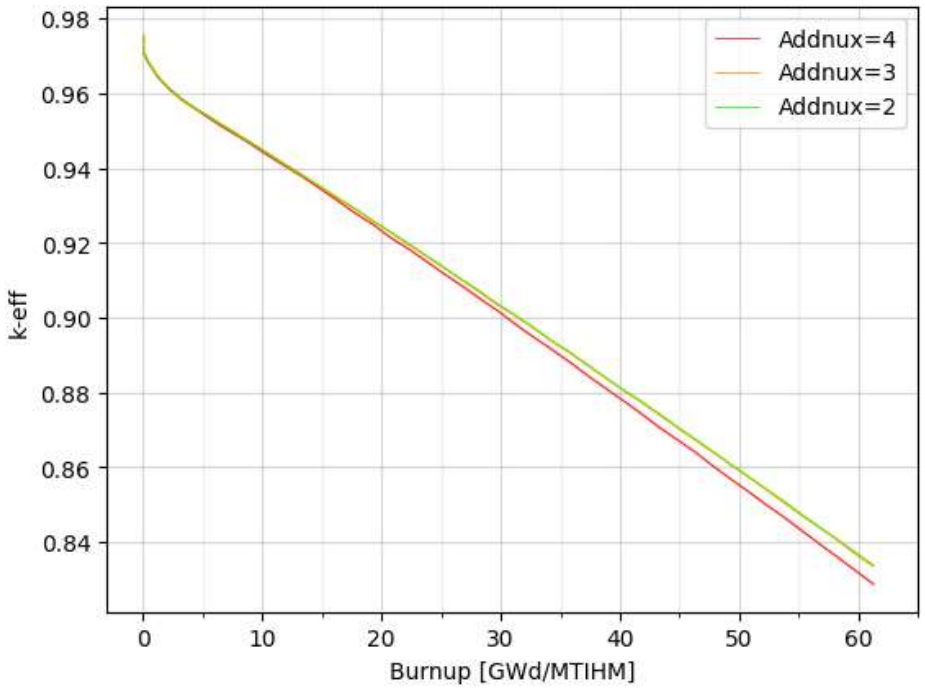

Figure 42. k_{eff} vs burnup of Scheme 10-4 for varying addnux parameters (±σ error bars are shown but are too small to be visible)

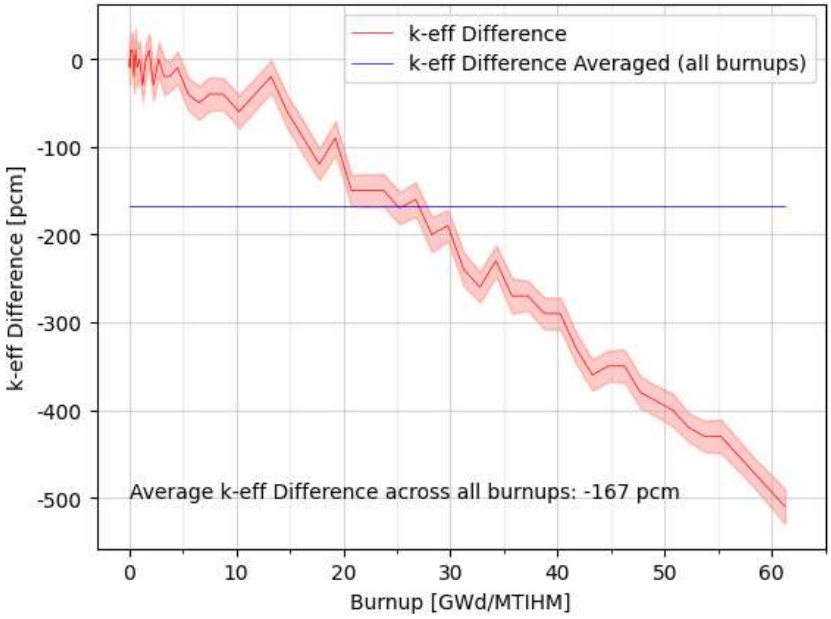

Figure 43. k_{eff} difference from addnux=2 to addnux=4 across all burnups

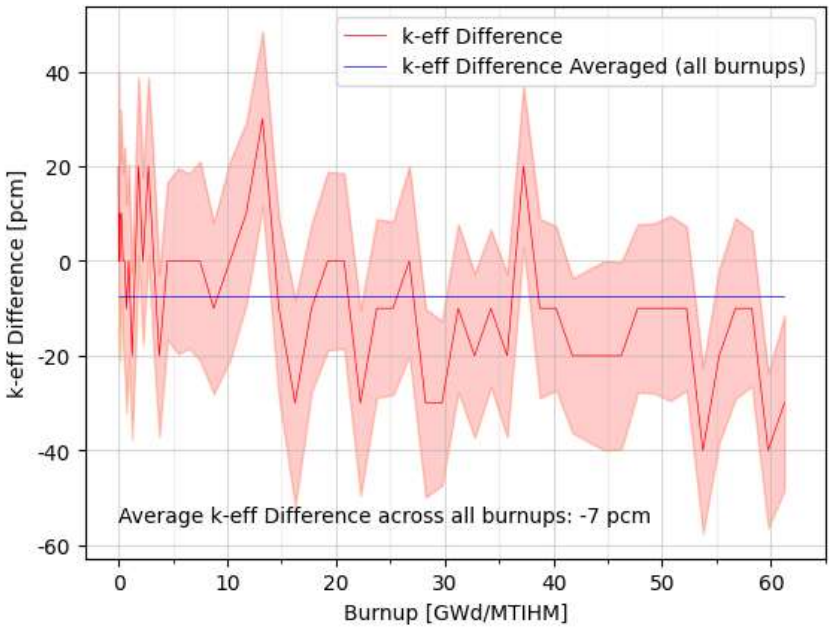

Figure 44. k_{eff} difference from addnux=2 to addnux=3 across all burnups

Analysis was also conducted on k_{eff} differences for CE addnux=2 to addnux=4. The results of which were indistinguishable from that of MG simulations and were thus not included.

3.3.3.2 Isotopic Concentrations

Due to the inability to analyze differences of the nuclides which were initialized in one addnux variation but not in the other, further analysis was conducted using only those nuclides of interest (Table 4) found in addnux=2 to ensure that all analyses would incorporate only mutually initialized and tracked nuclides; these nuclides can be found in Table 19.

Table 19. Nuclides of Interest found in addnux=2

Element	Z	N	SCALE Symbol
Zr	40	91	zr-91
Zr	40	93	zr-93
Zr	40	94	zr-94
Zr	40	95	zr-95
Mo	42	95	mo-95
Mo	42	97	mo-97
Mo	42	99	mo-99
Tc	43	99	tc-99
Ru	44	103	ru-103
Ru	44	106	ru-106
Pd	46	107	pd-107
Cd	48	113	cd-113
Sn	50	126	sn-126
I	53	129	i-129
Xe	54	131	xe-131
Xe	54	133	xe-133

Xe	54	135	xe-135
Cs	55	134	cs-134

Table 19 continued

Cs	55	135	cs-135
Cs	55	137	cs-137
Ba	56	140	ba-140
Ce	58	143	ce-143
Sm	62	149	sm-149
Sm	62	151	sm-151
Sm	62	153	sm-153
U	92	234	u-234
U	92	235	u-235
U	92	236	u-236
U	92	238	u-238
Np	93	237	np-237
Pu	94	238	pu-238
Pu	94	239	pu-239
Pu	94	240	pu-240
Pu	94	241	pu-241
Pu	94	242	pu-242
Am	95	241	am-241
Am	95	243	am-243
Am	95	242m	am-242m
Cm	96	242	cm-242
Cm	96	243	cm-243
Cm	96	244	cm-244

In Figure 45, the average maximum actinide percent difference from addnux=2 to addnux=4 is shown to be high at low burnups (~100% difference at 0.05 GWd/MTIHM) but converges to near-zero by ~10 GWd/MTIHM (average of 0.41% difference at >10 GWd/MTIHM). The disparity seen in the early transient stages is dominated by Am-243

and at burnups >1 GWd/MTIHM the near-zero difference is dominated exclusively by Cm-243.

Figure 47 shows again that these particular nuclides yield near-zero concentrations and thus any deviation may be through stochastic uncertainty. Significant nuclides in this case may be U-235 and Pu-240, which experience concentration differences of 10-grams and 25-grams, respectively. For thorough analysis of actinides, the actinide percent difference at EOL is provided in Figure 46.

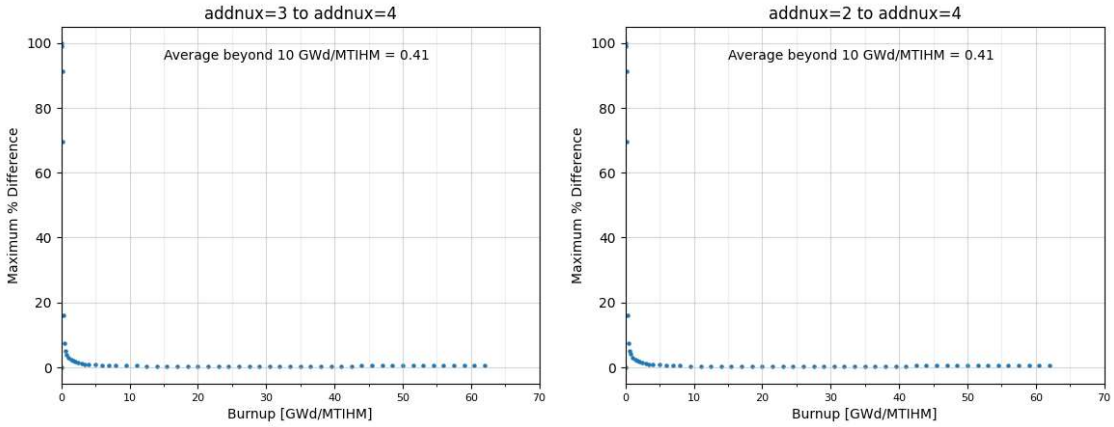

Figure 45. Maximum percent differences between addnux parameters for nuclides included in addnux=2.

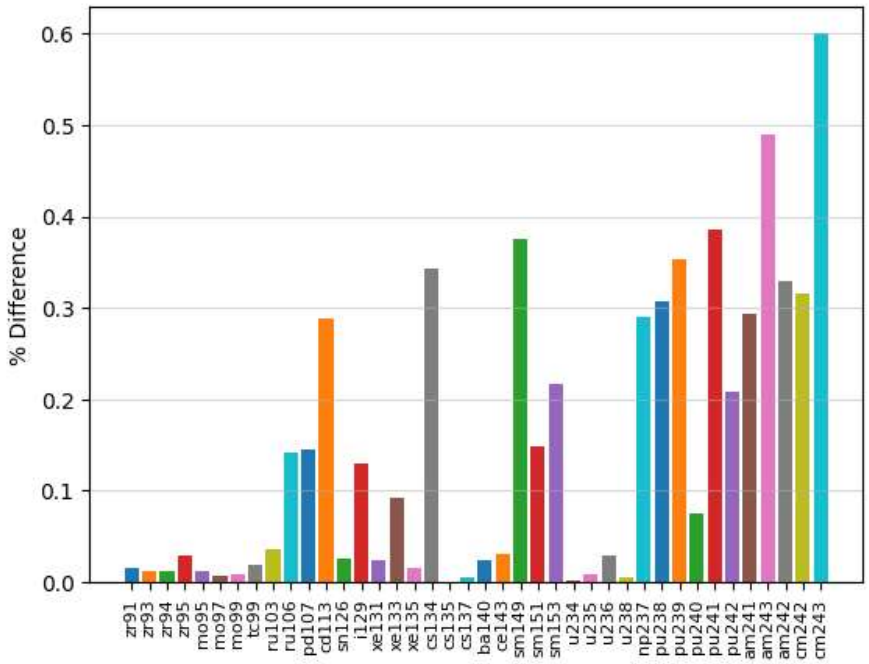

Figure 46. EOL percent differences from addnux=2 to addnux=4 of nuclides included in addnux=2.

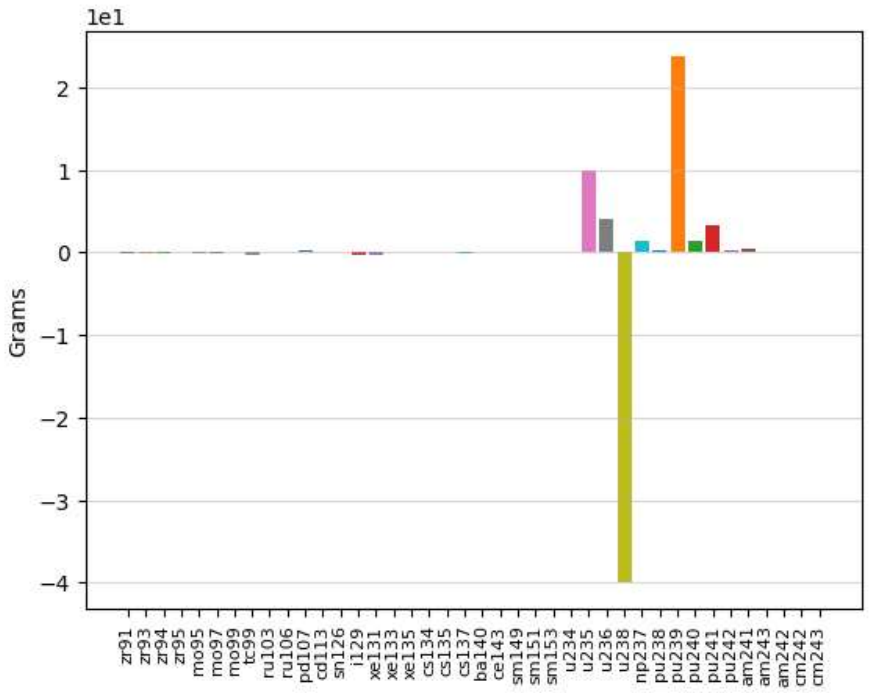

Figure 47. EOL mass differences from addnux=2 to addnux=4 of nuclides included in addnux=2.

Because of the questionable significance of the maximum percent difference of many actinides, Figure 48, Figure 49, and Figure 50 were used to analyze the most significantly radioactive nuclides, the FLiBe fuel nuclides, and Uranium isotopes of interest, respectively.

Figure 48 shows that, Curium nuclides yields the highest percent difference (~0.75%) at EOL from addnux=2 to addnux=4, which is again a near zero mass difference. The maximum percent difference is always dominated by Cm-244 nuclides across all burnups in this case. All analyzed significant radioactive isotopes differences yielded are below 1-gram. Across all burnups beyond 10 GWd/MTIHM, the average maximum % difference is 0.49%.

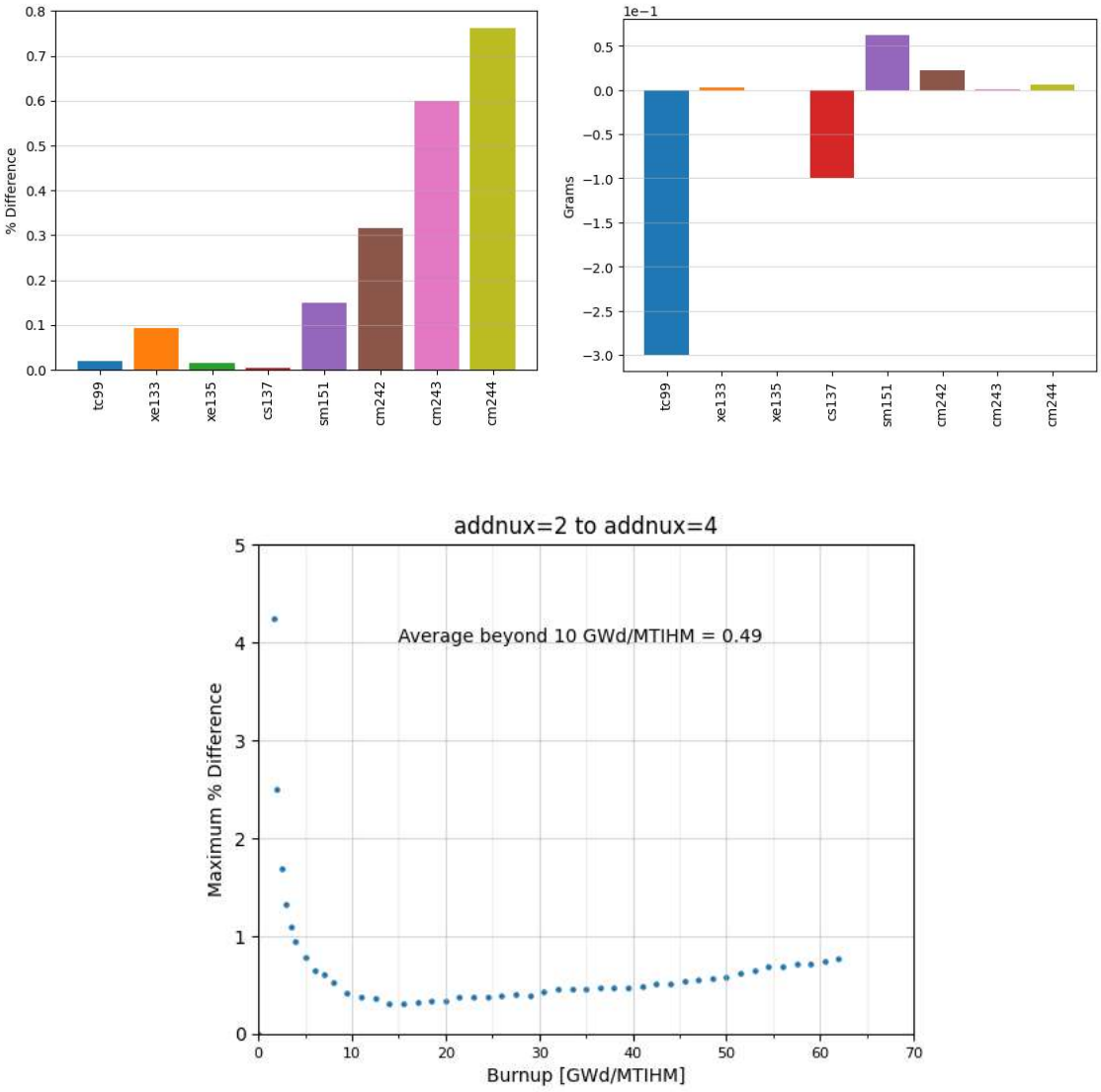

Figure 48. EOL concentration differences and maximum percent difference for significantly radioactive nuclides within addnux=2 from addnux=2 to addnux=4

Figure 49 and Figure 50 show that none of the fueled nuclides experience significant difference from addnux=2 to addnux=4, with the maximum percent difference across all burnups being less than 0.1%, and the maximum percent difference being primarily dominated by Li-6 at all burnups. Notably, U-235 experiences a significantly higher EOL percent difference from addnux=2 to addnux=4 than U-238, but both remain below 0.02%

difference. This is because the mass of U-235 in the system is significantly less than that of U-238.

Figure 50 shows that U-235 and U-238 experience extremely low maximum percent difference from addnux=2 to addnux=4 (on the order of single-atom difference). The reason for the seemingly random occurrence of datapoints jumping up and down (as seen at 20 GWd/MTIHM) is likely due to such a low percent change being shown only in the last significant decimal place (machine precision) combined with the stochastic uncertainty of the U-235 and U-238 concentrations.

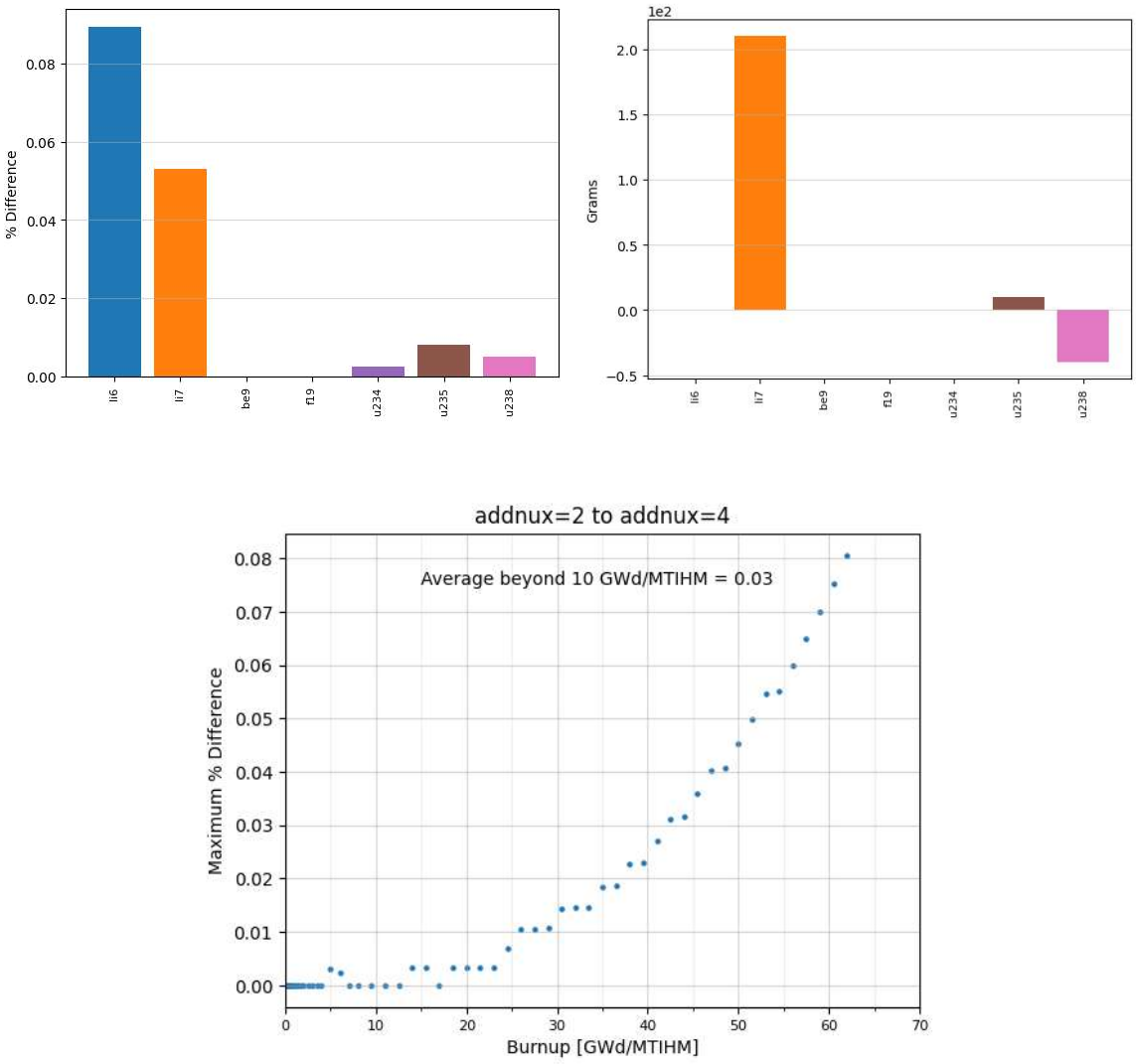

Figure 49. EOL concentration differences and maximum percent difference for fueled FLiBe from addnux=2 to addnux=4

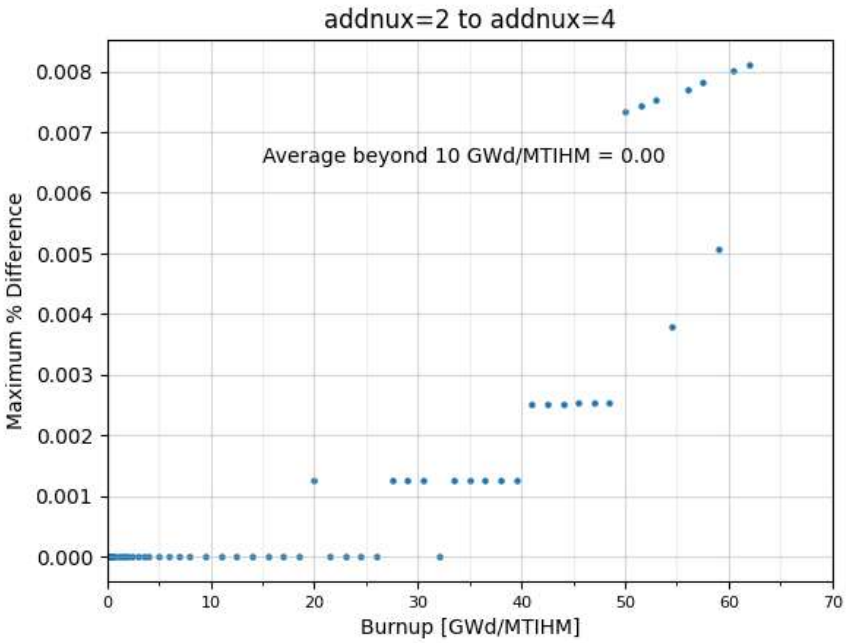

Figure 50. Maximum percent difference for uranium isotopes from addnux=2 to addnux=4

Analysis was also conducted on isotopic concentration differences for CE addnux=2 to addnux=4. The results of which were indistinguishable from that of MG simulations and were thus not included. Notably, the only distinguishable difference between CE addnux analysis and MG addnux analysis were Uranium-235 and U-238 concentrations (which have been seen and studied previously in 3.3.2.2 Isotopic Concentrations), and convergence of Li-7 concentrations from 0.05% in MG to ~0.00% in CE.

3.3.3.3 Computational Resources

Figure 51 shows the relationship between addnux parameter and estimated serial runtime for this particular MG model. As shown, the estimated runtime difference from addnux=2

to addnux=4 is relatively low (~6.3% increase in runtime) resulting in only a ~2.6-hour increase (from 24.9 hours to 27.4 hours).

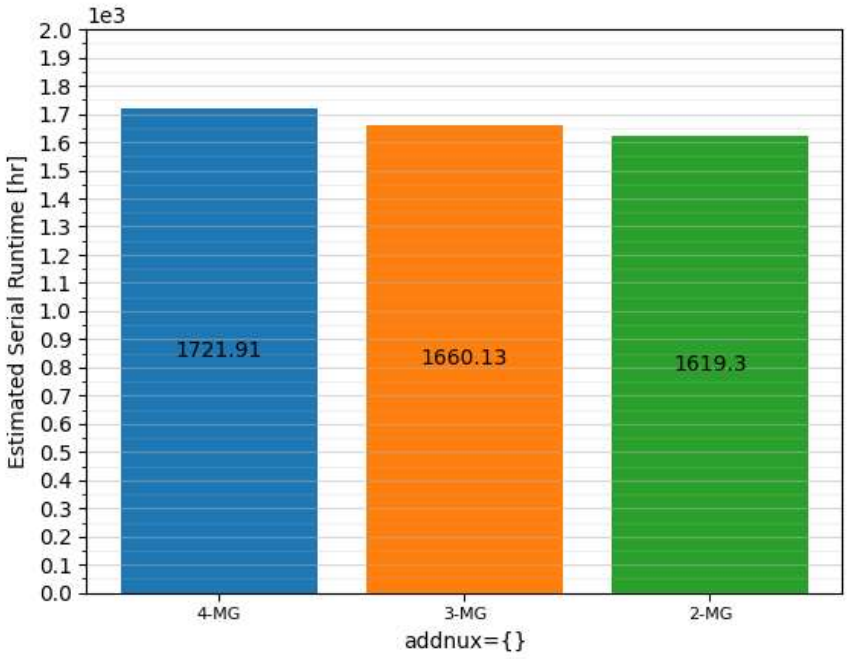

Figure 51. Est. serial runtime for varying addnux parameters for MG

Because of the addnux parameter changing the nuclides that are being tracked and analyzed, it can be understood that computational runtimes of addnux variations will be more significant when using CE over MG because of the significantly longer runtime associated with running and utilizing CE libraries in simulation. So, it is important to study the effects of CE addnux parameter variation rather than MG addnux parameter variation.

For CE, Figure 52 and Figure 53 show the relationship between addnux parameter and estimated serial runtime for this CE model. As shown, the estimated runtime difference from addnux=2 to addnux=4 is significant (~4.7x increased runtime).

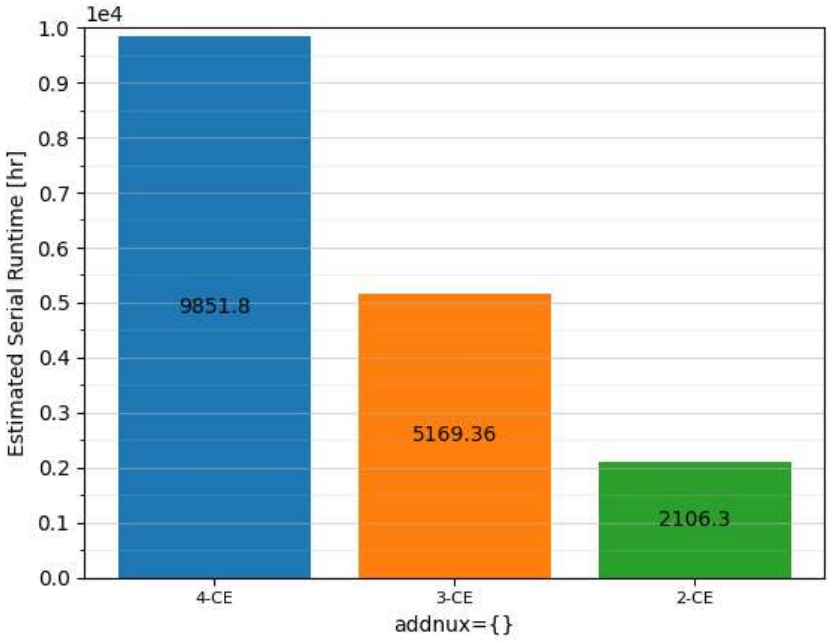

Figure 52. Est. serial runtime for varying addnux parameters for CE

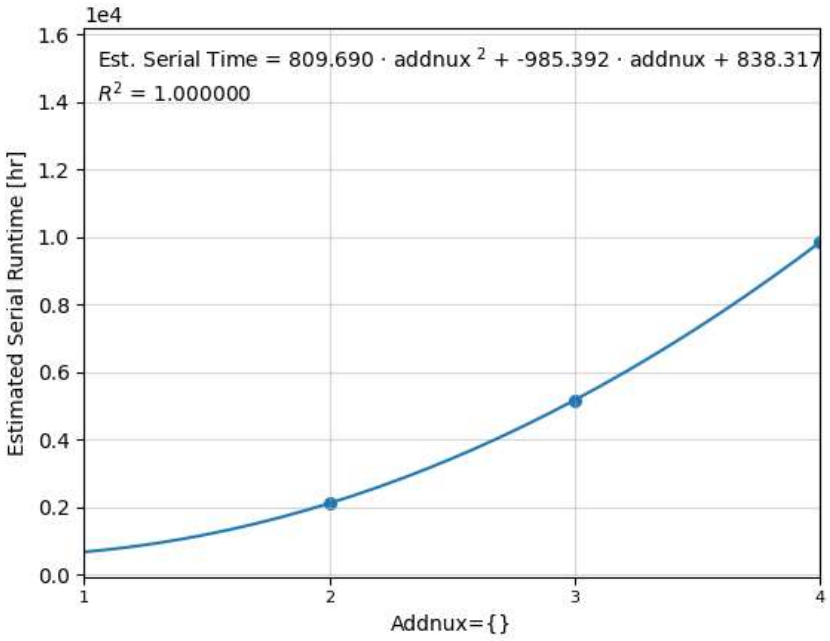

Figure 53. Estimated serial time vs addnux parameter for CE

3.3.4 Specific Power

Different MSR designs will experience different specific powers [MW/MTIHM], therefore analysis of the sensitivity of k_{eff} estimates and radionuclide concentrations on specific power is a crucial step in being able to extrapolate the results of this thesis outside of this particular MSR model.

For this analysis, replica simulations were run using specific powers of 10 MW/MTIHM and 20 MW/MTIHM. The simulations used in this study of specific power have been extracted from Table 10 and are presented in Table 20.

Table 20. Specific Power Simulations Used.

Model	Run	Addnux	Est. MTIHM	Depletion Scheme	Self-shielding	Library	Cluster	gen	npg	nsk	MPI Processes	Average Parallel Efficiency [%]	Wallclock time [hours]	Average k_eff Uncertainty [ncml
0002	v05	4	0.292513	20-8	CENTRM	MG	INL-ST	350	400000	50	240	26.427	54.051	10.2
0003	v05	4	0.292513	10-8	CENTRM	MG	INL-ST	350	400000	50	240	26.143	53.989	9.7

3.3.4.1 Multiplication factor k_{eff}

Figure 54 shows k_{eff} of the replica simulations with different specific powers of 10 and 20 MW/MTIHM. Figure 55 shows that k_{eff} from 10 to 20 MW/MTIHM experiences an average decrease of ~291-pcm with the k_{eff} difference converging to zero as burnup increases. This k_{eff} difference is due to the increased specific power yielding increased equilibrium concentrations of certain neutron absorber fission products (notably xenon and tellurium; discussed in 3.3.4.2 Isotopic Concentrations). Additionally, the reason for the

convergence of k_{eff} difference to zero as burnup increases may be explained by the higher neutron poison concentrations resulting in a harder neutron spectrum and thus converting more fissile plutonium as burnups increase. This would result in gradually compensating the effect of initially reduced k_{eff} and its slow rising back to the 10 MW/MTIHM simulation values in the 20 MW/MTIHM simulation, as seen in Figure 55.

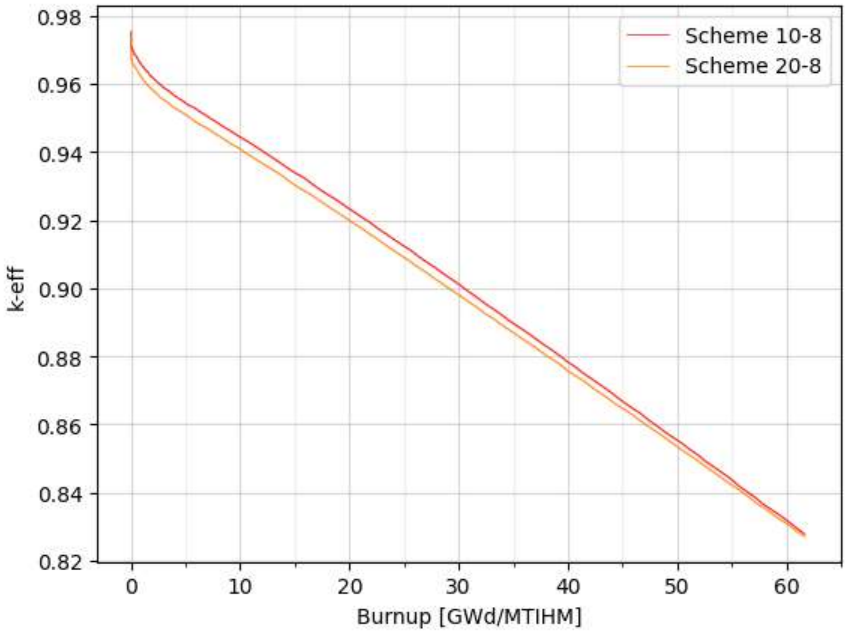

Figure 54. k_{eff} vs burnup varying specific power (±σ error bars are shown but are too small to be visible)

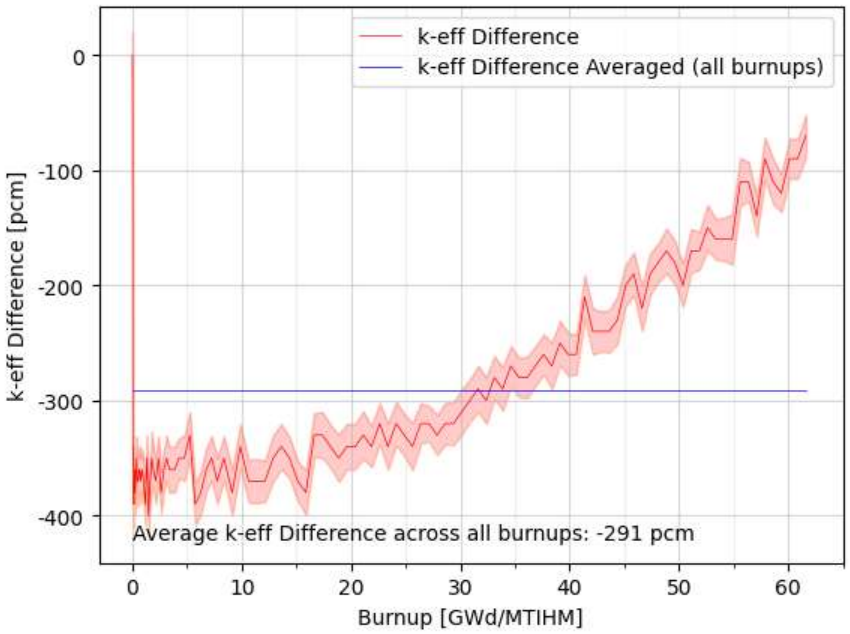

Figure 55. k_{eff} difference from 10 MW/MTIHM to 20 MW/MTIHM across all burnups

3.3.4.2 Isotopic Concentrations

In Figure 56, the average maximum percent difference between actinides of different depletion schemes are shown to converge to ~ 144.31% beyond 3 GWd/MTIHM. This was an expected result due to the fact that differeing specific powers should yield isotopic transmutation rates of relatively constant percent difference. This maximum percent difference is dominated by Pu-243 (half-life: 4.956 hours) until ~30 GWd/MTIHM, after which it is dominated by Cf-252 (half-life: 2.645 years). Both of these nuclides have short half-lives relative to the depletion lifetime, therefore the shortened depletion *time*-steps (same sized burnup steps) of the 20 MW/MTIHM simulation would yield higher concentrations of these isotopes at all burnups.

As expressed in Figure 58, the maximum percent difference in actinides is usually dominated by low-concentration nuclides, such as Pu-243, Ac-225, and Cf-252. Figure 59 shows that these particular nuclides yield near-zero concentrations, in alignment with previous analyses.

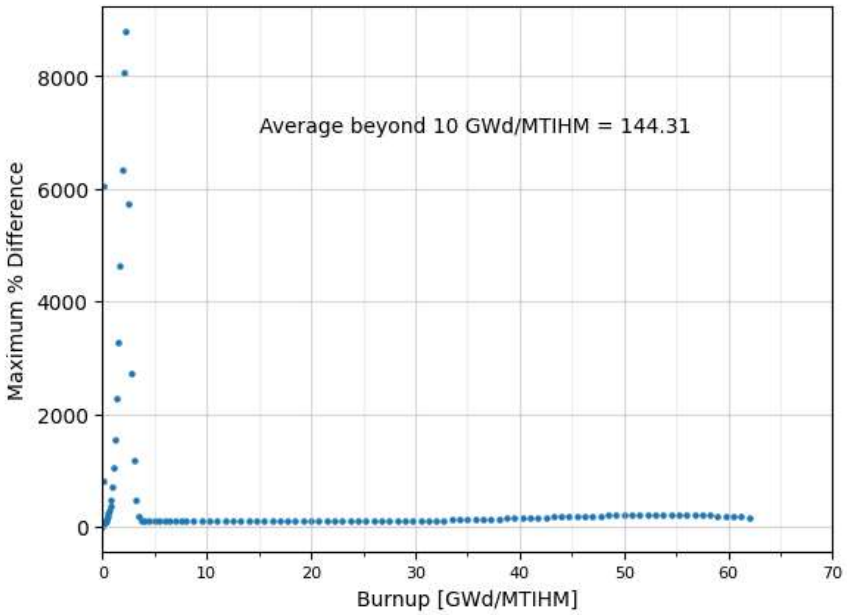

Figure 56. Maximum actinide percent differences across burnups from Scheme 10-8 to 20-8

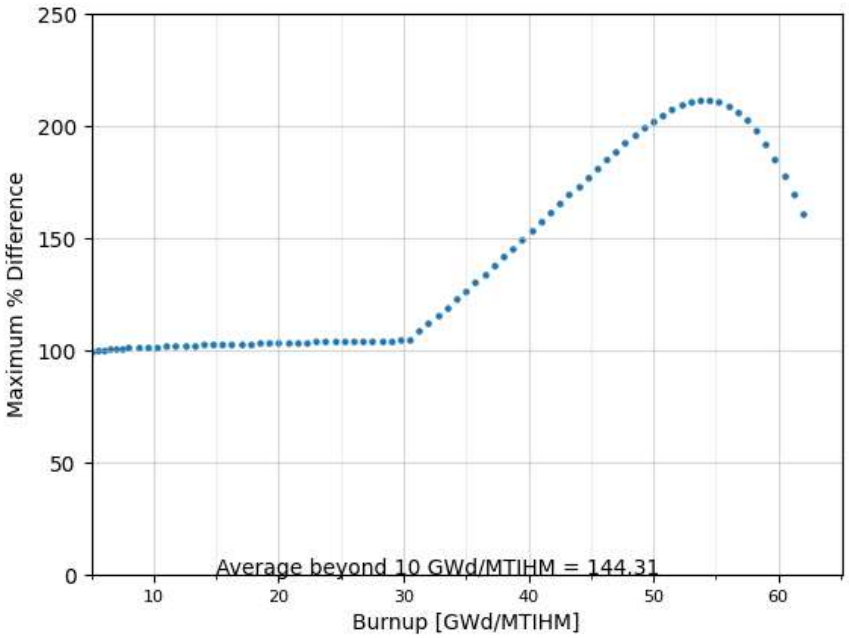

Figure 57. Zoom in of Figure 56.

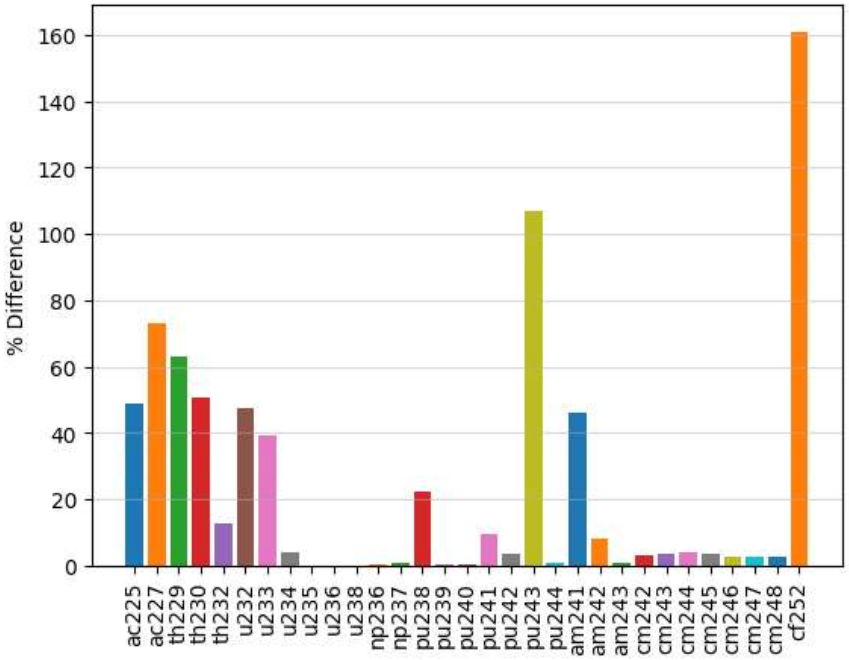

Figure 58. EOL actinide percent differences from Scheme 10-8 to 20-8

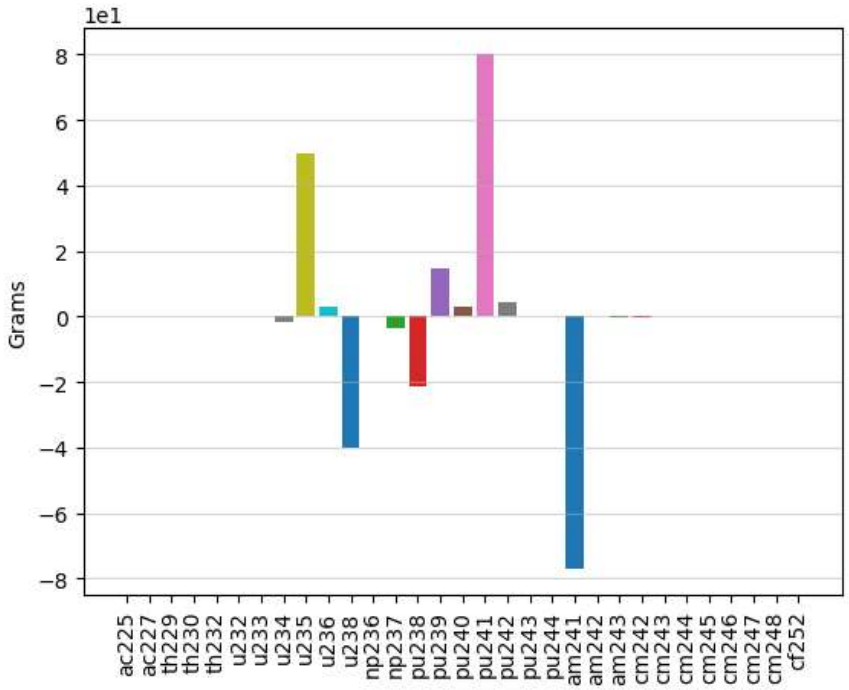

Figure 59. EOL actinide mass differences from Scheme 10-8 to 20-8

Due to the questionable significance of the maximum percent difference of actinides when some actinides yield such low concentrations, Figure 60, Figure 63, and Figure 64 were used to analyze the most significantly radioactive nuclides, the nuclides found in the FLiBe fuel, and Uranium isotopes of interest, respectively.

Figure 60 shows that Xe-133, Xe-135, Te-132, and Cf-252 yield the highest percent differences. The significant rise in percent difference starting at ~30 GWd/MTIHM is the point at which Cf-252 begins to experience increasing percent difference (i.e. the maximum percent difference is dominated exclusively by Cf-252 after 30 GWd/MTIHM while Xe-133, Xe-135, and Te-132 dominate before 30 GWd/MTIHM). The consistency of the Xenon and Tellurium percent difference at each burnup is represented in Figure 61 and

Figure 62, respectively. This is intuitive due to the difference in specific power yielding different equilibrium concentrations for varying nuclides, including Xenon and Tellurium.

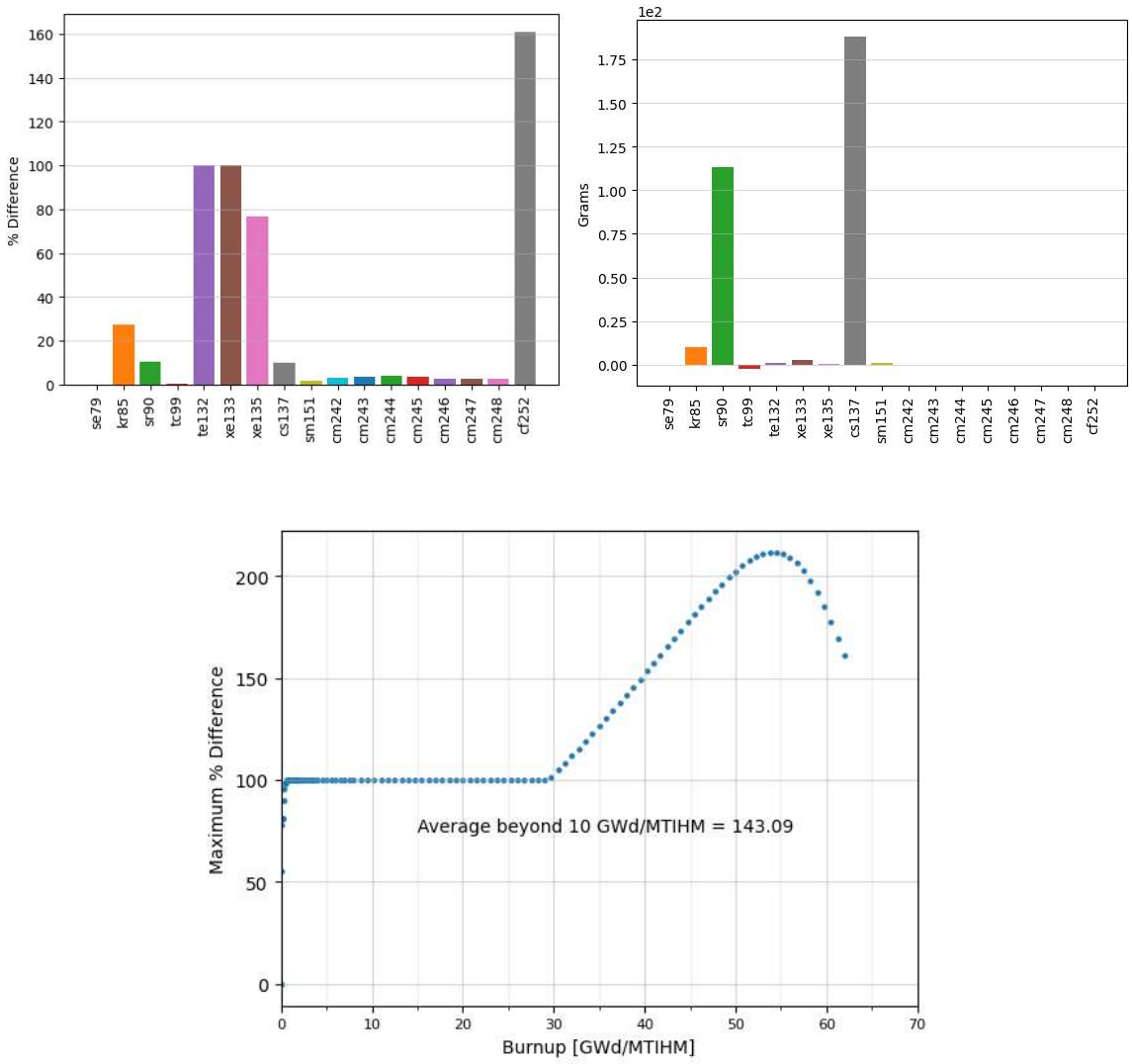

Figure 60. EOL concentration differences and maximum percent difference for significantly radioactive nuclides from Scheme 10-8 to 20-8

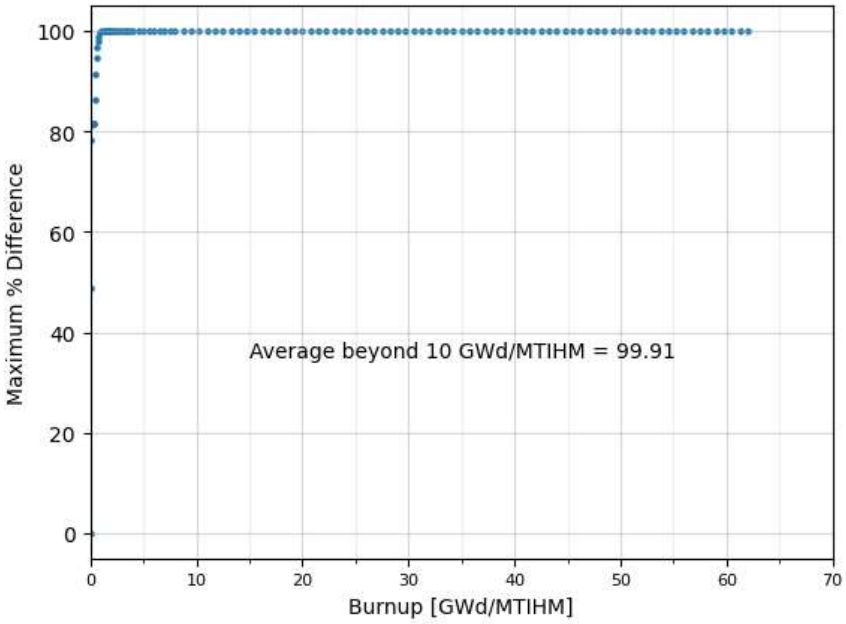

Figure 61. Max percent difference of Xe-133 and Xe-135

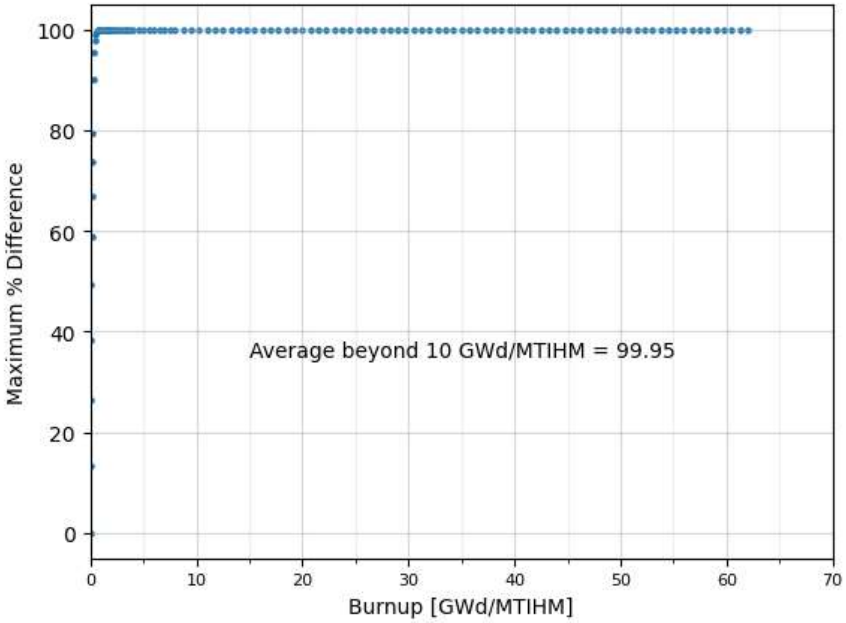

Figure 62. Max percent difference of Te-132

Figure 63 and Figure 64 show that U-234 experiences ~4% difference from 10 MW/MTIHM to 20 MW/MTIHM at EOL; however all other FLiBe fuel nuclides experience <2% difference at EOL. U-235 and U-238 experience ~0.01% difference at EOL.

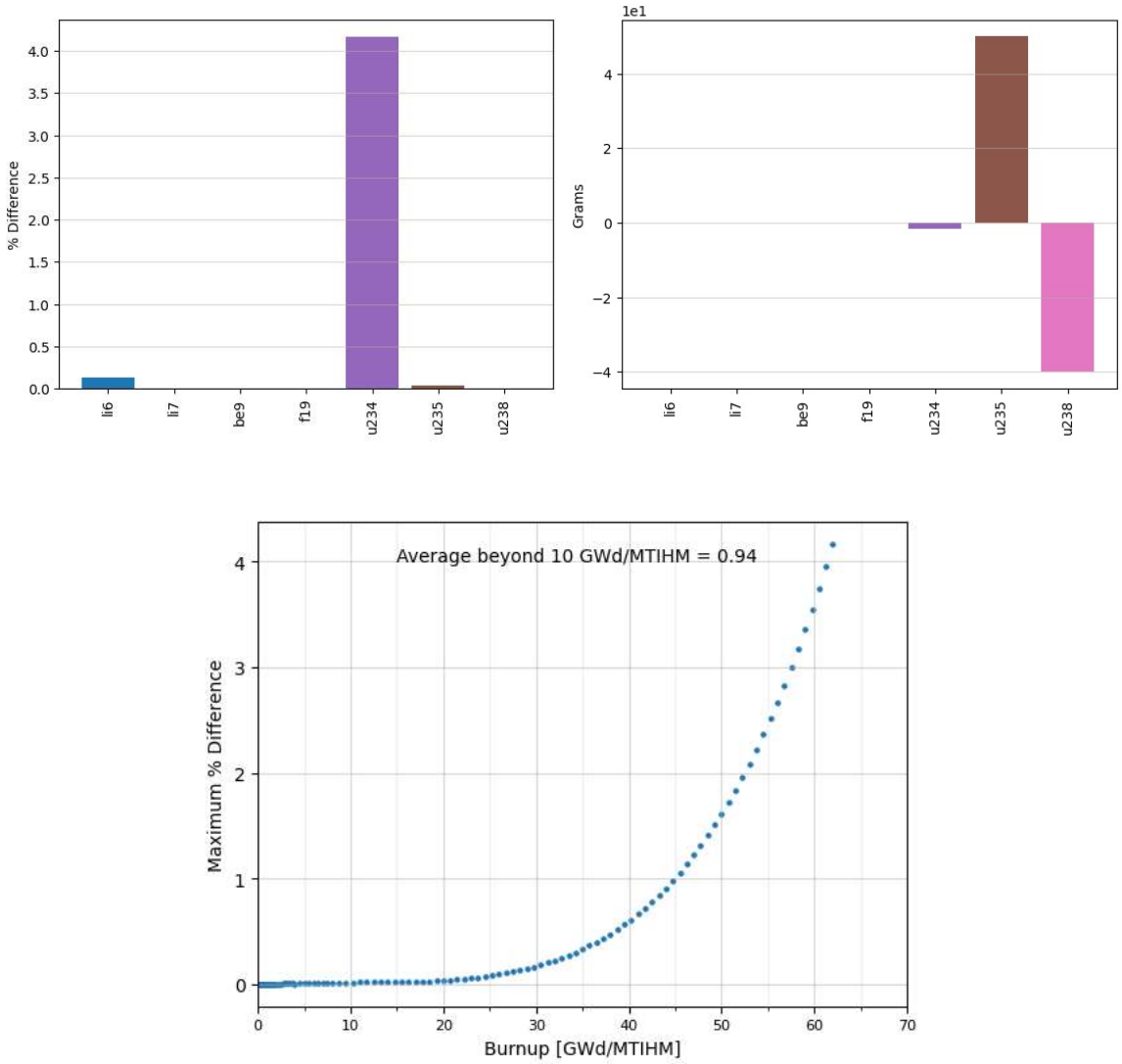

Figure 63. EOL concentration differences and maximum percent difference for fueled FLiBe from Scheme 10-8 to 20-8

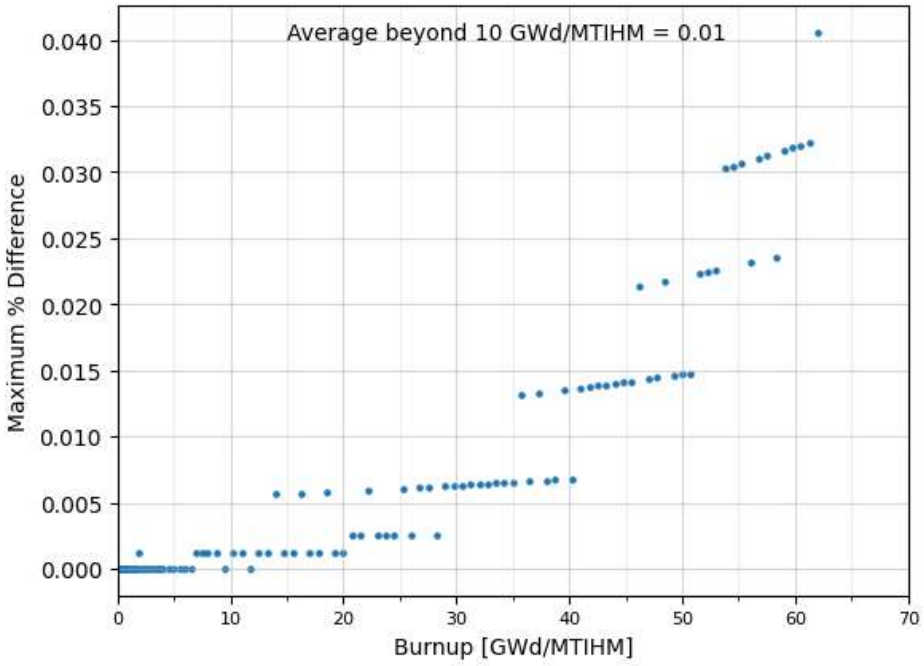

Figure 64. Maximum percent difference for uranium isotopes from Scheme 10-8 to 20-8

3.3.4.3 Computational Resources

Figure 65 shows that, intuitively, there was near-zero effect on computational serial time between specific powers. This is intuitive due to the fact that specific power does not change the rate at which computations may be performed.

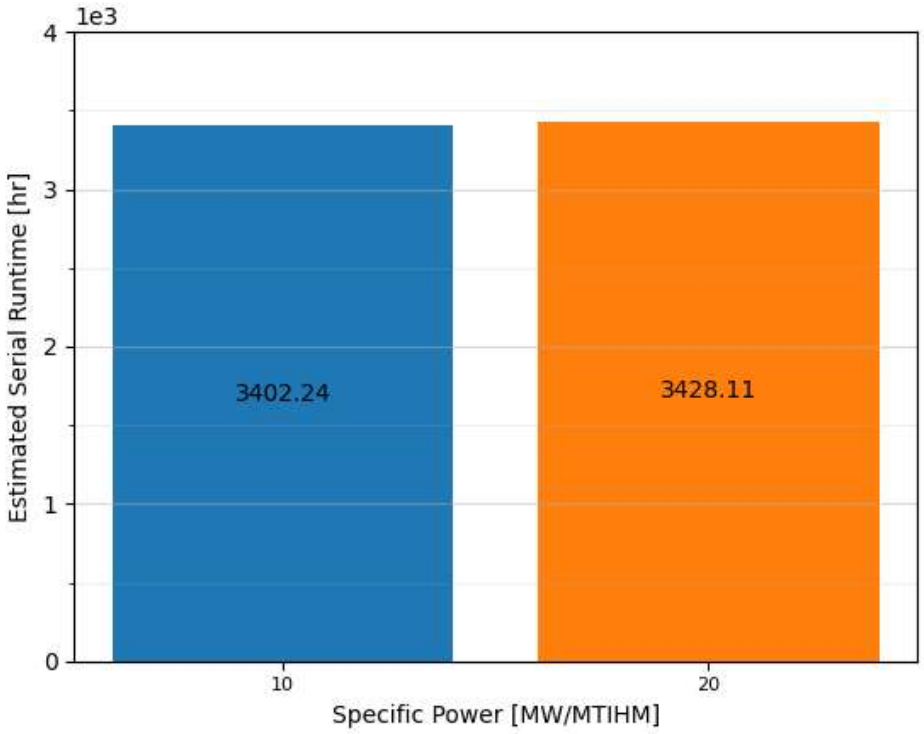

Figure 65. Estimated serial runtime vs specific power for 240 MPI processes on INL's Sawtooth cluster

4 SUMMARY OF FINDINGS, CONCLUSIONS AND RECOMMENDATIONS

The results of the analyses can be summarized into Table 21 which provides information on differences between replica simulations averaged across all burnups >10 GWd/MTIHM, and Table 22, which provides information on max percent and max mass differences at EOL.

Table 21. Parameters Effects on k_{eff}, Average Maximum Nuclide Concentration Percent Differences, and Serial Runtime.

Study	Depletion Sub-interval Scheme			Self-shielding Method	Cross-section Library	Trace Elements (only nuclides in addnux=2; MG)			Specific Power
	10-2 to 10-8	10-2 to 10-4	10-4 to 10-8	BONAMI to CENTRM	MG to CE	addnux=2 to addnux=4	addnux=2 to addnux=3	addnux=3 to addnux=4	10 to 20 MW/MTIHM
Average keff diff. [pcm]	<10	<10	<10	-226	148	-167	-7	-160	-291
Actinide max % diff.	0.32	0.28	0.22	2.51	6.97	0.41	-	0.41	144.31
Sig. radioactive max % diff.	5.10	-	-	2.51	4.09	0.49	-	-	143.09
FLiBe max % diff.	0.00	-	-	0.03	0.24	0.03	-	-	0.94
uranium max % diff.	0.00	-	-	0.03	0.06	0.00	-	-	0.01
% diff. on est. serial runtime [hr]	303.19	101.08	100.51	6.81	1038.75	6.33	2.52	3.72	~0.00

Table 22. Parameters Effects on EOL Nuclide Concentrations.

Study	Depletion Sub-interval Scheme		Self-shielding Method		Cross-section Library		Trace Elements (note the nuclides in addnux2)		Specific Power	
	10-2 to 10-8		BONAMI to CENTRM		MG to CE		addnux=2 to addnux=4		10 to 20 MW/MTIHM	
	Max % Diff.	Max Mass Diff.	Max % Diff.	Max Mass Diff.	Max % Diff.	Max Mass Diff.	Max % Diff.	Max Mass Diff.	Max % Diff.	Max Mass Diff.
Actinide	Pu-243	U-236	Cm-248	U-238	Cm-243	U-238	Cm-244	U-238	Cf-252	Pu-241
% Diff.	0.28	0.01	2.83	0.02	3.53	0.03	0.76	0.01	160.93	9.30
Δ Mass [g]	-5.30E-06	-1.00E+00	6.25E-10	-1.50E+02	-2.54E-03	2.70E+02	6.26E-03	-4.00E+01	3.17E-12	8.02E+01
Sig. Rad.	Xe-133	Tc-99	Cm-248	Sr-90	Cm-243	Sr-90	Cm-244	Sr-90	Cf-252	Cs-137
% Diff.	5.09	1.39	2.83	0.09	3.53	0.16	0.76	0.03	160.93	9.73
Δ Mass [g]	1.44E-01	2.24E+01	6.25E-10	1.00E+00	-2.54E-03	1.80E+00	6.26E-03	-3.00E-01	3.17E-12	1.88E+02
Fuel Salt	Li-6	Li-6	U-235	Li-7	U-234	U-238	Li-6	Li-7	U-234	U-235
% Diff.	0.00	0.00	0.07	0.05	0.42	0.03	0.09	0.05	4.17	0.04
Δ Mass [g]	1.00E-03	1.00E-03	9.00E+01	2.10E+02	-1.66E-01	2.70E+02	2.00E-02	2.10E+02	-1.66E+00	5.00E+01
Top 30 (by mass)	Mo-97	Mo-97	Cs-134	Li-7	Pu-242	U-238	Pu-241	Li-7	Cs-134	Cs-135
% Diff.	1.48	1.49	2.35	0.05	2.81	0.03	0.39	0.05	59.19	10.26
Δ Mass [g]	2.34E+01	2.34E+01	8.58E-01	2.10E+02	-3.78E+00	2.70E+02	3.31E+00	2.10E+02	2.22E+01	-2.20E+02

Overall, these analyses quantified several tradeoffs between simulation accuracy and required computational resources for SCALE fluoride-MSR simulation parameters. Decisions on whether to use a more accurate and more computationally expensive simulation, or a less accurate but significantly faster depletion will depend on each specific application; quantification provided here may help guide that decision.

4.1 Numerical Parameter Sensitivity

Analysis of k_{eff} and radionuclide concentration sensitivity to numerical parameters within this thesis is led by the study of varying depletion sub-interval schemes on this MSR model. Parallelization of SCALE 6.2.4 MSR models was also studied.

4.1.1 Parallelization

The study of parallelization and read/write processes was shown to be associated more with computer science than nuclear physics and engineering, so was left as a simple comparison between INL's Sawtooth cluster (INL-ST) and Georgia Institute of Technologies Firebird cluster (GT-FB). This comparison showed that while INL-ST yields more cores per node (thus less cross-node communication), it in fact performs calculation in SCALE 6.2.4 slower than GT-FB. The causes of this effect may be several, including less efficient parallel processing and less efficient read/write processing (e.g. slower to load cross-section libraries). These causes are suggested by the fact that both parallel and serial process times are longer than those on GT-FB for identical simulations. Technically, GT-FB yields faster performance than INL-ST; however INL-ST provides benefits through the sheer number of available cores (~100,000 on INL-ST compared to ~1000 for the equivalent export-controlled system on GT-FB) and through the free-use of INL-ST when

compared to the ~$0.0067 per CPUhr charge on GT-FB. In conclusion, although GT-FB may be able to compute faster (~40% faster) for this and similar MSR models, INL-ST offers ~9,900% more cores[f] for users and at no cost per CPUhr.

4.1.2 Depletion Sub-intervals

The study of depletion sub-intervals schemes proved that actinides and FLiBe fuel salt nuclides remain relatively stable from coarser to finer depletion schemes but several key radioactive nuclides, namely Tc-99, Mo-97, and Xe-133, undergo relatively significant changes. These depletion schemes correspond to ~3 GWd/MTIHM depletion burnup steps for the coarsest, and ~0.75 GWd/MTIHM depletion burnup steps for the finest (full depletion scheme found in Table 12 through Table 26). From the coarsest to the finest depletion schemes, the following was experienced (Table 21 and Table 22):

- Xe-133 concentrations experienced a 5.09% increase (0.144 grams)
- Tc-99 concentrations experienced a 1.39% increase (22.4 grams)
- Mo-97 concentrations experienced 1.48% increase (23.4 grams)
- All other Top 30 concentration nuclides (Table 9) were shown to experience a percent difference of < 0.06%
- k_{eff} experienced negligible effect (i.e. change in k_{eff} was within k_{eff} uncertainty)
- # of depletion sequences experienced a 4x increase, thus est. serial runtime experienced a ~4x increase

[f] Although there are more users on INL-ST than GT-FB, acquiring 1000+ cores (more than the entirety of GT-FB) on INL-ST is relatively easy

The reason for these relatively higher differences in Xe-133, Tc-99, and Mo-97 are due to their roles as short-lived fission products or daughters of decaying short-lived fission products. This is important because the depletion calculations within the early transient stage of the reactor core environment must occur in short enough time-steps to account for the rise in these short-lived nuclide concentrations and their convergence to equilibrium concentrations. The half lives for these radionuclides are presented in Table 23. In the case of Tc-99 (which has a longer half-life) its parent, Mo-99, can be considered due to its role as a significant fission product.

Table 23. Half-lives of Nuclides with Significant Concentrations Differences

Radionuclide	Half-life [days]
Xe-133	5.243E+00
Mo-97	stable
Mo-99	2.748E+00
Tc-99	7.705E+07
Tc-99m	2.504E-01

It can be concluded that, within a reasonable depletion scheme, coarser or finer will not significantly affect criticality estimates, actinide concentrations, or any FLiBe salt nuclides. However, depletion sub-intervals must account for fine steps in the transient stage of the reactor core environment when attempting to analyze fission products. The choice of coarse depletion schemes provides a significant benefit in the way of significantly

reducing computational runtime, so is a good tool for those attempting to model MSRs in SCALE with the understanding in mind that fission products, and especially short-lived fission products, may not be accurately represented below 5% concentration certainty.

4.2 Reactor Physics Model Sensitivity

4.2.1 Self-shielding method

The study of SCALE self-shielding methods proved that FLiBe fuel salt nuclides remain relatively stable from BONAMI to CENTRM self-shielding methods but higher actinides undergo relatively significant changes and lead to max percent differences of ~ 2.83% for both major actinides and major radioactive nuclides. From the BONAMI to the CENTRM, the following was experienced (Table 21 and Table 22):

- FLiBe and Uranium nuclides experienced average maximum of 0.03% difference across burnups >10 GWd/MTIHM
- Actinides and significant radioactive nuclides experienced average maximum difference of 2.51% across burnups >10 GWd/MTIHM (dominated exclusively by Curium nuclides higher than Cm-245)
- U-238 experienced the maximum actinide mass difference of -0.02% difference at EOL (-1.50E+02 grams)
- Sr-90 experienced the maximum significant radioactive nuclide mass difference of 0.09% difference at EOL (1 gram)
- U-235 experienced the maximum FLiBe fuel % difference of 0.07% difference at EOL (9.00E+01 grams)

- Li-7 experienced the maximum FLiBe fuel mass difference of 0.05% difference at EOL (2.10E+02 grams)
- Cs-134 experienced the maximum % difference for the top-30 nuclides by mass of 2.35% difference at EOL (8.58E-01 grams)
- k_{eff} decreased by 226-pcm (i.e. BONAMI overestimates k_{eff} compared to CENTRM)
- Est. serial runtime experienced relatively small increase from BONAMI to CENTRM (~6.81%)

The reason for these relatively higher differences in higher actinides, U-238, and U-235 are due to the self-shielding methods resulting in different flux spectrum. The effects from BONAMI to CENTRM can be seen to not only increase the rate of conversion into higher isotopes of Curium, but also the conversion rate of U-238 while the utilization rate of U-235 is decreased. This lends itself to the conclusion that the flux spectrum is hardened (i.e. higher energy on average) by the transition from BONAMI to CENTRM, leading to less absorption by U-235, greater conversion/utilization of U-238, and higher conversions from lower to higher isotopes of Curium.

It can be concluded that there is likely little reason to use BONAMI over CENTRM due to the general difference in flux spectrum leading to >1% difference in most-all transuranic actinides at EOL. The computational benefit of BONAMI only being a ~7% reduction in serial runtime compared to CENTRM is not a significant enough benefit to detract from the accuracy of transuranic nuclide concentrations.

4.2.2 Cross-section Library

The study of continuous-energy vs multigroup cross-section libraries proved that this studied parameter yields the largest effect on nuclide concentrations and runtime. From the 252-MG to CE (both within ENDF/B-VII.1), the following was experienced (Table 21 and Table 22):

- FLiBe nuclides experienced average maximum of 0.24% difference across all burnups >10 GWd/MTIHM
- U-235 and U-238 nuclides experienced average maximum of 0.06% difference across burnups >10 GWd/MTIHM
- Actinides experienced average maximum difference of 6.97% across burnups >10 GWd/MTIHM (dominated exclusively by U-233 until 35 GWd/MTIHM, at which point Cm-243 dominates)
- Significant radioactive nuclides experienced average maximum difference of 4.09% across burnups >10 GWd/MTIHM (dominated exclusively by Cm-242 and Cm-243)
- U-238 experienced the maximum actinide mass difference of 0.03% difference at EOL (2.70E+02 grams)
- Sr-90 experienced the maximum significant radioactive nuclide mass difference of 0.16% difference at EOL (1.80E+00 gram)
- U-234 experienced the maximum FLiBe fuel % difference of -0.42% difference at EOL (-1.66E-01 grams)
- U-238 experienced the maximum FLiBe fuel mass difference of 0.03% difference at EOL (2.70E+02 grams)

- Pu-242 experienced the maximum % difference for the top-30 nuclides by mass of -2.81% difference at EOL (-3.78E+00 grams)
- k_{eff} increased by 148-pcm (i.e. MG underestimated k_{eff} compared to CE)
- Est. serial runtime experienced significant increase from MG to CE (~1000%)

The reason for these relatively higher differences U-238, Pu-242, and lower Curium isotopes (Cm-242 and Cm-243) can be inferred to be caused by an effective increase in the absorption cross-section of U-238 through the multigroup process from CE to 252-MG. Evidence[g] that suggests this includes the decrease in U-238 and the increase in Pu-239 (i.e. U-238 conversion in to Pu-239) . Whereas the self-shielding method seemed to harden the neutron flux spectrum, the use of 252-MG over CE in this model seems to yield an increased effective U-238 absorption cross-section and has been shown to do so in similar studies [13].

4.2.3 Trace Elements (i.e. addnux)

The study of trace element tracking through the "addnux" SCALE parameter proved that actinides, significant radioactive nuclides, and FLiBe fuel salt nuclides all remain relatively stable from coarser to finer addnux (<0.5% difference). From the coarsest trace-element parameter (addnux=2) to the finest trace-element parameter (addnux=4), the following was experienced (Table 21 and Table 22):

- Due to extreme differences between untracked trace-elements, only those nuclides included in addnux=2 were considered (Table 19)

[g] Approaching the analysis from CE to MG requires that all effects from MG to CE be inverted

- FLiBe nuclides experienced average maximum of 0.03% difference across burnups >10 GWd/MTIHM, while U-235 and U-238 experienced ~0.00%
- Actinides and significant radioactive nuclides experienced average maximum difference of 0.41% and 0.49%, respectively, across burnups >10 GWd/MTIHM (dominated exclusively by Cm-244)
- U-238 experienced the maximum actinide mass difference of -0.01% difference at EOL (-4.00E+01grams)
- Tc-99 experienced the maximum significant radioactive nuclide mass difference of -0.02% difference at EOL (-3.00E-01 grams)
- Li-6 experienced the maximum FLiBe fuel % difference of 0.09% difference at EOL (2.00E-02 grams)
- Li-7 experienced the maximum FLiBe fuel mass difference of 0.05% difference at EOL (2.10E+02 grams)
- Pu-241 experienced the maximum % difference for the top-30 nuclides by mass of 0.39% difference at EOL (3.31E+00 grams)
- k_{eff} decreased by 167-pcm (i.e. addnux=2 overestimates k_{eff} compared to addnux=4)
- Est. serial runtime experienced relatively small increase from addnux=2 to addnux=4 (~6.33%)
- Usage of either CE or MG libraries yield indistinguishable results within actinides, and significant radioactive nuclides. FLiBe fuel nuclides concentration differences are also largely indistinguishable, except for Li-7 (which experiences an improved 0.00% difference between addnux parameters in CE) and uranium (which

experiences differences that follow the expectations set in previously discussed MG vs CE analysis).

For MG, it can be concluded that, despite the considerably small change in radionuclide concentrations, there is too large a k_{eff} difference (167-pcm) and too little est. runtime difference (~6%) between addnux=2 and addnux=4 to justify utilizing addnux=2. The same can be said in general between addnux=3 and addnux=4. However, in the consideration of limited computational resources, the studies conducted between the 3 addnux parameters yielded sometimes significant effects on computational memory load. For this reason, the use of lower addnux parameters might be useful in the event of limited computational memory.

For CE, it can be concluded that there is a very significant effect on the computational runtime (~4.7x longer) from addnux=2 to addnux=4 due to the lengthy amount of time necessary to load and utilize CE nuclide libraries in calculations. When using CE over MG, it becomes clear that the drawbacks of higher addnux parameters on computational runtime are much more considerable and the decision of addnux parameter must be considered on a case-by-case basis for the application that is intended for the depletion simulation results.

4.2.4 Specific Power

The analysis of specific power proved that actinides and FLiBe fuel salt nuclides remain relatively stable from coarser to finer depletion schemes but several key radioactive nuclides, namely Tc-99, Mo-97, and Xe-133, undergo relatively significant changes. These depletion schemes correspond to ~3 GWd/MTIHM depletion burnup steps for the coarsest, and ~0.75 GWd/MTIHM depletion burnup steps for the finest (full depletion scheme found

in Table 12 through Table 26). From the coarsest to the finest depletion schemes, the following was experienced (Table 21 and Table 22):

- FLiBe and Uranium nuclides experienced average maximum of 0.94% difference and 0.01% difference, respectively, across burnups >10 GWd/MTIHM
- Actinides experienced average maximum difference of 144.31% difference across burnups >10 GWd/MTIHM (dominated exclusively by Pu-243 until 30 GWd/MTIH, then dominated by Cf-252)
- Significant radioactive nuclides experienced average maximum difference of 143.09% difference across burnups >10 GWd/MTIHM (dominated exclusively by Te-132 until 29 GWd/MTIHM, then dominated by Cf-252
- Pu-241 experienced the maximum actinide mass difference of 9.3% difference at EOL (8.02E+01 grams)
- Cs-137 experienced the maximum significant radioactive nuclide mass difference of 9.73% difference at EOL (1.88E+02 grams)
- U-234 experienced the maximum FLiBe fuel % difference of -4.17% difference at EOL (-1.66E+00 grams)
- U-235 experienced the maximum FLiBe fuel mass difference of 0.04% difference at EOL (5.00E+01 grams)
- Cs-134 experienced the maximum % difference for the top-30 nuclides by mass of 59.19% difference at EOL (2.22E+01 grams)
- Cs-135 experienced the maximum % difference for the top-30 nuclides by mass of 10.26% difference at EOL (-2.20E+02 grams)
- k_{eff} decreased by 291-pcm (i.e. BONAMI overestimates k_{eff})

- Est. serial runtime experienced statistically no change

The reason for these significant differences is due to the inherent effects of differing specific powers in otherwise identical systems; the specific power must be increased by inducing more fissions and scaling the neutron flux is the only way to achieve this in identical systems. So, the flux is increased to match the increased power, thus the fission rate increases and fission product concentrations increase. As expected, certain fission products (Xe-133 and Te-132) that yield equilibrium concentrations within the reactor experienced exactly an exactly 100% greater equilibrium concentration from 10 MW/MTIHM to 20 MW/MTIHM (100% increase in power); and Xe-135 experienced almost an 80% increase in EOL concentration. These nuclides stood out in the significance of their differences between specific powers due to the neutron flux being tied to both their generation (through fission) and their destruction (through absorption). Most other fission products do not experience such significant differences due to the EOL burnup being held identical between the 10 MW/MTIHM and 20 MW/MTIHM simulations, thus the total power output and the number of fission events was generally held constant. When not accounting for Xe-133, Xe-135, Te-132, and Cf-252, the % differences of significant radioactive nuclides are shown to be significantly less (Figure 66 and Figure 67).

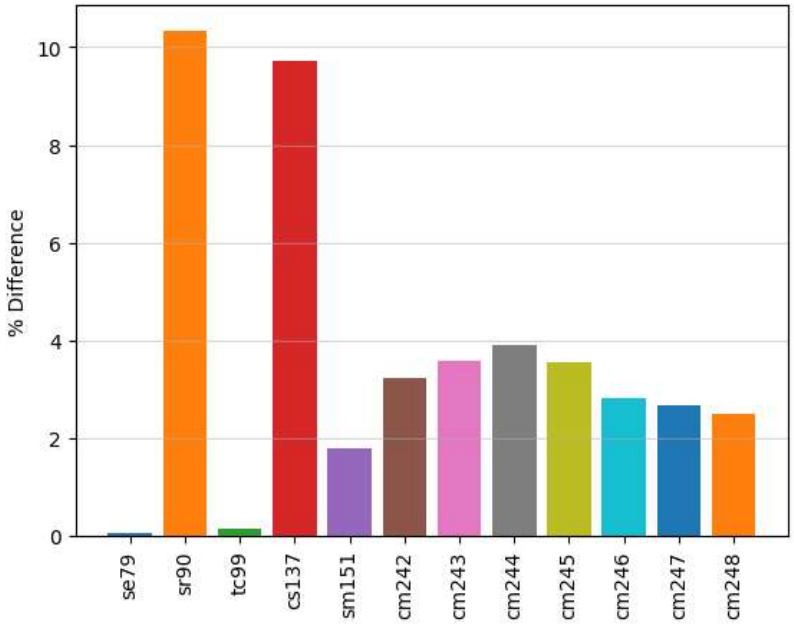

Figure 66. Significantly radioactive nuclide concentration percent differences from 10 MW/MTIHM to 20 MW/MTIHM (excluding xenon and tellurium)

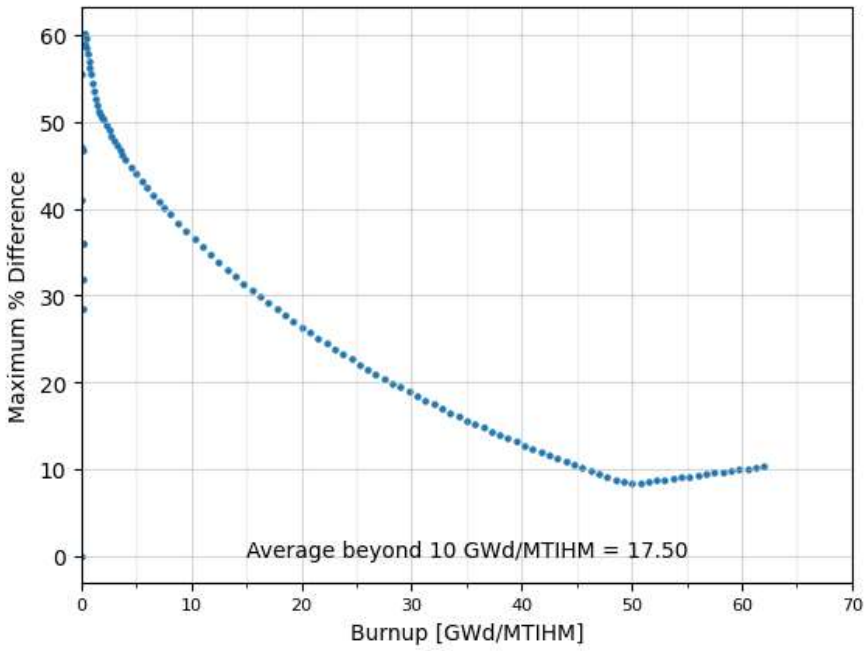

Figure 67. Significantly radioactive nuclide maximum concentration percent differences from 10 MW/MTIHM to 20 MW/MTIHM (excluding xenon and tellurium)

Additionally, the cause of the significant increase in certain actinide concentrations is due to these certain nuclides yielding shorter half-life. Thus, as the reactor is simulated for nearly 17 years in the 10 MW/MTIHM model to achieve 62 GWd/MTIHM, the 20 MW/MTIHM model only simulates ~ 8.5 years to achieve the same burnup. The same fissions being performed in half the time results in higher concentrations of these nuclides due to less time to decay before EOL is reached.

The purpose of this analysis was to determine the scalability of this the overall study of this thesis to different MSR systems. From the results, it can be concluded that clearly specific power will significantly affect the concentrations of those fission product that are strong neutron absorbers, but FLiBe, Uranium, and the majority of all other studied

nuclides are held relatively stable. This lends itself to the conclusion that performing the studies within this thesis on other MSR systems can be expected to yield similar results to those presented here.

5 FUTURE WORK

For thorough analysis of MSR modelling in SCALE, there are several studies that were considered, but not actualized, in this thesis. These most significant of these included:

- Performance of all studies within the scope of the 20 MW/MTIHM model
- Adjustment of lattice-cell input for self-shielding solutions (currently, the lattice cell for which self-shielding methodology is employed on is exact to the reactor core model and does not account for the annular salt content)
- Performance of studies on salt power-average modelling vs salt advection/diffusion modelling

The potential for future studies in the realm of MSR modelling is vast, and the special interest in MSRs as the nuclear industry pursues Generation IV reactors provides incentive to continue within this realm of study.

APPENDICES

A.1 (0001-v01 Convergence Test Results)

****
****

***** Shannon entropy tests *****

****
****

---|---
Test 1: Is the final fission source converged?	Test 1: passed

Test 1 details:

Is the mean square posterior relative entropy < the center mean square Shannon entropy?

(msq(D) < cmsq(H(S)))

generations skipped	msq	cmsq
10	7.14452E-08	8.41379E-06
25	7.14817E-08	8.26665E-06
40	7.06760E-08	8.31058E-06
55	7.05799E-08	8.31776E-06
70	7.02096E-08	8.53492E-06
85	7.06845E-08	8.04448E-06
100	7.07456E-08	8.40764E-06
115	7.11045E-08	8.68651E-06
130	6.99538E-08	8.15095E-06
145	6.92539E-08	8.21718E-06
160	6.77745E-08	7.86781E-06
175	6.75512E-08	8.15229E-06
190	6.65149E-08	8.99683E-06
205	6.58837E-08	9.43401E-06
220	6.56350E-08	9.12921E-06
235	6.13857E-08	9.53970E-06
250	5.92486E-08	8.33805E-06
265	5.67419E-08	9.15428E-06
280	5.25803E-08	9.26018E-06
295	4.61446E-08	7.84245E-06

---|---
Test 2: Are all the active generations within epsilon of the average?	Test 2: passed

Test 2 details:

Does the Shannon entropy of each active generation vary from the average Shannon entropy of the system?

(|D(S||T)-[H(T-H(S))]| < 0.1)

0 active generations failed the test.

The maximum value for the test is 8.53671E-03 which occurred for active generation 106.

---|---
Test 3: Are there adequate active generations after the source is converged?	Test 3: passed

Test 3 details:

Does the Shannon entropy for the last half of the active generations vary from the Shannon entropy of all active generations?

(|H(T) - Hb| < 0.1)

|H(T) - Hb| = 2.64181E-04

****

A.2 (Add. Depletion Sub-interval Schemes)

Table 24. Depletion Scheme 10-3.

Sub-interval [d]	Sub-interval [GWd/MTIHM]
0.00	0.00
6.60	0.07
13.40	0.13
20.00	0.20
40.00	0.40
60.00	0.60
80.00	0.80
120.00	1.20
160.00	1.60
200.00	2.00
266.60	2.67
333.40	3.33
400.00	4.00
533.40	5.33
666.60	6.67
800.00	8.00
1000.00	10.00
1200.00	12.00
1400.00	14.00
1600.00	16.00
1800.00	18.00
2000.00	20.00
2200.00	22.00
2400.00	24.00
2600.00	26.00

Table 24 continued

2800.00	28.00
3000.00	30.00
3200.00	32.00
3400.00	34.00
3600.00	36.00
3800.00	38.00
4000.00	40.00
4200.00	42.00
4400.00	44.00
4600.00	46.00
4800.00	48.00
5000.00	50.00
5200.00	52.00
5400.00	54.00
5600.00	56.00
5800.00	58.00
6000.00	60.00
6200.00	62.00

Table 25. Depletion Scheme 10-4.

Sub-interval [d]	Sub-interval [GWd/MTIHM]
0.00	0.00
5.00	0.05
10.00	0.10
15.00	0.15
20.00	0.20
35.00	0.35
50.00	0.50
65.00	0.65
80.00	0.80
110.00	1.10
140.00	1.40
170.00	1.70
200.00	2.00
250.00	2.50
300.00	3.00

Table 25 continued

350.00	3.50
400.00	4.00
500.00	5.00
600.00	6.00
700.00	7.00
800.00	8.00
950.00	9.50
1100.00	11.00
1250.00	12.50
1400.00	14.00
1550.00	15.50
1700.00	17.00
1850.00	18.50
2000.00	20.00
2150.00	21.50
2300.00	23.00
2450.00	24.50
2600.00	26.00
2750.00	27.50
2900.00	29.00
3050.00	30.50
3200.00	32.00
3350.00	33.50
3500.00	35.00
3650.00	36.50
3800.00	38.00
3950.00	39.50
4100.00	41.00
4250.00	42.50
4400.00	44.00
4550.00	45.50
4700.00	47.00
4850.00	48.50
5000.00	50.00
5150.00	51.50
5300.00	53.00
5450.00	54.50
5600.00	56.00
5750.00	57.50
5900.00	59.00

Table 25 continued

6050.00	60.50
6200.00	62.00

Table 26. Depletion Scheme 10-8.

Sub-interval [d]	Sub-interval [GWd/MTIHM]
0.00	0.000
2.50	0.025
5.00	0.050
7.50	0.075
10.00	0.100
12.50	0.125
15.00	0.150
17.50	0.175
20.00	0.200
27.50	0.275
35.00	0.350
42.50	0.425
50.00	0.500
57.50	0.575
65.00	0.650
72.50	0.725
80.00	0.800
95.00	0.950
110.00	1.100
125.00	1.250
140.00	1.400
155.00	1.550
170.00	1.700
185.00	1.850
200.00	2.000
225.00	2.250
250.00	2.500
275.00	2.750
300.00	3.000
325.00	3.250
350.00	3.500
375.00	3.750
400.00	4.000

Table 26 continued

450.00	4.500
500.00	5.000
550.00	5.500
600.00	6.000
650.00	6.500
700.00	7.000
750.00	7.500
800.00	8.000
875.00	8.750
950.00	9.500
1025.00	10.250
1100.00	11.000
1175.00	11.750
1250.00	12.500
1325.00	13.250
1400.00	14.000
1475.00	14.750
1550.00	15.500
1625.00	16.250
1700.00	17.000
1775.00	17.750
1850.00	18.500
1925.00	19.250
2000.00	20.000
2075.00	20.750
2150.00	21.500
2225.00	22.250
2300.00	23.000
2375.00	23.750
2450.00	24.500
2525.00	25.250
2600.00	26.000
2675.00	26.750
2750.00	27.500
2825.00	28.250
2900.00	29.000
2975.00	29.750
3050.00	30.500
3125.00	31.250
3200.00	32.000

Table 26 continued

3275.00	32.750
3350.00	33.500
3425.00	34.250
3500.00	35.000
3575.00	35.750
3650.00	36.500
3725.00	37.250
3800.00	38.000
3875.00	38.750
3950.00	39.500
4025.00	40.250
4100.00	41.000
4175.00	41.750
4250.00	42.500
4325.00	43.250
4400.00	44.000
4475.00	44.750
4550.00	45.500
4625.00	46.250
4700.00	47.000
4775.00	47.750
4850.00	48.500
4925.00	49.250
5000.00	50.000
5075.00	50.750
5150.00	51.500
5225.00	52.250
5300.00	53.000
5375.00	53.750
5450.00	54.500
5525.00	55.250
5600.00	56.000
5675.00	56.750
5750.00	57.500
5825.00	58.250
5900.00	59.000
5975.00	59.750
6050.00	60.500
6125.00	61.250
6200.00	62.000

REFERENCES

[1] W. A. Wieselquist, R. A. Lefebvre and M. A. Jessee, "SCALE Code System, Version 6.2.4," 2020.

[2] NEXT, "Abilene Christian University Molten Salt Research Reactor Preliminary Safety Analysis Report,", Revision 0, ML22227A201, US NRC 2022.

[3] B. R. Betzler, F. Heidet, B. Feng, C. Rabiti, T. Sofu and N. R. Brown, "Modeling and simulation functional needs for molten salt reactor licensing," *Nuclear Engineering and Design,* vol. 355, 2019.

[4] R. Bostelmann, S. Skutnik, E. Walker, G. Ilas and W. Wieselquist, "Modeling of the Molten Salt Reactor Experiment with SCALE," *Nuclear Technology,* vol. 208, 2022.

[5] NEA, "International Handbook of Evaluated Criticality Safety Benchmark Experiments,", NEA-1486/18, Organisation for Economic Co-operation and Development, Nuclear Energy Agency, 2020.

[6] B. R. Betzler, "Liquid-fueled Molten Salt Reactor Depletion Modeling," *2021 ANS Annual Meeting*, Providence, RI, June 13-16, 2021.

[7] J. W. Bae, B. R. Betzler and A. Worrall, "Molten Salt Reactor Neutronic and Fuel Cycle Sensitivity and Uncertainty Analysis,", *ANS Winter Meeting and Nuclear Technology Expo*, Washington, DC, November 17-21, 2019.

[8] PNNL, "Compendium of Material Composition Data for Radiation Transport Modeling,", 200-DMAMC-128170, PNNL-15870, Rev. 2, PNNL, 2021.

[9] B. R. Betzler, S. Robertson, E. Davidson, J. J. Powers, A. Worrall, L. Dewan and M. Massie, "Fuel cycle and neutronic performance of a spectral shift molten salt reactor design," *Annals of Nuclear Energy,* vol. 119, pp. pp.396-410, 2018.

[10] INL, *Nuclear Science User Facility (NSUF) High Performance Computing (HPC),* Idaho National Laboratory, 2023.

[11] M. L. Huang and B. Petrovic, "Use of MCDancoff factor correction for multi-group fuel depletion analyses of Liquid Salt Cooled Reactors," in *Proceedings of the International Conference on Physics of Reactors (PHYSOR 2014)*, Kyoto, Japan, 28 Sep - 3 Oct, 2014.

[12] M. L. Huang and B. Petrovic, "Development of methodology for efficient fuel design evaluation of the Advanced High Temperature Reactor (AHTR)," *Annals of Nuclear Energy,* vol. 121, pp. 646-660, 2018.

[13] C. E. Bayne and B. Petrovic, "Molten Salt Reactor Modeling in SCALE: Effects of Multigroup Libraries on Depletion Analysis," in *ANS Winter Metting 2022*, Phoenix, AZ, November 13-17, 2022.

[14] D. Wooten and J. J. Powers, "A Review of Molten Salt Reactor Kinetics Models," *Nuclear Science and Engineering,* vol. 191, 2018.

[15] M. L. Williams and K. S. Kim, "The Embedded Self-Shielding Method", *Physor 2012*, Knoxville, TN, April 15-20, 2012.

[16] M. L. Williams, K. S. Wiarda, M. A. Kim and M. A. Jessee, "Multigroup Data Processing for the Embedded Self-Shielding Method in SCALE,", *Physor 2016,* Sun Valley, ID, May 1-5, 2016.

[17] P. Vincent Valdez Jr, B. R. Bezler, W. A. Wieselquist and M. Fratoni, "Modeling Molten Salt Reactor Fission Product Removal with SCALE", ORNL/TM-2019/1418, Oak Ridge National Laboratory, 2020.

[18] N. Shoman and B. B. Cipiti, "Development of a Liquid-Fueled Molten Salt Reactor Safeguards Model,", SAND2019-7415, Sandia National Laboratory, 2019.

[19] D. Shen, G. Ilas and J. J. Powers, "Reactor Physics Benchmark of the First Criticality in the Molten Salt Reactor Experiment," *Nuclear Science and Engineering,* vol. 195, 2021.

[20] K. M. Ramey and B. Petrovic, "Monte Carlo modeling and simulations of AHTR fuel assembly to support V&V of FHR core physics methods," *Annals of Nuclear Energy,* vol. 118, 2018.

[21] G. Radulescu, I. C. Gauld, G. Ilas and J. C. Wagner, "Approach for Validating Actinide and Fission Product Compositions for Burnup Credit Criticality Safety Analyses," *Nuclear Technology,* vol. 188, 2017.

[22] V. Pathirana, O. Chvala and S. Skutnik, "Depletion dependency of molten salt reactor dynamics," *Annals of Nuclear Energy,* vol. 168, 2022.

[23] L. Mei, X. Cai, D. Jiang, J. Chen, Y. Zhu and Y. Liu, "The investigation of thermal neutron scattering data for molten salt Flibe," *Jounral of Nuclear Science and Technology,* vol. 50, 2012.

[24] A. E. Isotalo and W. A. Wieselquist, "A method for including external feed in depletion calculations with CRAM and implementation into ORIGEN," *Annals of Nuclear Energy,* vol. 85, 2015.

[25] D. Huang, U. Mertyurek and H. Abdel-Khalik, "Verification of the sensitivity and uncertainty-based criticality safety validation techniques: ORNL's SCALE case study," *Nuclear Engineering and Design,* vol. 361, 2020.

[26] I. C. Gauld, G. Ilas and G. Radulescu, "Uncertainties in Predicted Isotopic Compositions for High Burnup PWR Spent Nuclear Fuel,", NUREG/CR-7012 ORNL/TM-2010/41, US NRC, 2011.

[27] M. Fratoni, D. Shen, G. Ilas and J. Powers, "Molten Salt Reactor Experiment Benchmark Evaluation,", DOE-UCB-8542, US DOE, 2020.

[28] M. P. Dion, L. G. Worrall, S. Croft and L. M. Scott, "Molten Salt Reactor Signatures and Modeling Study,", ORNL/SPR-2020/1836, Oak Ridge National Laboratory, 2020.

[29] F. Bostelmann, G. Ilas, C. Celik, A. M. Holcomb and W. A. Wieselquist, "Nuclear Data Assessment for Advanced Reactors,", NUREG/CR-7289 ORNL/TM-2021/2002, US NRC, 2021.

[30] F. Bostelmann and W. W. A. Ilas, "Key Nuclear Data Impacting Reactivity in Advanced Reactors,", ORNL/TM-2020/1557, Oak Ridge National Laboratory, 2020.

[31] B. R. Betzler, J. J. Powers and A. Worrall, "Molten salt reactor neutronics and fuel cycle modeling and simulation with SCALE," *Annals of Nuclear Energy,* vol. 101, pp. 489-503, 2017.

[32] B. R. Betzler, K. B. Bekar, W. A. Wieselquist, S. W. Hart and G. Stimpson S, "MOLTEN SALT REACTOR FUEL DEPLETION TOOLS IN SCALE,", *Global/Top Fuel 2019,* Seattle, WA, September 22-27, 2019.

[33] B. R. Betzler, J. J. Powers, N. R. Brown and B. T. Rearden, "Implementation of Molten Salt Reactor Tools in SCALE,", *M&C 2017,* Jeju, Korea, April 16-20, 2017.

[34] M. L. Huang and B. Petrovic, "Automated MCDancoff Factor Generation for Liquid Salt Cooled Reactor Parametric Studies," *ANS Transactions,* vol. 113, pp. 1254-1257, 2015.

[35] PACE, "{P}artnership for an {A}dvanced {C}omputing {E}nvironment ({PACE})," Atlanta, GA, 2017.